UNIVERSITÀ DEGLI STUDI DI UDINE

Facoltà di Ingegneria

Dottorato in Ingegneria Industriale e dell'Informazione

Tesi di Dottorato

FILTER BANK TRANSCEIVER SYSTEMS: DESIGN AND PERFORMANCE ANALYSIS

Relatore:
Prof. ANDREA TONELLO

Dottorando:
NICOLA MORET

Dicembre 2011

ANNO ACCADEMICO 2011/2012

a Dio
perché Tutto viene da Lui,
a Salvatore
il mio compagno
di viaggio in quest'avventura

Contents

List of Tables

List of Figures

Abstract

In this thesis we consider transceiver architectures based on the filter bank (FB) theory. We begin by introducing the general system model and its mathematical representation, by closely focusing on two particular FB schemes that are Orthogonal Frequency Division Multiplexing (OFDM) and Filtered Multitone Modulation (FMT).

We introduce a notation based on operators that enables us to derive the efficient FB realizations by exploiting a unique framework in the time domain. In particular we consider three efficient architectures that deploy time-invariant filtering.

We then consider one particular efficient realization among the three discussed, and we describe its mathematical representation in a matrix form, in order to derive the equations to design an orthogonal prototype pulse. We propose a method that considerable simplifies the design of the orthogonal prototype pulse for certain choices of the parameters and for arbitrarily large number of sub-channels, so that no inter-symbol and no inter-channel interference is present in an ideal channel. A FB system that deploys orthogonal pulses will be referred in this thesis to as orthogonal FMT or Short-Orthogonal FMT (SO-FMT). Several examples of pulses are reported and the performance in typical wireless multi-path fading channels are shown.

Then, we consider orthogonal FMT with orthogonal pulse, in combination with an MMSE frequency domain equalizer to cope with the inter-channel interference, and a DFE equalizer to cope with the residual inter-symbol interference, when transmission is over a frequency selective channel. Numerical results show that orthogonal FMT in conjunction with the MMSE/DFE equalizer has the potentiality to sensibly improve the capacity in the WLAN scenario compared to OFDM

Furthermore, we investigate the use of an adaptive FB modulation scheme over WLAN channels. Concerning this topic, we propose a hybrid architecture, herein referred to as hybrid FMT (H-FMT), which is based on the deployment of adaptive OFDM (A-OFDM) and SO-FMT. We show that H-FMT provides significant achievable rate gains compared to OFDM with a static CP and it

marginal increases the computational complexity.

By considering the multiple antenna communication scenario, we present a multiple-input multiple-output (MIMO) transceiver based on FB modulation, and on the polynomial singular value decomposition (PSVD). We show the performance in terms of capacity in typical WLAN MIMO channels.

Finally, we analyze the effect of phase noise on FB transmission systems by considering OFDM and FMT. We report a general analysis of the distortion due to the Common Phase Error (CPE), and the interferences using a stationary model for the phase noise impairment process. We consider a non-coherent and a one-tap coherent receiver. Theoretical and simulation results are presented for the Bit-Error-Rate (BER) of FMT and OFDM. It is shown that FMT provides somewhat better performance than OFDM in the presence of phase noise.

Sommario

In questa tesi consideriamo i sistemi di modulazione basati sull'architettura a banchi di filtri (FB). Nel capitoli introduttivi viene presentato il modello di sistema generale e la sua descrizione analitica . In particolare vengono descritte due specifiche architetture FB, che sono rispettivamente Orthogonal Frequency Division Multiplexing (OFDM) e Filtered Multitone modulation (FMT), le quali saranno considerate in dettaglio lungo tutto lo sviluppo della tesi.

In seguito consideriamo la descrizione analitica di alcune architetture efficienti relative ai transricevitori a FB. A tal proposito, introduciamo una notazione ad operatori che permette di derivare e descrivere le realizzazioni efficienti dei sistemi FB nel dominio del tempo. In particolare consideriamo e confrontiamo tre architetture efficienti che sfruttano filtraggi tempo-invarianti.

Partendo da una di queste architetture efficienti, ne sviluppiamo il modello matematico in forma matriciale, dal quale ricaviamo le equazioni necessarie per progettare un filtro prototipo ortogonale. In questo contesto, introduciamo un metodo che semplifica sensibilmente il progetto del filtro prototipo ortogonale per un certo insieme di parametri e un arbitrario numero di sottocanali. Lungo questa trattazione ci riferiremo al sistema FB che utilizza i suddetti filtri ortogonali con il nome di FMT ortogonale, altrimenti denotato con SO-FMT. Presentiamo di seguito diversi esempi di impulsi con le relative performance in canali wireless.

Consideriamo quindi il sistema FMT ortogonale sin qui sviluppato, combinato con un equalizzatore a errore quadratico medio minimo (MMSE) per ridurre l'effetto di interferenza di inter-canale, e un ulteriore blocco di equalizzazione a retroazione (DFE) per far fronte all'interferenza di inter-simbolo residua. Vengono riportati numerosi risultati numerici in termini di capacità, confrontando il sistema FMT ortogonale equalizzato, con il sistema OFDM.

Abbiamo poi investigato sulla possibilità di progettare un sistema FB ibrido (H-FMT) combinando le potenzialità dei sistemi SO-FMT e OFDM. Mostriamo come questo sistema possa sensibilmente incrementare le performance con una minima introduzione di complessità.

Proseguendo, consideriamo lo scenario applicativo di trasmissioni che sfrutta

l'utilizzo di antenne multiple. In questo constesto, progettiamo un trasmettitore FB con un sistema di precodifica ed equalizzazione, basato sull'algoritmo di decomposizione SVD per polinomi (PSVD), mostrando le prestazioni in termini di capacità.

Infine analizziamo i sistemi FB considerando l'effetto di distorsione causato dal rumore di fase degli oscillatori (PN). Confrontiamo i sistemi FMT e OFDM, riportando un'analisi generica sull'errore di fase comune (CPE). Considerando sia un ricevitore non-coerente che un ricevitore coerente, presentiamo le performance dei due sistemi in termini di Bit Error Rate (BER), e ne confrontiamo i risultati con quelli ottenuti dalla trattazione teorica sviluppata.

Chapter 1

Introduction

Modulated filter bank (FB) transmission systems, sometimes referred as to multicarrier modulation, has been successfully applied to a wide variety of digital communications applications over the past several years.

FB transceivers employ a transmission technique where a set of narrow band signals are transmitted simultaneously over a broad band channel, by adopting transmission filters that confine the energy of each narrow-band signal around several tones. The low rate signals are obtained by a serial-to-parallel conversion of the input information data. The original idea was introduced many years ago [1] and it was originated by the goal of simplifying the equalization task in highly frequency selective channels that introduce severe inter-symbol interference (ISI). The simplification of the equalization stage is possible since the wide band channel is divided in a number of narrow band channels that exhibit a nearly flat frequency response. If the number of sub-channels is sufficiently large, and the inter-channel interference (ICI) is negligible, then a single tap equalizer per sub-channel is sufficient for data detection.

The most famous modulated FB scheme is indeed Orthogonal Frequency Division Multiplexing (OFDM) [2] that has been adopted by several important standards in communications. Regarding wireless data transfer applications, it is employed in local-area-networks (LAN) with the IEEE 802.11a,g,n standards [3], and metropolitan area network (MAN) with the WiMAX (IEEE 802.16) standard [4]. Moreover, it is also utilized for terrestrial broadcasting of digital

audio (DAB) [5] and video (DVB) [6] signals. Due to its capability to cope with the frequency selective fading channels, OFDM has also attracted a lot of interest for high speed transmission in a mobile scenario, and the 3rd Generation Partnership Project (3GPP) has considered Long Term Evolution (LTE) and LTE Advanced [7] that employ OFDM, as the new frontier of cellular systems. Concerning wireline applications, OFDM was adopted in Asymmetric Digital Subscriber Line (ADSL). The IEEE P1901 [8] and HomePlug AV [9] standards that were developed for powerline applications also use OFDM.

Although OFDM has been chosen as the physical layer standard for all these important standards, the theory, algorithms and implementation techniques are still of high interest. This is because OFDM presents some drawbacks. First of all it suffers from a non-optimal spectral efficiency since it exploits the cyclic prefix technique to cope channel dispersion, and this affects the transmission bit-rate. Furthermore, OFDM is very sensitive to fast time-variant channels, and also to hardware impairments such as the frequency offset and the phase noise.

FB theory gives us some tools to develop alternative algorithms and schemes to counteract all these drawbacks. This is due to the fact that OFDM itself can be viewed as a particular realization of a general modulated FB system. Thus, exploiting FB theory, we can analyze and design a FB transceiver by considering all degrees of freedom that could normally remain hidden and we can bring out some new light.

One of the reasons that renders OFDM so popular is that its realization requires a very low computational complexity, since its architecture only requires the computation of a Discrete Fourier Transform (DFT) that can be realized exploiting the Fast Fourier Transform (FFT) algorithm. As it will be shown in this thesis, the use of alternatives FB schemes can lead to an improvement of the performance, but the price paid is an increment of computational complexity that sometimes might not be justified. More generally, any FB scheme requires higher complexity w.r.t. OFDM, and this is why the community research spent much effort over the years to propose alternatives efficient implementations to cope with this issue.

The efficient realizations are not only important for lowering the computation

complexity but they also leads to a mathematical representation of the FB system in matrix form that can be exploited to ease the treatment of some classical problems such as the design the filters deployed by the transceiver.

Many others multicarrier schemes have been presented in literature as alternatives of classic OFDM. They range from simple variation of OFDM such as Windowed-OFDM (WOFDM), Pulse-Shaped OFDM [10], to more complex architectures such as Filtered Mutitone (FMT) [11] and Offset-QAM [12].

In this thesis, we present a study of alternatives FB architectures that follows the philosophy introduced by the Filtered Multitone (FMT) paradigm. FMT was presented in [11], and was initially considered for the evolution of the ADSL. Subsequently, it was also investigated for wireless and powerline applications. As it will be explained in next chapters, one of the major issues of OFDM is that it deploys sub-channel filters that are not well confined in frequency, that cannot completely separate the sub-channels. The idea of FMT is to adopt pulses that can concentrate the energy of the narrow-band signals around equally spaced tones, and this renders the sub-channel signals independent from each others. Clearly, this achievement can be paid in terms of an increment of computation complexity.

The contribution of this thesis is summarized as follows:

Chapter 2

We introduce the modulated FB architecture with its mathematical description. We aim at describing the general philosophy behind the FB transceivers, presenting the general model that can be adapted to various schemes already presented in literature like OFDM and FMT, simply by changing some parameters such as the number of sub-channels, the sampling-interpolation factor, and the prototype pulses deployed. Furthermore, we introduce the channel model representative of the WLAN scenario that will be often adopted along this thesis to present numerical results.

Chapter 3

We present a general framework that is useful for deriving the efficient realization of the FB transceivers in the time domain. We consider three schemes that have been each described by Tonello in [13], by Cvetković, Vetterli in the context of signal coding [14], (and more recently by Siclet, Siohan, Pinchon in [15] and by McGee in [16]), and another one by Weiss, Stewart in [17]. They are all based on the deployment of a DFT and a polyphase FB network. We aim at describing the differences and similarities between them. Instead of deriving the realizations in the Z-domain, we introduce a notation based on operators, that helps us to distinguish the processing blocks, and explicitly detail the implementation steps. This also leads to a mathematical treatment of the efficient architectures that can be easily expressed with a matrix structure which enables us to derive alternatives mathematical representations.

Chapter 4

The frequency selective channel may introduce inter-channel interference (ICI) and inter-symbol interference (ISI) that can be minimized with the design of time-frequency confined pulses. We investigate the design of a prototype pulse that merges the characteristic of both OFDM and FMT, in the sense that it would be desirable that the prototype pulse holds the orthogonality property like OFDM (i.e., absence of interference in an ideal channel), and also it also has an high frequency confinement like FMT. We exploit one of the efficient architectures presented in Chapter 3 from which we extract a matrix representation and then the orthogonality equations. We propose a simplified design method that generates orthogonal prototype pulses for a wide set of parameters. We then consider the FB system that deploys an orthogonal prototype pulse, that will be referred as to orthogonal FMT. If the pulse has minimal length the scheme is referred to as short-orthogonal FMT (SO-FMT). We compare its performance with those of canonical FMT and OFDM schemes.

Chapter 5

The orthogonal FMT system presented in Chapter 4 suffers from a non-negligible ICI since the prototype pulses cannot effectively separate the sub-channels. In this chapter we present the design of a frequency domain equalizer that mitigates the unwanted ICI distortion effect. In conjunction with this linear equalization stage, we further propose to improve the performance by adopting a Decision Feedback Equalizer (DFE) to compensate the remaining inter-symbol interference effects. We present extensive numerical results considering the WLAN channel model [18], evaluating the performance in terms of capacity of orthogonal FMT, and comparing the results with the baseline system represented by the OFDM used in the IEEE 802.11 protocol.

Chapter 6

In this chapter we present a novel hybrid transceiver scheme based on the modulated FB theory that exploits the peculiarities of two different FB architectures, namely OFDM and SO-FMT. We aim at setting up a system that can switch between the two architecture considered by choosing the one that grant the maximum information capacity as a function of the channel state information.

Chapter 7

We then focus on the wireless scenario where Multiple-Output Multiple-Input (MIMO) transmission multiple antennas is used. Under the assumption of full channel state information, and considering flat-frequency fading channels, a precoding and an equalizer based on the singular value decomposition (SVD) can be adopted to effectively counteract the inter-antenna interference (IAI). To remove the IAI when the channel is frequency selective, FB modulation is adopted to render the channel frequency response approximately flat on each sub-channel. Nevertheless, when the number of tones is not sufficient to assume the sub-channel response to be flat, some IAI arises if simple SVD precoding and equalization is employed. In such a case, singular value decomposition (SVD) of polynomial matrices (PSVD) can be deployed. We analyze the possibility of combining the PSVD decomposition of the broadband MIMO channel with the

FMT modulation transmission system, and we compare its performance to that of MIMO-OFDM.

Chapter 8

Hardware impairments such as non-linear amplification, carrier frequency-offset and phase noise are a major issue in communications. In this chapter, we study the effect of phase noise due to non ideal oscillators when FB modulation systems are deployed. In particular, we analyze the FMT system and the OFDM system. We provide a general framework to the analysis of the Common Phase Error (CPE) and the interference components in FB modulation. We propose approximated expressions of the symbol error rate for M-PSK and M-QAM constellations with both a non-coherent and a one-tap coherent receiver, using a stationary model for the PN impairment process and under the Gaussian interference assumption. Several simulation results are reported to validate the theoretical results. It is shown that FMT provides somewhat better performance than OFDM in the presence of phase noise.

Related Publications

The main results of this thesis have been the subject of the publications listed below.

Journal papers:

- N. Moret, A. M. Tonello, *"Performance of Filter Bank Modulation with Phase Noise,"* IEEE Trans. on Wireless Communications, pag. 3121-3126, October 2011.

- N. Moret, A. M. Tonello, *"Design of Orthogonal Filtered Multitone Modulation Systems and Comparison among Efficient Realizations,"* EURASIP Journal on Advances in Signal Processing, Special issue: Filter Banks for Next Generation Wireless Multicarrier Systems, 2010.

Conference papers:

- N. Moret, A. M. Tonello, S. Weiss, *"MIMO Precoding for Filter bank Modulation Systems Based on Polynomial Singular Value Decomposition,"* Proc. of IEEE VTC 2011 Spring, Budapest, Hungary, May 15-18, 2011.

- S. D'Alessandro, N. Moret, A. M. Tonello, *"Green Hybrid-FMT for WLAN Communications,"* Proc of IFIP Wireless Days 2010, Venice (Italy), October 20-22, 2010.

- S. D'Alessandro, N. Moret, A. M. Tonello, *"Hybrid FMT for WLAN Applications,"* Proc of. PIMRC 2010, Instanbul, Sept. 27-30, 2010.

- N. Moret, A. M. Tonello, *"Filter Bank Transmission Systems: Analysis with Phase Noise,"* Proc.of International Symposium on Wireless Communication System (ISWCS) 2009, Siena, Italy, pp.498-501, September 9-11, 2009.

- N. Moret, A. M. Tonello, *"Similarities and Differences among Filtered Multitone Modulation Realizations and Orthogonal Filter Bank Design,"* Proc. of EUSIPCO 2009, Glasgow, Scotia, August 24-28, 2009.

Public deliverables (http://www.ict-omega.eu/):

- Home Gigabit Access project, *"Deliverable D2.4: Performance Report of advanced PHY and MAC mechanisms"*.

- Home Gigabit Access project, *"Deliverable D2.5: Performance report of the radio convergence layer"*.

- Home Gigabit Access project, *"Deliverable D2.6: Performance report of cross-layer mechanisms"*.

- Home Gigabit Access project, *"Deliverable D2.7: Radio - Final evaluation report"*.

Chapter 2

Modulated Filter Bank Transceivers

2.1 General Filter Bank Architecture

In this chapter, we introduce a transmission technique based on the modulated filter bank (FB) architecture which has received much attention from the community research since it can easily cope with frequency selective fading channels. In a FB transceiver, several narrow band streams of data symbols are parallel processed deploying interpolation filters. Then, they are summed together resulting in a wide band signal which is transmitted over the transmission media. The modulated FB assumes the filters to be obtained by considering a unique prototype pulse, and by shifting its spectrum around equally spaced sub-channels. The receiver in FB is generally the dual version of the transmitter, since the received signal is processed by some parallel sampling filters, that give at the output the reconstructed version of the transmitted signals. In this chapter, we aim at describing the general philosophy behind the FB transceivers, presenting a general model that can be adapted to various schemes already presented in the literature simply by changing some parameters such as the number of sub-channels, the sample-interpolation factor, and the prototype pulses deployed.

We now present in detail the mathematical representation of a modulated FB transceiver depicted in Fig. 2.1. We consider M low-rate signals representing data-symbols belonging to a certain constellation (e.g., M-QAM), and herein denoted as $a^{(k)}(Nn)$, with $k = 0, \ldots, M-1$. The signals $a^{(k)}(Nn)$ are upsampled

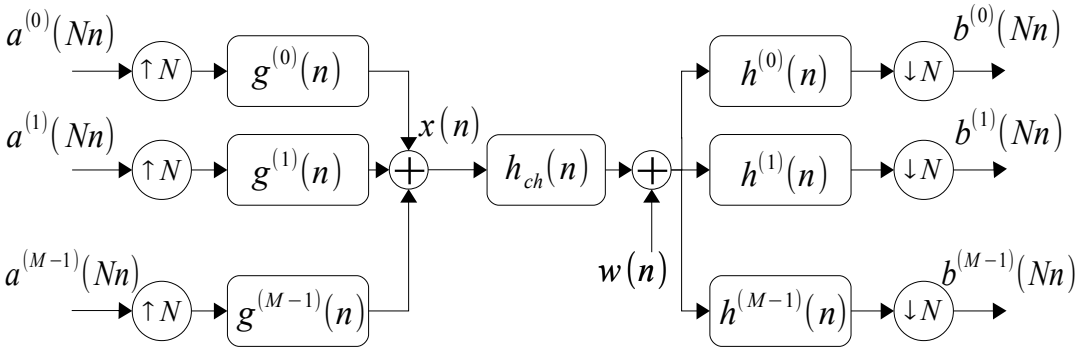

Figure 2.1: FB scheme.

by a factor N, and are filtered by the pulses defined as

$$g^{(k)}(n) = g(n)W_M^{-kn}, \tag{2.1}$$

that are the modulated version of the prototype pulse $g(n)$ of the synthesis bank, where $W_M^{kn} = e^{-j\frac{2\pi}{M}kn}$. Thus, as mentioned above the filters deployed are obtained by uniformly shifting in frequency the spectrum of the prototype pulse. Then, the sub-channel signals are summed, and the transmitted signal reads

$$x(n) = \sum_{k=1}^{M-1} \sum_{\ell \in \mathbb{Z}} a^{(k)}(N\ell) g^{(k)}(n - N\ell).$$

After propagation through the channel, we obtain the signal $y(n)$ defined as

$$y(n) = x * h_{ch}(n) + w(n), \tag{2.2}$$

where we denoted with $*$ the convolution operation, and with $h_{ch}(n)$ the channel impulse response and is the noise modeled as an Additive White Gaussian Noise (AWGN) process. The signal $y(n)$ is processed by the sub-channel modulated pulses defined as

$$h^{(k)}(n) = h(n)W_M^{-kn}, \tag{2.3}$$

where $h(n)$ is the prototype pulse of the analysis bank. The obtained signals

are then sampled by a factor N. Therefore, the signal received in the i-th sub-channel, with sampling with period N, can be written as

$$b^{(i)}(Nn) = \sum_{m\in\mathbb{Z}} y(m)h^{(i)}(Nn-m). \tag{2.4}$$

If we explicitly write the received signal $b^{(i)}(Nn)$ as a function of the transmitted symbols $a^{(k)}(Nn)$, we obtain

$$\begin{aligned} b^{(i)}(Nn) = &\sum_{k=1}^{M-1}\sum_{\ell\in\mathbb{Z}} a^{(k)}(N\ell)\sum_{p\in\mathbb{Z}} g^{(k)}(p-N\ell) \\ &\times \sum_{m\in\mathbb{Z}} h_{ch}(m-p)h^{(i)}(Nn-m) + w^{(i)}(Nn), \end{aligned} \tag{2.5}$$

where we defined the received noise component as

$$w^{(i)}(Nn) = \sum_{\ell\in\mathbb{Z}} w(\ell)h^{(i)}(Nn-\ell). \tag{2.6}$$

Now, we separate the useful signal from the interferences components and (2.5) reads

$$\begin{aligned} b^{(i)}(Nn) &= a^{(i)}(Nn)g_{eq}^{(i,i)}(0) \\ &\quad + \sum_{\substack{\ell\in\mathbb{Z}\\ \ell\neq n}} a^{(k)}(N\ell)g_{eq}^{(i,i)}(Nn-N\ell) \\ &\quad + \sum_{\substack{k=0\\ k\neq i}}^{M-1}\sum_{\ell\in\mathbb{Z}} a^{(k)}(N\ell)g_{eq}^{(i,k)}(Nn-N\ell) + w^{(i)}(Nn) \\ &= a^{(i)}(Nn)g_{eq}^{(i,i)}(0) + ISI^{(i)}(Nn) \\ &\qquad + ICI^{(i)}(Nn) + w^{(i)}(Nn), \end{aligned} \tag{2.7}$$

where we defined the sub-channel equivalent impulse response as

$$g_{eq}^{(i,k)}(Nn) = g^{(k)} * h_{ch} * h^{(i)}(Nn). \tag{2.8}$$

Thus, (2.7) reveals that in general the received symbol at the ith sub-channel at the instant Nn denoted as $b^{(i)}(Nn)$ equals the transmitted symbol $a^{(i)}(Nn)$ multiplied by the complex number $g_{eq}^{(i,i)}(0)$, plus the interference components here represented by the terms $ISI^{(i)}(Nn)$ and $ICI^{(i)}(Nn)$, namely the inter-symbol interference (ISI) and the inter-channel interference (ICI).

2.2 Orthogonal Frequency Division Multiplexing (OFDM)

The Orthogonal Frequency Division Multiplexing (OFDM) scheme, sometimes referred to as Discrete Multitone (DMT), is probably the most popular modulated FB technique. In OFDM, the interpolation factor equals the number of sub-channels M, i.e., $N = M$, and the prototype pulses have rectangular impulse response. So the filters can be written as

$$\begin{cases} g(n) = rect(n/M) \\ h(n) = g(-n) \ , \end{cases} \tag{2.9}$$

where we defined the rectangular pulse as

$$rect(n/M) = \begin{cases} 1 & \text{if} \quad n \in \{0, \cdots, M-1\} \\ 0 & \text{otherwise} \ . \end{cases} \tag{2.10}$$

This scheme holds the orthogonal property only in ideal signal propagation conditions. In Fig. 2.2 the frequency response of OFDM pulses with $M = 8$ sub-channels are reported. When the channel is frequency selective the critically sampled OFDM scheme suffers from ISI and ICI. In particular the ICI contribution is heavy because of the frequency response of the prototype pulse that does not effectively attenuate the signal energy present outside the sub-channel band.

There is a method that enables the system to hold its PR even in the presence of a dispersive channel. This technique consists in setting the interpolation factor

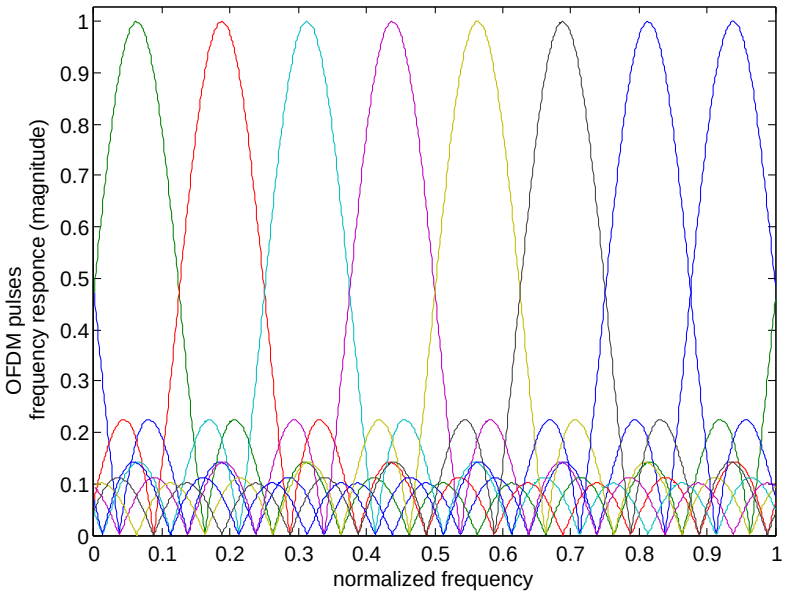

Figure 2.2: Frequency responce (magnitude) of OFDM pulses for a FB with a number of sub-channels equal to $M = 8$.

$N > M$, and replacing the prototype pulses with

$$\begin{cases} g(n) = rect(n/N) \\ h(n) = rect(-n/M) \ . \end{cases} \tag{2.11}$$

This solution is known as cyclically prefixed OFDM, and yields a PR system only if the cyclic prefix (CP) lasts longer than the channel duration. The relation between the CP in number of samples and the sampling-interpolation factor N is

$$\beta = N - M. \tag{2.12}$$

However, the increment of N (or equivalently an adoption of a longer CP), reflects on a decrement of the transmission rate. Furthermore, the deployment of non-matched filters lowers the signal to noise ratio (SNR) experienced by

the received signals $b^{(i)}(Nn)$, and this leads to a further degradation of the performance.

2.3 Filtered Multitone (FMT)

Another popular modulated FB technique is Filtered Multitone (FMT). It has been originally proposed for application over broadband wireline channels [11], and subsequently it has also been investigated for wireless [19],[20] and power line [21] applications.

The main characteristic that distinguishes FMT from OFDM is the different prototype pulse deployed. FMT in general privileges frequency confined pulses that render the sub-channels well separated, and this limits the inter-channel interference (ICI) introduced by the frequency selective channel. A common choice is to deploy truncated root-raised cosine (rrc) as prototype pulse for both the synthesis and the analysis banks. The frequency response of the rrc pulse has the following expression

$$RRC(f) = \begin{cases} 1 & \text{if} |f| \leq \frac{1-\rho}{2} \\ \sqrt{\frac{1}{2}[1 + cos(\frac{\pi}{\rho}[|f| - \frac{1-\rho}{2}])]} & \text{if} \quad \frac{1-\rho}{2} \leq |f| \leq \frac{1+\rho}{2} \\ 0 & \text{otherwise} , \end{cases} \tag{2.13}$$

where $\rho \in [0, 1]$ denotes the roll-off factor. In Fig 2.3, the frequency response of rrc FMT pulses with $\rho = 0.2$ and pulse length $L_g = 24N$ and $M = 8$ sub-channels are reported.

Since the prototype pulse of the synthesis and the analysis bank are equivalents, the receiver deploys matched filtering, i.e.,

$$g^{(k)}(n) = h^{(k)^*}(-n). \tag{2.14}$$

Whenever the the prototype pulse achieves a high level of spectral containment, the sub-channels are quasi-orthogonal to each other and this renders the inter-channel interference negligible. Clearly, the frequency confinement characteristic is obtained by choosing filters with length equal to several symbol periods,

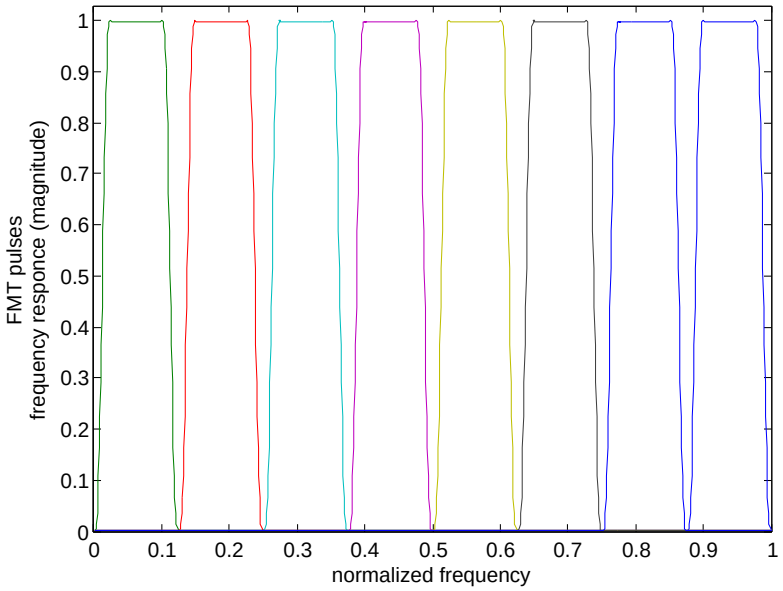

Figure 2.3: Frequency response (magnitude) of FMT pulses for a FB with number of sub-channels equal to $M = 8$ and $N = 10$.

and this, in addition to increase the computational complexity, introduces considerable inter-symbol interference, when transmitting over a multipath channel. The ISI component introduced by the frequency selectivity can be mitigated with sub-channel equalization [19],[22],[23].

2.4 IEEE Tgn Channel Model

In this thesis we will often consider the Tgn channel model described in [18] and developed for the indoor Multiple-Input Multiple-Output (MIMO) WLAN scenario.

This model consists of six classes of channels labeled (A,B,C,D,E,F) representing different environments, i.e. small office, large open space/office. Both small scale multipath fading and large scale path loss fading as a function of distance are incorporated in this model. A single channel realization assumes the impulse response modeled by clusters. Each cluster contains taps generated with a certain power delay profile. The number of clusters varies from 2 to 6,

depending on the model, and the clusters can overlap. The angular spread, angle of arrival, and angle of departure values are assigned to each tap and cluster using statistical model. The channel model can be used for both 2 GHz and 5 GHz frequency bands. However, the path loss model is frequency dependent. In Table 2.1 the root mean square (rms) delay spread for each channel model class are summarized.

Class	Rms delay spread
A	0 ns
B	15 ns
C	30 ns
D	50 ns
E	100 ns
F	150 ns

Table 2.1: Root mean square (rms) delay spread

Chapter 3

Filter Bank Efficient Realizations

3.1 Introduction

In this chapter we present a general framework useful for deriving the efficient realization of the FB transceivers in the time domain. Research on low computational complexity architectures mainly covers two important issues: firstly, it is desirable to have high performance systems, with an increment of computational complexity that justifies the benefits given by the system itself. Secondly, the mathematical treatment of the efficient architectures can be easily expressed with a matrix structure which enables one to derive alternatives representations of classical problems, such as the design of the prototype filter that satisfies the orthogonal constraints of the FB.

In the literature several efficient schemes for FB have been proposed. Some of them deploy a time variant filtering, resulting in a difficult practical realization [11]. Herein, we consider efficient implementations of FB where the polyphase network has time-invariant filtering that results desirable for practical purpoises.

In particular in this chapter we consider three schemes that have been described one by Tonello in [13], one by Cvetković, Vetterli in the context of signal coding [14], (and more recently by Siclet, Siohan, Pinchon in [15] and by McGee in [16]), and another one by Weiss, Stewart in [17]. They are all based on the deployment of a DFT and a polyphase FB network. The method described in [13], that herein will be referred as to Method A, was derived in the time domain

while the schemes described in [14], and [17], that will be referred as to Method B and Method C, were derived in the Z-domain.

Although at the first glance the three schemes seems to be identical, they are not. They present some peculiarities at a processing level that differ from each other. Furthermore the approach of their derivation follows different philosophies. We aim at describing the differences and similarities between them, and instead of deriving the realizations in the Z-domain, we introduce a notation based on operators, that helps us to identify the processing blocks, and explicitly detail the implementation steps. We also compute the complexity of the architectures in terms of number of complex operations per second. The analysis done shows that the three methods require similar memory space and achieve identical reductions in complexity, but differ in the elegance of their representation.

This chapter is organized as follows. In Section 3.2, we report the notation useful for deriving the efficient realization in the time domain. Section 3.3 , we recall the FMT system model using the novel notation, while in Sections 3.4-3.6 we derive the three efficient realizations. The differences/similarities and the complexity analysis is reported in Section 3.7.

3.2 Notation

The notation related to the operators, constants and signals used in this chapter is summarized in Tab. 3.1. A discrete time signal is denoted either with x or $x(Nn)$. It is a function

$$x : Z(N) \to \mathbb{C},$$

where $Z(N)$ is the set of integer numbers multiple of N, with N belonging to the set $\mathbb{N}$ of natural number, i.e.,

$$Z(N) = \{-\infty, \cdots, -N, 0, N, 2N, \cdots, +\infty\},$$

and $\mathbb{C}$ is the set of complex numbers. The notation $x(Nn)$ explicitly shows the definition domain of the signal.

3.2.1 Operators

To derive the FMT realizations presented in this paper it is convenient to use the notation of operators, in particular, the translation, sampling and interpolation. They are defined as follows:

1. *Operator* τ^a: translation of signal $x : Z(P) \to \mathbb{C}$ by $a \in \mathbb{Z}$.

$$\tau^a[x] = x(P(n+a)). \tag{3.1}$$

2. *Operator* $\mathcal{C}_N$: sampling of signal $x : Z(P) \to \mathbb{C}$ by $N \in \mathbb{N}$.

$$\mathcal{C}_N[x] = x(NPn). \tag{3.2}$$

3. *Operator* $\mathcal{I}_N$: interpolation of signal $y : Z(K) \to \mathbb{C}$ by $N \in \mathbb{Z}$, with $K = PN$, and $P \in \mathbb{N}$.

$$\mathcal{I}_N[y] = \begin{cases} y(Pn) & \text{if} \quad n \in Z(N) \\ 0 & \text{otherwise.} \end{cases} \tag{3.3}$$

We often write signals with the specification of the definition domain, e.g. $\tau^a[x](Pn)$ instead of $\tau^a[x]$, as in Tab. 3.1. The properties of the operators that are exploited in this paper are listed below.

1. *Translation properties*:

$$\tau^a[x+y] = \tau^a[x] + \tau^a[y] \qquad \text{Additive property} \qquad (3.4)$$

$$\tau^a[xy] = \tau^a[x]\tau^a[y] \qquad \text{Multiplicative property} \qquad (3.5)$$

$$\tau^a[\tau^b[x]] = \tau^b[\tau^a[x]] = \tau^{a+b}[x] \qquad \text{Commutative property.} \qquad (3.6)$$

2. *Sampling properties*:

$$\mathcal{C}_M[x+y] = \mathcal{C}_M[x] + \mathcal{C}_M[y] \qquad \text{Additive property} \qquad (3.7)$$

$$\mathcal{C}_M[xy] = \mathcal{C}_M[x]\mathcal{C}_M[y] \qquad \text{Multiplicative property} \qquad (3.8)$$

$$\mathcal{C}_M[\mathcal{C}_N[x]] = \mathcal{C}_N[\mathcal{C}_M[x]] = \mathcal{C}_{MN}[x] \qquad \text{Commutative property} \qquad (3.9)$$

$$\mathcal{C}_N[\tau^{Na}[x]] = \tau^a[\mathcal{C}_N[x]] \qquad \text{Sampling-translation property} \qquad (3.10)$$

3. *Interpolation properties*:

$$\mathcal{I}_M[x+y] = \mathcal{I}_M[x] + \mathcal{I}_M[y] \qquad \text{Additive property} \qquad (3.11)$$

$$\mathcal{I}_M[xy] = \mathcal{I}_M[x]\mathcal{I}_M[y] \qquad \text{Multiplicative property} \qquad (3.12)$$

$$\mathcal{I}_M[\mathcal{I}_N[x]] = \mathcal{I}_N[\mathcal{I}_M[x]] = \mathcal{I}_{MN}[x] \qquad \text{Commutative property} \qquad (3.13)$$

$$\mathcal{I}_N[\tau^a[x]] = \tau^{Na}[\mathcal{I}_N[x]] \qquad \text{Interpolation-translation property} \qquad (3.14)$$

4. *Convolution Properties*:

$$\tau^a[x * y] = x * \tau^a[y] = \tau^a[x] * y \qquad \text{Convolution-translation property} \tag{3.15}$$

$$\mathcal{I}_N[x] * \mathcal{I}_N[h] = \mathcal{I}_N[x * h] \qquad \text{Noble identity 1} \tag{3.16}$$

$$\mathcal{C}_N\left[x * \mathcal{I}_N[h]\right] = \mathcal{C}_N[x] * h \qquad \text{Noble identity 2} \tag{3.17}$$

$$x \ * \ (h\, w^{(k)}) = \left((x\, w^{(-k)}) \ * \ h\right)\ w^{(k)} \qquad \text{Convolution-modulation property} \tag{3.18}$$

where in (18) $w^{(k)}(n) = W_M^{kn}$, and $W_M = e^{-j\frac{2\pi}{M}}$.

3.2.2 Polyphase decomposition

The *M-order polyphase decomposition* of a signal $x : Z(P) \to \mathbb{C}$ generates M low-rate signals $x_i : Z(MP) \to \mathbb{C}$ with $i \in \{0, 1, \cdots, M-1\}$ that are referred to as *polyphase components*. They are defined as

- *A-type polyphase components*:

$$x_i(MPn) = x(MPn + Pi) = \mathcal{C}_M\left[\tau^i[x]\right]. \tag{3.19}$$

- *B-type polyphase components*

$$x_{-i}(MPn) = x(MPn - Pi) = \mathcal{C}_M\left[\tau^{-i}[x]\right]. \tag{3.20}$$

We can recover the original signal x from the polyphase components as follows

- *Signal recontruction from the A-type type polyphase components*:

$$x(Pn) = \sum_{i=0}^{M-1} \mathcal{I}_M[x_i](Pn - Pi) \tag{3.21}$$

$$= \sum_{i=0}^{M-1} \tau^{-i} \left[\mathcal{I}_M[x_i]\right](Pn). \tag{3.22}$$

- *Signal recontruction from the B-type type polyphase components*:

$$x(Pn) = \sum_{i=0}^{M-1} \tau^{i} \left[\mathcal{I}_M[x_{-i}]\right](Pn). \tag{3.23}$$

It is worth noting that the A-type polyphase components in (3.19) can be obtained with a serial-to-parallel (S/P) conversion, while (3.22) corresponds to a parallel-to-serial (P/S) conversion.

OPERATOR NOTATION	
Convolution	$[\, x \ * \ h \,](n)$
Translation	$\tau^a[x](Pn) = x(P(n+a))$ $(x:Z(P)\to\mathbb{C})$
Sampling	$\mathcal{C}_N[x](NPn) = x(NPn)$ $(x:Z(P)\to\mathbb{C})$
Interpolation	$\mathcal{I}_N[y](Pn) = \begin{cases} y(Pn) & \text{if} \quad n \in Z(N) \\ 0 & \text{otherwise} \end{cases}$ $(y:Z(K)\to\mathbb{C} \text{ and } K=NP)$
SIGNALS AND CONSTANTS	
M	number of sub-channels
N	sampling - interpolation factor
M_1	$l.c.m.(M,N)$ (least common multiple)
M_0	M_1/N
N_0	M_1/M
L_f	prototype filter length
L_M	L_f/N
L_N	L_f/M
W_M	$e^{-j\frac{2\pi}{M}}$
$a^{(k)}(Nn)$	data input at the $k-th$ sub-channel
$b^{(k)}(Nn)$	output at the $k-th$ sub-channel
$g(n)$	synthesis bank prototype filter
$h(n)$	analysis bank prototype filter
$\tilde{a}^{(k)}(Nn)$	$a^{(k)}(Nn)\, W_M^{kNn}$
$\tilde{b}^{(k)}(Nn)$	$b^{(k)}(Nn)\, W_M^{-kNn}$
$g^{(k)}(n)$	$g(n)\, W_M^{-kn}$
$h^{(k)}(n)$	$h(n)\, W_M^{-kn}$
$div[A,B]$	$floor(A/B)$
$mod[A,B]$	$A - div[A,B]\, B$
$y_a = \sum_{b=0}^{N_0-1} x_{a+Mb}$ $a \in \{0,..,M-1\}$	$M-$ periodic repetition of x_i $i \in \{0,..,N_0M-1\}$
$x_a = y_{mod[a,M]}$ $a \in \{0,..,N_0M-1\}$	N_0- cyclic extension of y_i $i \in \{0,..,M-1\}$

Table 3.1: Operator notation and useful signals and constants.

3.3 Filter Bank Scheme with the Operators Notation

In this section we consider a FB scheme as depicted in Fig. 3.1 and we describe it exploiting the operator notation. We briefly recall what has been already presented in the Section 2.1. The discrete-time transmitted signal at the output of the synthesis FB, $x : Z(1) \to \mathbb{C}$, is obtained by the modulation of M data streams at low rate $a^{(k)} : Z(N) \to \mathbb{C}$, with $k \in \{0, 1, \cdots, M-1\}$, that belong to the QAM signal set. Using the operator notation, as summarized in Tab. 3.1, the transmitted signal can be written as

$$x(n) = \sum_{k=0}^{M-1} \sum_{l \in \mathbb{Z}} a^{(k)}(Nl) g^{(k)}(n - Nl) = \sum_{k=0}^{M-1} \left[\mathcal{I}_N[a^{(k)}] * g^{(k)} \right](n), \tag{3.24}$$

where M is the number of sub-channels of the transmitter, and N is the sampling-interpolation factor. According to (3.24), the signals $a^{(k)}(Nl)$ are upsampled by a factor N and are filtered by the modulated pulses $g^{(k)}(n) = g(n)W_M^{-kn}$, with $g(n)$ being the prototype filter of the synthesis bank and $W_M^{kn} = e^{-j\frac{2\pi}{M}kn}$. Then, the sub-channel signals are summed and sent over the transmission media.

After propagation through the transmission media, the received signal $y(n)$ is processed by the analysis FB whose outputs are

$$b^{(k)}(Nn) = \sum_{m \in \mathbb{Z}} y(m) h^{(k)}(Nn - m) = \mathcal{C}_N \left[y * h^{(k)} \right](Nn). \tag{3.25}$$

We refer to the direct implementation of (3.24),(3.25) as the inefficient realization since it requires a bank of high rate filters. Fortunately, the FB scheme can be efficiently realized via three DFT based architectures that we describe in the following.

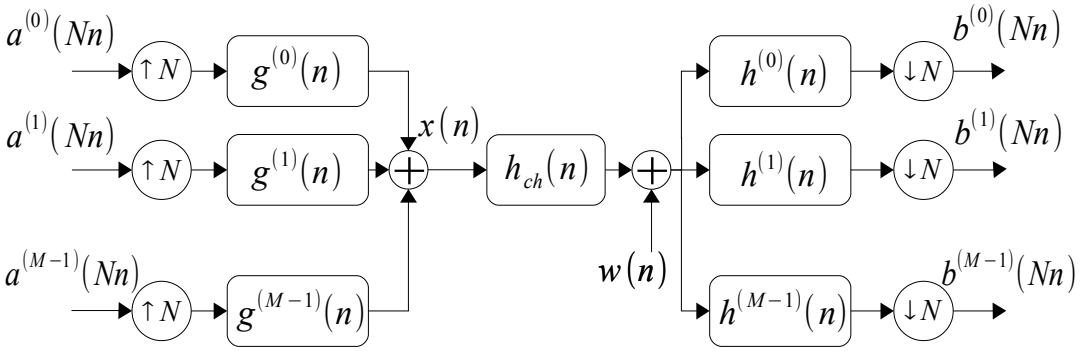

Figure 3.1: General modulated filter tranceiver.

3.4 Realization A: M_1-Order Polyphase Decomposition of the Signals

3.4.1 Synthesis bank in Method A

A first efficient realization of the synthesis bank [13] is derived if we perform a polyphase decomposition of order $M_1 = M_0N = N_0M = l.c.m.[M, N]$ of the signal x in (3.24). M_0 and N_0 are integers numbers. The $i-th$ polyphase component $x_i : Z(M_1) \to \mathbb{C}$ with $i \in \{0, \cdots, M_1 - 1\}$ can be written as

$$x_i(M_1 n) = \sum_{k=0}^{M-1} \sum_{l \in \mathbb{Z}} a^{(k)}(Nl) g(M_1 n + i - Nl) W_M^{-k(M_1 n + i - Nl)} \tag{3.26}$$

$$= \sum_{l \in \mathbb{Z}} \sum_{k=0}^{M-1} a^{(k)}(Nl) W_M^{kNl}\ g_i(M_1 n - Nl) W_M^{-ki}, \tag{3.27}$$

where $g_i : \mathbb{Z}(N) \to \mathbb{C}$ is the $i-th$ N-order polyphase decomposition of the pulse g. If we define

$$\tilde{a}^{(k)}(Nl) = a^{(k)}(Nl)\ W_M^{kNl} \tag{3.28}$$

$$\tilde{A}^{(i)}(Nl) = \sum_{k=0}^{M-1} \tilde{a}^{(k)}(Nl)\ W_M^{-ki}, \tag{3.29}$$

where $\tilde{a}^{(k)}(Nl)$ is the signal obtained by modulating the data symbols by W_M^{kNl}, and $\tilde{A}^{(i)} : \mathbb{Z}(N) \to \mathbb{C}$ for $i \in \{0, \cdots, M_1 - 1\}$, is the Inverse Discrete Fourier Transform (IDFT) of the signal $\tilde{a}^{(k)}$ for $k \in \{0, \cdots, M - 1\}$, we obtain

$$x_i(M_1 n) = \sum_{l \in \mathbb{Z}} \tilde{A}^{(i)}(Nl)\, g_i(M_0 N n - Nl) \tag{3.30}$$

$$= \mathcal{C}_{M_0} \left[\tilde{A}^{(i)} \, * \, g_i \right] (M_1 n). \tag{3.31}$$

Now, in order to better understand the structure of the polyphase filters we use the operator notation which helps us to greatly simplify the derivation. First, we redefine the index i as

$$i = \alpha + N\beta = p + Mm, \tag{3.32}$$

with

$$\begin{cases} \alpha & = mod[i, N] \\ \beta & = div[i, N] \\ p & = mod[i, M] \\ m & = div[i, M], \end{cases}$$

where we defined

$$div[A, B] = \lfloor A/B \rfloor$$
$$mod[A, B] = A - \lfloor A/B \rfloor \, B,$$

and the sets of α, β, p, and m are

$$\begin{cases} \alpha \in \{0, \ldots, N - 1\} \\ \beta \in \{0, \ldots, M_0 - 1\} \\ p \in \{0, \ldots, M - 1\} \\ m \in \{0, \ldots, N_0 - 1\}. \end{cases}$$

Then, we have that $\tilde{A}^{(i)} = \tilde{A}^{(p+mM)} = \tilde{A}^{(p)} = \tilde{A}^{(mod[i,M])}$ and

$$
\begin{aligned}
g_i &= g_{\alpha+N\beta} && (3.33)\\
&= \mathcal{C}_N \left[\tau^{\alpha+N\beta}[g]\right] && \text{(using (3.19))} \quad (3.34)\\
&= \tau^{\beta}\left[\mathcal{C}_N\left[\tau^{\alpha}\left[g\right]\right]\right] && \text{(using (3.5) and (3.10))} \quad (3.35)\\
&= \tau^{div[i,N]}\left[g_{mod[i,N]}\right] && \text{(using (3.19) and substituting } \alpha \text{ and } \beta). \quad (3.36)
\end{aligned}
$$

Finally, the $i-th$ polyphase component of the transmitted signal x can be written as

$$
x_i(M_1 n) = \mathcal{C}_{M_0}\left[\tilde{A}^{(mod[i,M])} * \tau^{div[i,N]}\left[g_{mod[i,N]}\right]\right](M_1 n), \tag{3.37}
$$

and the transmitted signal $x(n)$ is

$$
x(n) = \sum_{i=0}^{M-1} \tau^{-i}\left[\mathcal{I}_M[x_i]\right](n). \tag{3.38}
$$

Therefore, as shown in Fig. 3.2, the synthesis FB realization comprises the following operations. The blocks of data $\tilde{a}^{(k)}$ are processed by an M-point IDFT. Each output block is cyclically extended to the block $\tilde{A}^{(mod[i,M])}$ of size M_1. The signals $\tilde{A}^{(i)}$ are filtered, after a delay, with the N-order polyphase components of the prototype pulse. Finally, the filter outputs are sampled by a factor M_0 and parallel-to-serial converted.

3.4.2 Analysis bank in Method A

According to [13] the efficient realization of the analysis FB is obtained with a M_1-order polyphase decomposition of the signal $y(n)\, W_M^{kn}$ at the receiver. We can re-arrange the analysis bank equation (3.25) as

$$
\begin{aligned}
b^{(k)}(Nn) &= \sum_{i\in\mathbb{Z}} y(i)\, h(Nn-i) W_M^{-k(Nn-i)} && (3.39)\\
&= \left(\sum_{i\in\mathbb{Z}} y(i) W_M^{ki}\, h(Nn-i)\right) W_M^{-kNn}. && (3.40)
\end{aligned}
$$

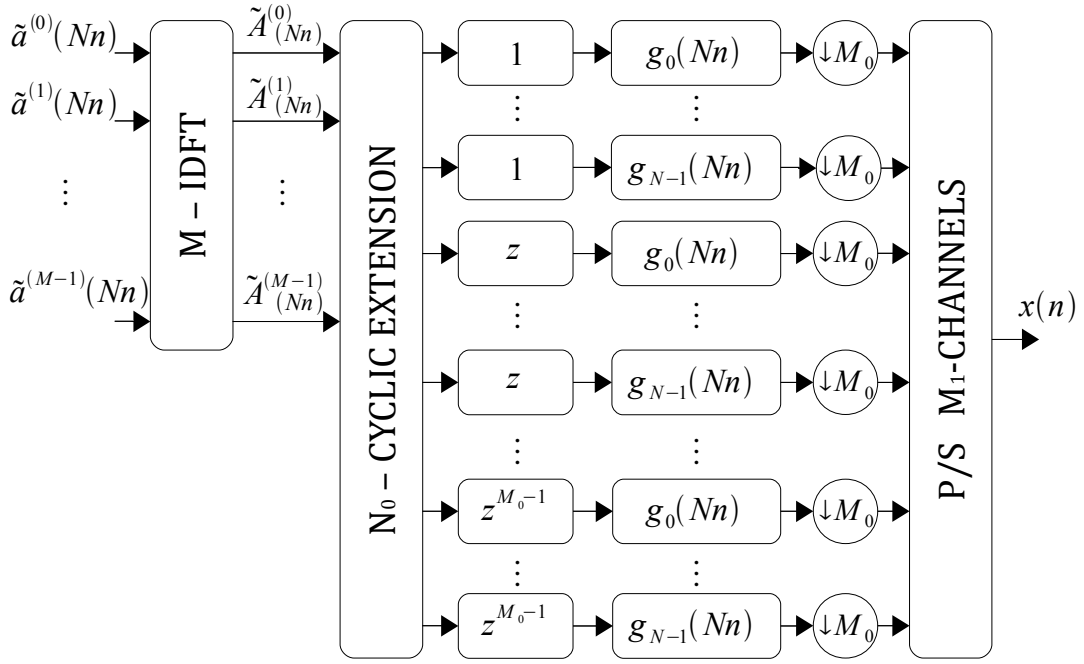

Figure 3.2: Syntesis bank (method A).

Now, if we define

$$\tilde{b}^{(k)}(Nn) = \sum_{i\in\mathbb{Z}} y(i) W_M^{ki}\, h(Nn-i), \tag{3.41}$$

and we perform a polyphase decomposition of order $M_1 = l.c.m.(M,N) = M_0 N = N_0 M$ on the signal $y(i)W_M^{ki}$, we obtain

$$\begin{aligned}
\tilde{b}^{(k)}(Nn) &= \sum_{l=0}^{M_1-1} \sum_{i\in\mathbb{Z}} y(M_1 i + l) W_M^{k(M_1 i+l)}\, h(Nn - M_1 i - l) && (3.42)\\
&= \sum_{l=0}^{M_1-1} \sum_{i\in\mathbb{Z}} y_l(M_1 i)\, h_{-l}(Nn - M_1 i)\, W_M^{kl} && (3.43)\\
&= \sum_{l=0}^{M_1-1} \left[\mathcal{I}_{M_0}[y_l] \;*\; h_{-l}\right](Nn)\, W_M^{kl}. && (3.44)
\end{aligned}$$

If we redefine

$$\begin{aligned} l &= p + Mm \\ &= \alpha + N\beta, \end{aligned} \tag{3.45}$$

with

$$\begin{cases} m \in \{0, \ldots, N_0 - 1\} \\ p \in \{0, \ldots, M - 1\} \\ \alpha \in \{0, \ldots, N - 1\} \\ \beta \in \{0, \ldots, M_0 - 1\}, \end{cases}$$

as in (3.32) and (3.33), we obtain

$$h_{-l} = h_{-\alpha - N\beta} \tag{3.46}$$

$$= \mathcal{C}_N \left[\tau^{-\alpha - N\beta}[h]\right] \qquad \text{(using (3.19))} \tag{3.47}$$

$$= \tau^{-\beta} \left[\mathcal{C}_N \left[\tau^{-\alpha}\,[h]\right]\right] \qquad \text{(using (3.5) and (3.10))} \tag{3.48}$$

$$= \tau^{-div[l,N]} \left[h_{-mod[l,N]}\right] \quad \text{(using (3.19) and substituting } \alpha \text{ and } \beta\text{).} \tag{3.49}$$

Substituting (3.49) in (3.44) we obtain the final expression as follows

$$\begin{aligned} \tilde{b}^{(k)}(Nn) = \sum_{p=0}^{M-1} W_M^{kp} \Bigg(\sum_{m=0}^{N_0-1} [\mathcal{I}_{M_0}[y_{p+Mm}] \\ * \ \tau^{-div[p+Mm,N]}[h_{-mod[p+Mm,N]}]\big]\,(Nn)\Big)\,. \end{aligned} \tag{3.50}$$

Therefore, as shown in Fig. 3.3, the analysis FB realization comprises the following operations. The received signal is serial-to-parallel converted with a converter of size M_1. The output signals are upsampled by a factor M_0, filtered with the N-order polyphase components of the prototype pulse. Then, after a delay, we compute the periodic repetition with period M of the block of coefficients of size M_1. Finally, the M-point DFT is performed.

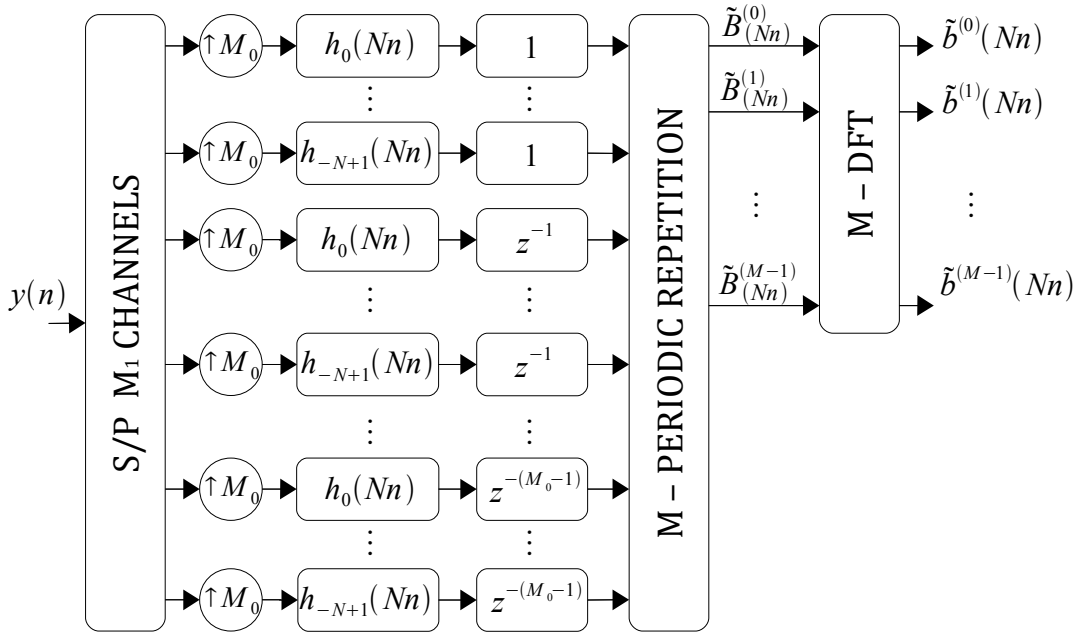

Figure 3.3: Analysis bank (method A).

3.5 Realization B: M_1-order Polyphase Decomposition of the Pulses

3.5.1 Synthesis bank in Method B

In a second method [14], [15] the efficient realization of the synthesis FB is obtained by performing an M_1-order polyphase decomposition of the filter $g^{(k)}$, with $M_1 = l.c.m(M, N)$. In the Appendix A a detailed derivation in the time-domain is reported and it shows that the polyphase components $x_\alpha : \mathbb{Z}(N) \to \mathbb{C}$, with $\alpha \in \{0, 1, \cdots, N-1\}$, of the transmitted signal x can be written as (see the Appendix A)

$$x_\alpha(Nn) = \sum_{\beta=0}^{M_0-1} \left[A^{(mod[\alpha+N\beta, M])} \ * \tau^{-\beta} \left[\mathcal{I}_{M_0}[g_{\alpha+N\beta}] \right] \right] (Nn). \tag{3.51}$$

In (3.51), $A^{(l)} : Z(N) \to \mathbb{C}$, with $l \in \{0, 1, \cdots, M-1\}$, is the M-point IDFT

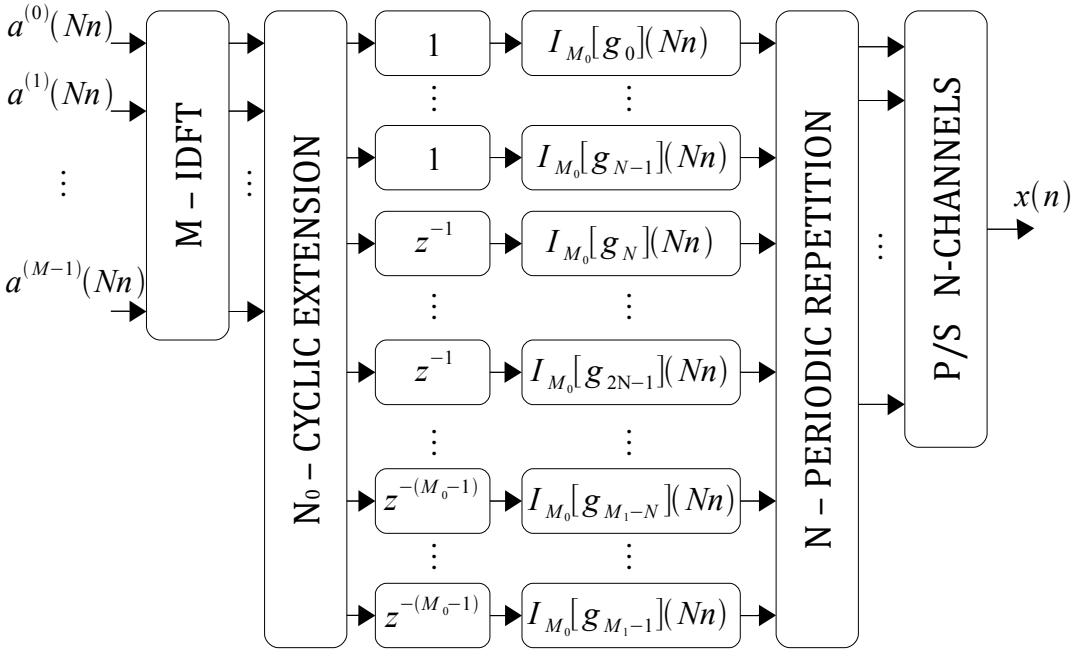

Figure 3.4: Synthesis bank (method B).

of $a^{(k)}$, $k \in \{0, \cdots, M-1\}$, i.e.,

$$A^{(l)}(Nn) = \sum_{k=0}^{M-1} a^{(k)}(Nn) W_M^{-kl}, \tag{3.52}$$

and $g_i : \mathbb{Z}(M_1) \to \mathbb{C}$, are the M_1-order polyphase components of the prototype filter g that are defined as

$$g_i(M_1 n) = \mathcal{C}_{M_1}\left[\tau^i[g]\right](M_1 n) \qquad i \in \{0, 1, \cdots, M_1 - 1\}. \tag{3.53}$$

Therefore, as shown in Fig. 3.4, the sythesis FB realization comprises the following operations. The blocks $a^{(k)}$ of data are processed with an M-IDFT. The output block is cyclically extended to a block of size M_1. The sub-channel signals are filtered, after a delay, with the M_1-order polyphase components of the prototype pulse interpolated by M_0. The output blocks of size M_1 are periodically repeated with period N and parallel-to-serial converted by a converter of size N.

3.5.2 Analysis bank in Method B

In this second method [14], [15], the efficient realization of the analysis FB is obtained by exploiting the M_1-order polyphase decomposition of the pulses $h^{(k)}$ with $k \in \{0, 1, \cdots, M-1\}$. The FB outputs can be written as (see the Appendix A)

$$b^{(k)}(Nn) = \sum_{p=0}^{M-1} \left(W_M^{kp} \sum_{m=0}^{N_0-1} \left[\tau^{div[p+Mm,N]} \left[y_{mod[p+Mm,N]} \right. \right. \right. \\ \left. \left. \left. * \ \mathcal{I}_{M_0}[\, h_{-p-Mm}]] \,] \,(Nn) \,) \right. \right., \tag{3.54}$$

where $y_i : \mathbb{Z}(N) \to \mathbb{C}$, are the N-order polyphase components of the received signal y that are defined as

$$y_i(Nn) = \mathcal{C}_N \left[\, \tau^i[y] \right] (Nn) \qquad\qquad i \in \{0, 1, \cdots, N-1\}. \tag{3.55}$$

The M_1-order polyphase components of the prototype filter h are defined as

$$h_{-l}(M_1 n) = \mathcal{C}_{M_1} \left[\, \tau^{-l}[h] \right] (M_1 n) \qquad\qquad l \in \{0, 1, \cdots, M_1 - 1\}. \tag{3.56}$$

Therefore, as shown in Fig. 3.5, this realization comprises the following operations. The received signal is serial-to-parallel converted by a size N converter. The outputs of the S/P converter are cyclically extended M_0 times. Then, the signals are filtered with the M_1-order polyphase components of the prototype pulse after appropriate delays. Finally, a periodic repetition with period M on the output blocks is computed, and an M-DFT is performed.

3.6 Realization C: L_f-order Polyphase Decomposition of the Pulses

3.6.1 Synthesis bank in Method C

The third method of realizing the synthesis FB is described in [17]. It starts from the assumption that the prototype pulse g has length $L_f = L_M N = L_N M$,

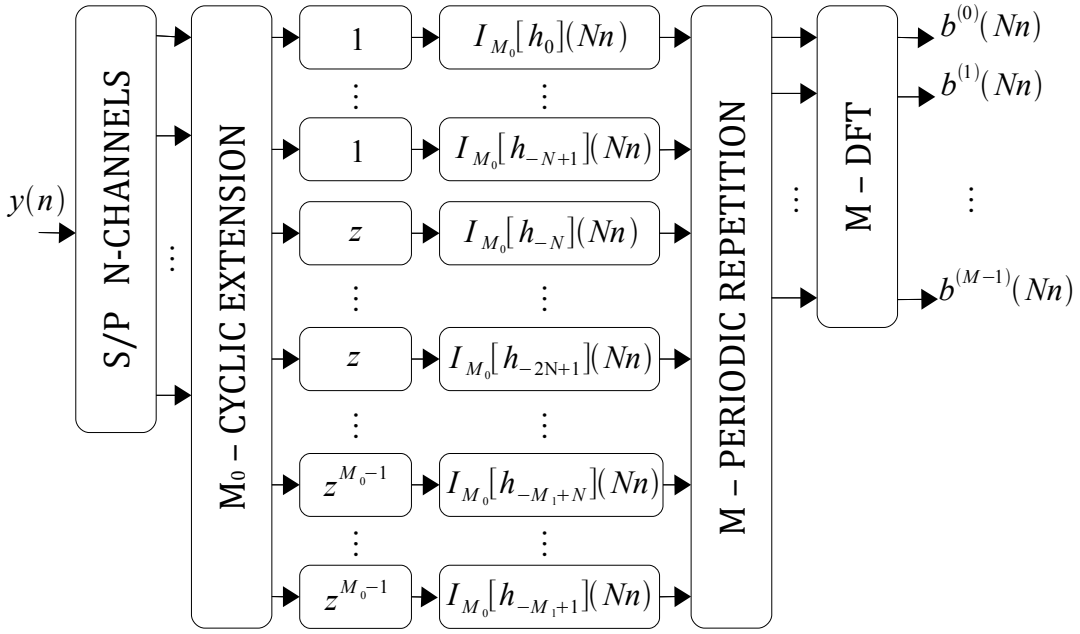

Figure 3.5: Analysis bank (method B).

i.e., without loss of generality, a multiple of both M and N. Then, if we exploit the L_f-order polyphase decomposition of the filters $g^{(k)}$, each having a single coefficient, the α-th N-order polyphase component of the signal x can be written as

$$x_\alpha(Nn) = \sum_{\beta=0}^{L_M-1} \tau^{-\beta} \left[A^{(mod[\alpha+N\beta,M])} \times g(\alpha+N\beta)\right](Nn). \tag{3.57}$$

In (3.57), $A^{(l)} : Z(N) \to \mathbb{C}$, with $l \in \{0,1,\cdots,M-1\}$, is the M-point IDFT of $a^{(k)}$, $k \in \{0,\cdots,M-1\}$, (see (51)) and $g(i)$ are the prototype pulse coefficients that correspond to the L_f-order polyphase components. The proof is given in Appendix B

Therefore, as shown in Fig. 3.6, the realization comprises the following operations. The data signals $a^{(k)}$ are processed with an M-IDFT. The output blocks are cyclically extended, to form a block of size $L_N M$. Then, the outputs after a proper delay are multiplied by the polyphase coefficients of the prototype filter. Each output block is periodically repeated with period N, and parallel-to-serial

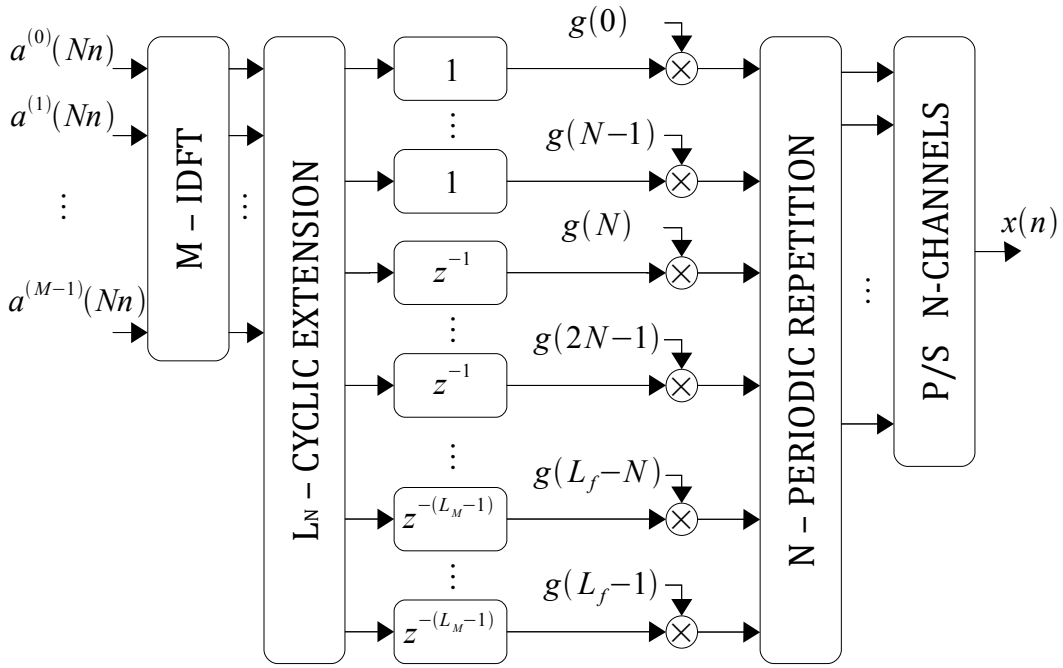

Figure 3.6: Synthesis bank (method C).

converted with a converter of size N.

3.6.2 Analysis bank in Method C

We assume, according to [17], without loss of generality the pulse $h(n)$ to be anticausal and defined for $n \in \{-L_f + 1, \cdots, 0\}$. The efficient realization of the analysis FB is obtained exploiting the L_f-order polyphase decomposition of the filter $h^{(k)}$ with $k \in \{0, 1, \cdots, M-1\}$. In the Appendix B we show that the FB outputs are obtained as follows

$$b^{(k)}(Nn) = \sum_{p=0}^{M-1} W_M^{kp} \left(\sum_{m=0}^{L_N-1} \tau^{div[p+Mm,N]} \left[y_{mod[p+Mm,N]} \right.\right. \\ \left.\left. \times h(-p-Mm)\right](Nn) \right), \tag{3.58}$$

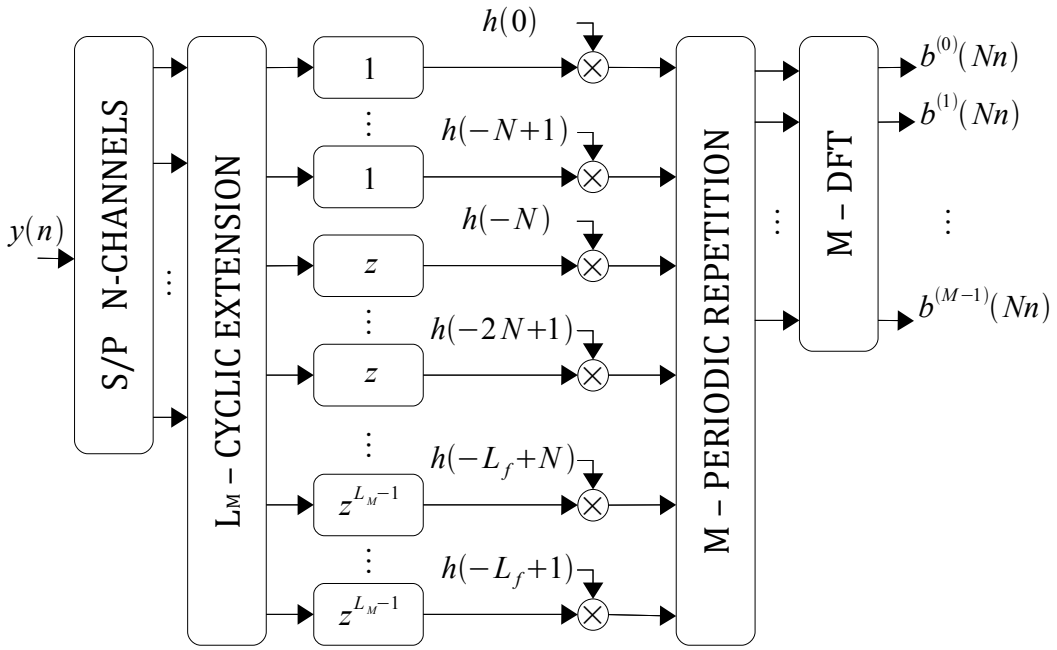

Figure 3.7: Analysis bank (method C).

where $y_i : \mathbb{Z}(N) \to \mathbb{C}$, are the N-order polyphase components of the received signal y that are defined as

$$y_i(Nn) = \mathcal{C}_N \left[\tau^i[y] \right] (Nn) \qquad i \in \{0, 1, \cdots, N-1\}, \tag{3.59}$$

and $h(i)$ are the prototype pulse coefficients that correspond to the L_f-order polyphase components.

Therefore, as shown in Fig. 3.7, the received signal is serial-to-parallel converted with a converter of size N. The outputs of the S/P converter are cyclically extended M_0 times. Then, the signals are delayed and multiplied with the coefficients of the prototype filter. The resulting block is periodically repeated with period M, and finally, an M-DFT is applied.

3.7 Comparison among FMT realizations

All three realizations deploy an M-point DFT, and essentially differ in the MIMO polyphase FB network which has size $M_1 \times M_1$ in the first and second realization, while it has size $L_f \times L_f$ in the third realization. Furthermore, the polyphase components of the pulses for method A, B, and C have different length that is respectively equal to L_f/N, L_f/M_1 and 1. When $L_f = M_1$ the implementations B and C are identical.

The complexity of the three structures in terms of number of complex operations (additions and multiplications) per unit sampling time is identical and it has order equal to $(\alpha M \log_2 M + 2\, L_f)\, /N$ for both the synthesis and the analysis bank which can be proved following the detailed calculation for realization A in [21]. The factor α depends on the FFT algorithm [24]. As an example, assuming $M = 64$, $N = 80$, $\alpha = 1.2$ and a pulse with length $L_f/N = \{1, 2, 3\}$ the complexity for realization A, B, and C respectively equals $\{7.8,\ 9.8,\ 11.8\}$ oper./samp. for both the transmitter the receiver.

The three schemes require the same memory usage that we define in terms of memory units per output sample (MUPS), where a memory unit is the space required to store one coefficient. Without taking into account the memory requirements of the DFT stages (identical for all three realizations), the synthesis and the analysis polyphase FB respectively require $(ML_M + N)/N$ and $(L_f + M)/M$ MUPS. As an example, assuming again $M = 64$, $N = 80$, and a pulse with length $L_f/N = \{1, 2, 3\}$ the MUPS for realization A, B, and C respectively equal $\{1.8,\ 2.6,\ 3.4\}$ for the synthesis bank, and $\{2.3,\ 3.5,\ 4.8\}$ for the analysis bank. It should however to be noted that as discussed in [25], depending on the DSP architecture and the specific processing procedures, the memory requirements may slightly change.

Another difference is that when we derive the perfect reconstruction (orthogonality) conditions in matrix form from the efficient realization, we obtain a different factorization of the system matrix that can be exploited in the design and search of optimal orthogonal pulses. This is discussed in the next chapter.

3.8 Conclusions

In this chapter we have compared three efficient realizations of FB modulation. We have introduced a notation based on operators that enables one to derive the efficient FB architectures by exploiting a unique framework in the time domain. We have shown that these implementations have the same complexity in terms of complex operations, and similar memory requirements, but they are different in terms of hardware implementation and matrix representation due to a different polyphase FB structure.

Chapter 4

Orthogonal Prototype Pulse Design

4.1 Introduction

When FB systems are employed in communications, the transmission over a time-frequency selective channel may introduce inter-channel interference (ICI) and inter-symbol interference (ISI) that can be minimized with the design of time-frequency confined pulses. Then, if the ICI is negligible, we can cope with the residual interference either via simplified sub-channel equalization [11], or optimal and iterative multi-channel equalization [26], [27]. The design of well localized pulses in modulated FB systems has been treated by several authors [28]- [32].

In this chapter we aim at designing a prototype pulse which satisfies the orthogonal property for modulated FB. The orthogonality is attained if the FB is designed to be with perfect reconstruction (PR), and if the analysis bank pulses are matched with those of the syntheses bank. In general a FB is with PR if the sub-channel signals received at the analysis bank are free of interference when transmitting in condition where the propagating media is considered to be ideal (time invariant channel without multi-path fading).

The design of the orthogonal prototype pulse is somehow easy for the case of $M = N$, i.e., the number of sub-channels equals the interpolation factor. In this condition the FB is referred to as critically sampled. It results that the orthogonality property is satisfied if the prototype pulse has length equal

to $L_g = M$, thus the prototype pulse length must equal the number of sub-channels. A popular choice is to deploy a rectangular shape pulse obtaining the classic OFDM scheme.

In our work we want to extend the search of orthogonal pulses when the FB is redundant, i.e., $N > M$, since this condition assures the system to be more robust to the interference.

In literature some methods for the design of quasi-orthogonal modulated FB has been proposed [22],[23]. Recently, simple pulse design criteria for non-orthogonal FMT have been reported in [33]. In [19] the performance limits of FMT modulation has been studied, and a design guidelines have been given such that frequency and time diversity gains are attainable with optimal multi-channel equalization. However, if complexity is an issue, linear single channel equalizers are desirable. Their performance in doubly dispersive fading channels has been studied in [20] assuming a rectangular, a sinc, a root-raised-cosine (rrc), and a Gaussian pulse.

The FB design described in [28]-[33] is not orthogonal, i.e., the FB does not grant perfect reconstruction even in the presence of an ideal channel. This condition eases the pulse design problem. The goal of achieving orthogonality is desirable but it makes the FB design more challenging. The construction of orthogonal DFT FB has been discussed in [14], [15]. Examples of pulses with practical relevance have been reported in [15] where however it is recognized that the design becomes significantly complex as the number of sub-channels increases. Therefore, it has been proposed to perform polynomial fitting of the parameters to decrease the number of variables which however yields a quasi-orthogonal FB. In this chapter, we bring new insights to this problem. We show that the polyphase decomposition of the signals used in the realization [13] allows one to derive the orthogonal FB equations and writing them in a number of uncoupled subsets. Each subset needs a small number of parameters, which simplifies the search of optimal pulses. The search of optimal pulses is carried out with the objective of maximizing the in-band to total pulse energy, or minimizing the mean square error between the pulse and a target frequency response. A numerical method is presented to obtain well frequency confined sub-channel pulses for an arbitrary large number of sub-channels. Some examples of

pulses with minimal length are then reported.

Finally, the performance in terms of average signal-to-interference power ratio of the orthogonal FMT system in typical multi-path fading channels is reported and compared to that obtained with a conventional truncated root-raised-cosine pulse. Then, we report a comparison in terms of achievable rate between FMT and cyclically prefixed OFDM using the IEEE 802.11 WLAN channel model in [18]. It is found that even deploying minimal length pulses and with single tap equalization, in the considered scenario, the achievable rate of FMT is higher than that of OFDM.

4.2 Perfect reconstruction and orthogonality

To derive the perfect reconstruction conditions for the FB, we can exploit the realization A of Fig. 3.2 and 3.3. Perfect reconstruction is achieved if the M-IDFT output coefficients at the transmitter $\tilde{A}^{(k)}$ are identical (despite a delay) to the input block $\tilde{B}^{(k)}$ of coefficients to the M-DFT at the receiver. The signal of the a-th sub-channel at the input of the DFT receiver is given by

$$\tilde{B}^{(a)}(Nn) = \sum_{b=0}^{N_0-1} \left[\mathcal{I}_{M_0}[x_{a+Mb}] * h_{-a-Mb}\right](Nn). \tag{4.1}$$

The analysis sub-channel pulse has been obtained by the the N-order polyphase decomposition of the prototype filter h, i.e., $h_l = \mathcal{C}_N[\tau^{-l}[h]]$ with $l \in \{0, 1, \cdots, M_1 - 1\}$. We now perform a further M_0-order polyphase decomposition of the sub-channel pulse and we obtain that it equals the M_1-order polyphase component of h. This is shown in what follows

$$\begin{aligned}
&\mathcal{C}_{M_0}[\tau^{\beta}[h_{-a-Mb}]] = \mathcal{C}_{M_0}[\tau^{\beta}[\mathcal{C}_N[\tau^{-a-Mb}[h]]] = \\
&= \mathcal{C}_{M_0}[\mathcal{C}_N[\tau^{N\beta}[\tau^{-a-Mb}[h]]]] = \mathcal{C}_{M_1}[\tau^{N\beta-a-Mb}[h]] = \\
&= h'_{N\beta-a-Mb} \ .
\end{aligned}$$

Now, (4.1) can be rewritten as

$$\begin{aligned}\tilde{B}^{(a)}(Nn) &= \sum_{b=0}^{N_0-1}\left[\mathcal{I}_{M_0}[x_{a+Mb}] * \sum_{\beta=0}^{M_0-1}\tau^{-\beta}[\mathcal{I}_{M_0}[h'_{N\beta-a-Mb}]]\right](Nn)\\ &= \sum_{\beta=0}^{M_0-1}\tau^{-\beta}[\mathcal{I}_{M_0}[\sum_{b=0}^{N_0-1} x_{a+Mb} * h'_{N\beta-a-Mb}](Nn)\\ &= \sum_{\beta=0}^{M_0-1}\tau^{-\beta}[\mathcal{I}_{M_0}[\tilde{B}^{(a)}_{\beta}]](Nn),\end{aligned}$$

where we have defined

$$\begin{aligned}\tilde{B}^{(a)}_{\beta}(M_1n) &= \sum_{b=0}^{N_0-1}\left[x_{a+Mb} * h'_{N\beta-a-Mb}\right](M_1n)\\ &= \sum_{b=0}^{N_0-1}\left[\mathcal{C}_{M_0}[\tilde{A}^{(a+Mb)} * g_{a+Mb}] * h'_{N\beta-a-Mb}\right](M_1n)\ .\end{aligned} \tag{4.2}$$

Similarly to what has been done for the pulses h_l, we can perform an M_0-order polyphase decomposition of the pulses g_l, and obtain that it equals the M_1-order polyphase decomposition of the prototype pulse g, i.e.,

$$\mathcal{C}_{M_0}[\tau^{-\alpha}[g_{a+Mb}]] = \mathcal{C}_{M_1}[\tau^{a+Mb-N\alpha}[g]] = g'_{a+Mb-N\alpha}\ .$$

It follows that (4.2) can be written as

$$\begin{aligned}&\tilde{B}^{(a)}_{\beta}(M_1n) =\\ &= \sum_{b=0}^{N_0-1}\left[\mathcal{C}_{M_0}[\tilde{A}^{(a)} * \sum_{\alpha=0}^{M_0-1}\tau^{\alpha}[\mathcal{I}_{M_0}[g'_{a+Mb-N\alpha}]]] * h'_{N\beta-a-Mb}\right](M_1n)\\ &= \sum_{\alpha=0}^{M_0-1}\left[\mathcal{C}_{M_0}[\tau^{\alpha}[\tilde{A}^{(a)}]] * \sum_{b=0}^{N_0-1} g'_{a+Mb-N\alpha} * h'_{N\beta-a-Mb}\right](M_1n)\ .\end{aligned}$$

Finally, if we define with $\tilde{A}^{(a)}_{\alpha} = \mathcal{C}_{M_0}[\tau^{\alpha}[\tilde{A}^{(a)}]]$ the M_0-order polyphase com-

ponent of $\tilde{A}^{(a)}$, we can write

$$\tilde{B}^{(a)}_{\beta}(M_1 n) = \sum_{\alpha=0}^{M_0-1} \left[\tilde{A}^{(a)}_{\alpha} * \sum_{b=0}^{N_0-1} g'_{a+Mb-N\alpha} * h'_{N\beta-a-Mb} \right] (M_1 n),$$

where the signal $\tilde{A}^{(a)}_{\alpha} : Z(M_1) \to \mathbb{C}$ and $\tilde{B}^{(a)}_{\beta} : Z(M_1) \to \mathbb{C}$ with $\alpha, \beta \in \{0, 1, \cdots, M_0 - 1\}$ are the M_0 order polyphase components of $\tilde{A}^{(a)}$ and $\tilde{B}^{(a)}$:

$$\tilde{A}^{(a)}_{\alpha}(M_1 n) = \mathcal{C}_{M_0} \left[\tau^{\alpha}\, \tilde{A}^{(a)} \right] (M_1 n) \qquad \alpha \in \{0, 1, \cdots, M_0 - 1\} \tag{4.3}$$

$$\tilde{B}^{(a)}_{\beta}(M_1 n) = \mathcal{C}_{M_0} \left[\tau^{\beta}\, \tilde{B}^{(a)} \right] (M_1 n) \qquad \beta \in \{0, 1, \cdots, M_0 - 1\}, \tag{4.4}$$

The pulses $g'_i : \mathbb{Z}(M_1) \to \mathbb{C}$, $h'_i : \mathbb{Z}(M_1) \to \mathbb{C}$ with $i \in \{0, 1, \cdots, M_1 - 1\}$ are the i-th component of the M_0 order polyphase components of g_i and h_i. They are equal to the M_1-order polyphase components of the prototype pulse g and h, i.e.,

$$g'_i(M_1 n) = \mathcal{C}_{M_1} \left[\tau^i [\, g] \right] (M_1 n) \qquad i \in \{0, 1, \cdots, M_1 - 1\} \tag{4.5}$$

$$h'_i(M_1 n) = \mathcal{C}_{M_1} \left[\tau^i [\, h] \right] (M_1 n) \ . \tag{4.6}$$

Therefore, from (4.3) the *perfect reconstruction* condition becomes

$$\sum_{b=0}^{N_0-1} \left[g'_{Mb+a-N\alpha} * h'_{N\beta-a-Mb} \right] (M_1 n) = \delta(M_1 n)\, \delta(\alpha - \beta), \tag{4.7}$$

with $\delta(k)$ being the Kronecker delta. Applying the Z-transform to (4.7) the relation becomes

$$\sum_{b=0}^{N_0-1} G'_{Mb+a-N\alpha}(z)\, H'_{N\beta-a-Mb}(z) = \delta(\alpha - \beta) \ . \tag{4.8}$$

Thus, if we define the following $M_0 \times N_0$ matrix:

$$\mathbf{G}_a(z) = \begin{bmatrix} G'_a(z) & \cdots & G'_{(N_0-1)M+a}(z) \\ G'_{a-N}(z) & \cdots & G'_{(N_0-1)M+a-N}(z) \\ \vdots & \vdots & \vdots \\ G'_{a-(M_0-1)N}(z) & \cdots & G'_{(N_0-1)M+a-(M_0-1)N}(z) \end{bmatrix}^T , \tag{4.9}$$

and we assume a matched analysis FB, i.e., $\mathbf{H}_{-a}(z) = \mathbf{G}_a^{T*}(1/z^*)$ the perfect reconstruction conditions become the orthogonality conditions so that they can be written in matrix form as

$$\mathbf{H}_{-a}(z)\,\mathbf{G}_a(z) = \mathbf{I}_{M_0} \qquad a \in \{0, 1, \cdots, M-1\} \ . \tag{4.10}$$

It is interesting to note that the FB is orthogonal when every sub-matrix (4.10) is orthogonal. Further, when M and N are not prime among them, i.e., $l.c.m.(M, N) \neq 1$, each sub-matrix contains pulse coefficients that are distinct from those in another sub-matrix. Consequently, the orthogonality conditions are imposed on distinct sub-sets of pulse coefficients.

We note that for $N = M$ the sub-matrices are squared therefore the only possible solution is to choose the prototype filter with length M (submatrices are polynomial so their inverse is polynomial if and only if each sub-matrix component is a monomial). It follows that, a plausible solution is the rectangular pulse, which yields the OFDM scheme. If $N > M$, the sub-matrices become rectangular enhancing the degrees of freedom in the choice of the shape and the length of the prototype filter.

4.3 Orthogonal FMT system design

Orthogonal matrices can be constructed via the parametrization of the pulse coefficients with angles as proposed in [15], i.e., expressing the pulse coefficients with trigonometric functions of the angles. For every choice of the angles the FB is orthogonal. Then, the search of optimal pulses can be done defining an objective function (metric). In this paper we consider either the maximization

of the in-band energy to the total pulse energy, or the minimization of the mean squared error between the pulse spectrum and a target frequency response. The metrics are the following

1. METRIC 1: Maximum in-band to total energy

$$\arg\max_{\boldsymbol{\theta}} \frac{\int_{-1/2M}^{1/2M} |G(f,\boldsymbol{\theta})|^2 \; df}{\int_{-\infty}^{\infty} |G(f,\boldsymbol{\theta})|^2 \; df}, \tag{4.11}$$

   where $G(f,\boldsymbol{\theta})$ is the frequency response of the pulse obtained for a certain choice of the angles stored in the vector $\boldsymbol{\theta}$.

2. METRIC 2: Least squares

$$\arg\min_{\boldsymbol{\theta}} \int_{-\infty}^{\infty} |G(f,\boldsymbol{\theta}) - H(f)|^2 \, df, \tag{4.12}$$

   where $H(f)$ is the target frequency response.

Since the efficient realization requires an M-point DFT, we can impose $M = 2^n$ with n integer in order to allow for an efficient fast Fourier transform based implementation. Now, we can choose $N_0 = M_0 + 1$ such that we minimize the amount of redundancy, i.e., minimize the ratio $N/M = N_0/M_0$. It results that

$$\begin{aligned} N &= 2^n \frac{N_0}{M_0} \\ &= 2^n + \frac{2^n}{M_0}. \end{aligned} \tag{4.13}$$

Since N must be integer, from (4.13) we derive that M_0 must also be an integer power of two, and $M_0 \leq 2^n$. Furthermore, we can choose M and N not to be relatively prime which simplifies the orthogonal FB design. If it is further desired to have non-polynomial sub-matrices, we can choose the pulse length $L_f = M_1 = M_0 N$.

For example, if we assume $M = 1024$ sub-channels, and we choose $M_0 = 2$ and $N_0 = 3$ (which implies $N = 1536$), and a pulse with length $L_f = M_0 N = 3072$, the orthogonality relations yield 512 sub-matrices with 2 variables each.

In turn, this implies that we need to independently solve 512 subsystems with only 2 variables each.

4.3.1 Simplified optimization for large number of sub-channels

The FB design procedure is based on the parametrization of the pulse coefficients with angles such that we fulfill the orthogonality conditions, and we deal with a minimal set of free variables [34]. Then, the next step is to find the set of angles such that a certain metric is satisfied (in our case we use (4.11) or (4.12)). The problem becomes complex as the number of sub-channels M increases since the number of variables becomes large. For instance,with $M = 1024$, $M_0 = 2$, $N_0 = 3$ and $L_f = 2N$, the amount of angles is 1024. Consequently, it becomes difficult to obtain an acceptable solution with standard methods of optimization, e.g., the conjugate gradient method.

To simplify the problem, in [15] it has been proposed to reduce the number of angles by polynomial fitting of them. However, this procedure does not allow obtaining a perfectly orthogonal FB solution. We instead propose an alternative method that significantly simplifies the orthogonal FB design for arbitrarily large M and it maintains the perfect orthogonality. The procedure is iterative and comprises two steps. In the first step, we design the pulse for a value of M that allows to use conventional optimization methods, i.e., for a number of sub-channels that yields a manageable number of variables. In a second iterative step, we increase the number of sub-channels by a factor of two and obtain the pulses via interpolation and adjustment of the coefficients such that orthogonality is granted. The procedure is detailed in the following.

First step. We minimize for instance the metric (4.12) for the case $M = M_0$. This step can be easily performed since the number of variables is small, e.g., for $M = M_0$ and $L_f = N$ the subsystem has only one variable, and the optimal solution is determined. We denote the prototype pulse obtained at this step with $\hat{g}_{M_0}$ where the subscript denotes that the filter is designed for the system with M_0 channels.

Second step. We interpolate $\hat{g}_{M_0}$ by a factor 2 with a low pass filter and

we obtain the filter $\hat{h}_{2M_0} = \mathcal{I}_2[\hat{g}_{M_0}]$ which has the same spectrum of $\hat{g}_{M_0}$. The preliminary pulse $\hat{h}_{2M_0}$ has the length required for the FB with $M = 2M_0$ and $L_f = N$, i.e., for the system with double the number of sub-channels of the one at the previous step. We note that the even coefficients of $\hat{h}_{2M_0}$ are the coefficients of $\hat{g}_{M_0}(n)$ and the odd are those derived from interpolation. The filter $\hat{h}_{2M_0}$ is not orthogonal for the system $M = 2M_0$ but starting from it we can obtain an orthogonal filter with similar frequency response. The FB of size $2M_0$ has a system matrix of size that is double that of the FB of size M_0. The system matrix is block diagonal, and the even coefficients of the pulse $\hat{h}_{2M_0}$ already grant half of the matrix sub-blocks to be orthogonal. The odd coefficients do not grant the remaining sub-blocks to be orthogonal. To achieve orthogonality we keep some of the odd coefficients identical to those obtained via interpolation while we adjust the remaining odd coefficients by solving the set of orthogonality conditions associated to the sub-block. We denote this new filter as $\hat{g}_{2M_0}(n)$. Its spectrum is very close to that of the filter $\hat{h}_{2M_0}$. Furthermore, the FB with this new filter is orthogonal.

The procedure at step 2 can be iteratively repeated starting from $\hat{g}_{2M_0}(n)$ such that we can easily design FBs with prototype pulses $\hat{g}_{2^k M_0}(n)$ for every $k \in \mathbb{N}$, i.e., arbitrarily large number of sub-channels.

4.3.2 Design of minimum length FMT prototype pulses

The design of minimal length pulses is very important because it allows minimizing the FMT system realization complexity. In this section we discuss the design of pulses of length $L_f = N$ and $L_f = 2N$ and we report a detailed description of their construction. We use the least square metric with a root-raised cosine target frequency response. The optimization procedure is the one described in the previous section.

In the following, to simplify the notation, we define the prototype pulse coefficients as

$$g(n) = h^*(-n) = p_n \quad . \tag{4.14}$$

Example of prototype pulse design ($M_0 = 2$, $N_0 = 3$, and $L_f = \{N, 2N\}$). Let

us assume a transmission system with M being a power of 2, $M_0 = 2$, $N_0 = 3$, and $L_f = 2N$. Hence, $N = 3M/2$. The sub-matrices in (4.10) have the following structure

$$\mathbf{G}_a(z) = \begin{bmatrix} p_a & p_{M+a} & p_{2M+a} \\ z^{-1}\, p_{M_1+(a-N)} & z^{-1}\, p_{M_1+(M+a-N)} & p_{2M+a-N} \end{bmatrix}^T , \tag{4.15}$$

where according to (4.14) p_n are the coefficients of the prototype pulse and $a \in \{0, 1, \cdots, M/M_0 - 1\}$. If a filter coefficient is present in the submatrix $\mathbf{G}_i$, it cannot be present in any other sub-matrix $\mathbf{G}_j$ with $j \neq i$. This implies that the subsystems are uncoupled.

From (4.15) we can derive the orthogonal conditions also for $L_f = N$ simply setting certain elements to zero, as detailed in the following.

Case $L_f = N$. For the case $L_f = N$ the orthogonality conditions for the a-th subsystem are given by the following equations

$$\begin{cases} p_a^2 + p_{M+a}^2 = 1 \\ p_{2M+a-N}^2 = 1 \end{cases} , \tag{4.16}$$

with $a \in \{0, 1, \cdots, M/M_0 - 1\}$. In order to solve the system using a minimal set of variables, we can parameterize the pulse coefficients with angles as follows

$$\begin{cases} p_a = cos(\theta_{a,1}) \\ p_{M+a} = sin(\theta_{a,1}) \\ p_{2M+a-N} = 1 \end{cases} . \tag{4.17}$$

Case $L_f = 2N$. Now, the orthogonality conditions for the a-th subsystem are given by the following equations

$$\begin{cases} p_a^2 + p_{M+a}^2 + p_{2M+a}^2 = 1 \\ p_{M_1+(a-N)}^2 + p_{M_1+(M+a-N)}^2 + p_{2M+a-N}^2 = 1 \\ p_a\, p_{M_1+(a-N)} + p_{M+a}\, p_{M_1+(M+a-N)} = 0 \\ p_{2M+a}\, p_{2M+a-N} = 0 \end{cases} , \tag{4.18}$$

with $a \in \{0, 1, \cdots, M/M_0 - 1\}$. Choosing $p_{2M+a} = 0$, and parameterizing the pulse coefficients with angles the system solution is

$$\begin{cases} p_a = cos(\theta_{a,1}) \\ p_{M+a} = sin(\theta_{a,1}) \\ p_{2M+a} = 0 \\ p_{2M+a-N} = cos(\theta_{a,2}) \\ p_{M_1+(a-N)} = -sin(\theta_{a,1})\ sin(\theta_{a,2}) \\ p_{M_1+(M+a-N)} = cos(\theta_{a,1})\ sin(\theta_{a,2}) \ . \end{cases} \tag{4.19}$$

For every choice of $(\theta_{a,1}, \theta_{a,2})$ with $a \in \{0, 1, \cdots, M/M_0 - 1\}$ the FMT scheme is orthogonal. We then define the vectors $\boldsymbol{\theta}_1 = [\theta_{0,1}, \theta_{1,1}, \cdots, \theta_{M/M_0,1}]$ and $\boldsymbol{\theta}_2 = [\theta_{0,2}, \theta_{1,2}, \cdots, \theta_{M/M_0,2}]$ and we search for pulses that satisfy the metric (4.11) and (4.12). The search is done according to the algorithm described in Section IX.A. In Fig. 4.1 and Fig. 4.2 we show the obtained pulses for $M = 64,\ 256,\ 1024$.

Example of prototype pulse design ($M_0 = 4$, $N_0 = 5$, and $L_f = \{N, 2N, \cdots, M_0N\}$). For the case $M_0 = 4$, $N_0 = 5$ and $L_f = M_0N$ the submatrices have the following structure:

$$\mathbf{G}_a = \begin{bmatrix} p_a & p_{M+a} & p_{2M+a} \\ z^{-1}\, p_{M_1+(a-N)} & z^{-1}\, p_{M_1+(M+a-N)} & p_{2M+a-N} \\ z^{-1}\, p_{M_1+(a-2N)} & z^{-1}\, p_{M_1+(M+a-2N)} & z^{-1}\, p_{M_1+(2M+a-2N)} \\ z^{-1}\, p_{M_1+(a-3N)} & z^{-1}\, p_{M_1+(M+a-3N)} & z^{-1}\, p_{M_1+(2M+a-3N)} \end{bmatrix}$$
$$\begin{bmatrix} p_{3M+a} & p_{4M+a} \\ p_{3M+a-N} & p_{4M+a-N} \\ p_{3M+a-2N} & p_{4M+a-2N} \\ z^{-1}p_{M_1+(3M+a-3N)} & p_{4M+a-3N} \end{bmatrix}^T . \tag{4.20}$$

The (4.20) can be used to derive the orthogonality conditions for the cases $L_f < M_0N$ simply setting certain elements to zero, as detailed in following.

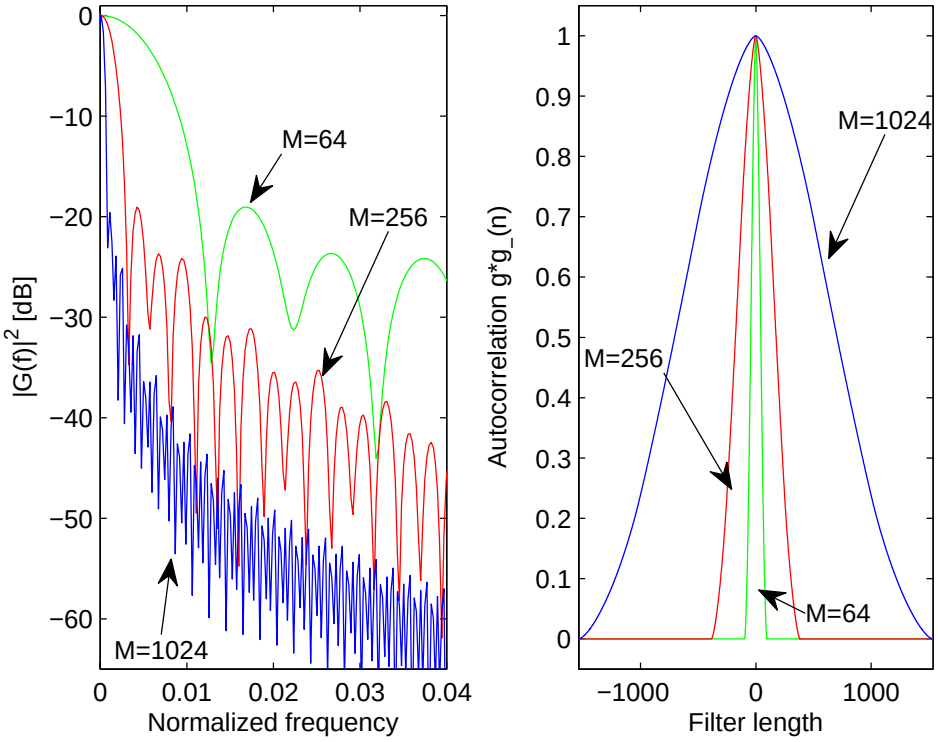

Figure 4.1: Frequency response and pulse autocorrelation for parameters $M_0 = 2$, $N_0 = 3$ and $L_f = N$.

Case $L_f = N$. Setting $p_i = 0$ with $i \in \{6, \cdots, 19\}$, the orthogonality condition for the a-th subsystem yields the following equations:

$$\begin{cases} p_a^2 + p_{M+a}^2 = 1 \\ p_{2M+a-N}^2 = 1 \\ p_{3M+a-2N}^2 = 1 \\ p_{4M+a-3N}^2 = 1 \end{cases} . \tag{4.21}$$

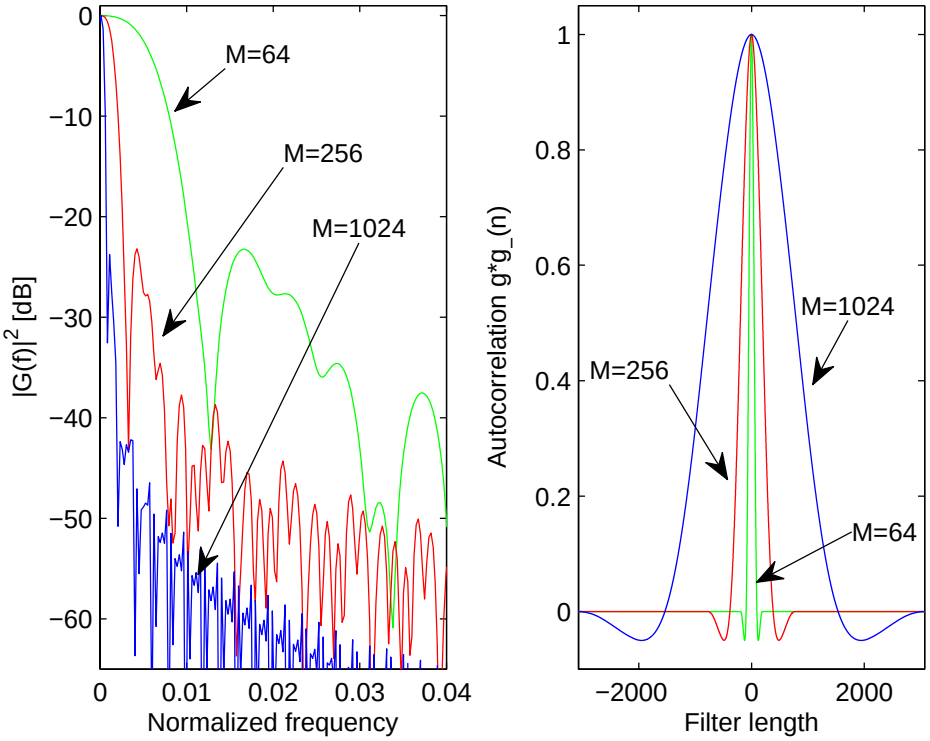

Figure 4.2: Frequency response and pulse autocorrelation for parameters $M_0 = 2$, $N_0 = 3$ and $L_f = 2N$.

The system can be parameterized with angles which yields

$$\begin{cases} p_a = cos(\theta_{a,1}) \\ p_{M+a} = sin(\theta_{a,1}) \\ p^2_{2M+a-N} = 1 \\ p^2_{3M+a-2N} = 1 \\ p^2_{4M+a-3N} = 1 \end{cases} . \tag{4.22}$$

Case $L_f = 2N$. Setting $p_i = 0$ with $i \in \{11, \cdots, 19\}$. The orthogonality

property for the a-th subsystem is determined by the following equations:

$$\begin{cases} p_a^2 + p_{M+a}^2 + p_{2M+a}^2 = 1 \\ p_{2M+a-N}^2 + p_{3M+a-N}^2 = 1 \\ p_{M_1+(a-2N)}^2 + p_{3M+a-2N}^2 + p_{4M+a-2N}^2 = 1 \\ p_{M_1+(a-3N)}^2 + p_{M_1+(M+a-3N)}^2 + p_{4M+a-3N}^2 = 1 \\ p_a p_{M_1+(a-3N)} + p_{M+a} p_{M_1+(M+a-3N)} = 0 \\ p_a p_{M_1+(a-2N)} = 0 \\ p_{2M+a-N} + p_{2M+a} = 0 \\ p_{3M+a-2N} p_{3M+a-N} = 0 \\ p_{4M+a-3N} p_{4M+a-2N} = 0 \ . \end{cases} \tag{4.23}$$

Setting $p_{M_1+(M+a-3N)} = p_{3M+a-2N} = p_{2M+a} = p_{M_1+(a-2N)} = 0$ we obtain

$$\begin{cases} p_a = cos(\theta_{a,1}) \\ p_{M+a} = sin(\theta_{a,1}) \\ p_{2M+a-N} = cos(\theta_{a,2}) \\ p_{3M+a-N} = sin(\theta_{a,2}) \\ p_{4M+a-2N} = 1 \\ p_{M_1+(a-3N)} = sin(\theta_{a,1}) \\ p_{M_1+(M+a-3N)} = -cos(\theta_{a,1}) \ . \end{cases} \tag{4.24}$$

In Fig. 4.3 and Fig. 4.4 we show the obtained pulses for $M = 64,\ 256,\ 1024$.

Generic design for $M_0 = 2^n$, $N_0 = M_0 + 1$ and $L_f = N$. The previous examples can be generalized to the case given by the parameters $M_0 = 2^n$, $N_0 = M_0 + 1$ and $L_f = N$. To do so we simply set $p_i = 0$ for $i > N_0$, then the orthogonality conditions for the a-th subsystem yield the following equations:

$$\begin{cases} p_a^2 + p_{M+a}^2 = 1 \\ p_{(k+1)M+a-kN}^2 = 1 \qquad k \in \{1, \cdots, M_0 - 1\} \ . \end{cases} \tag{4.25}$$

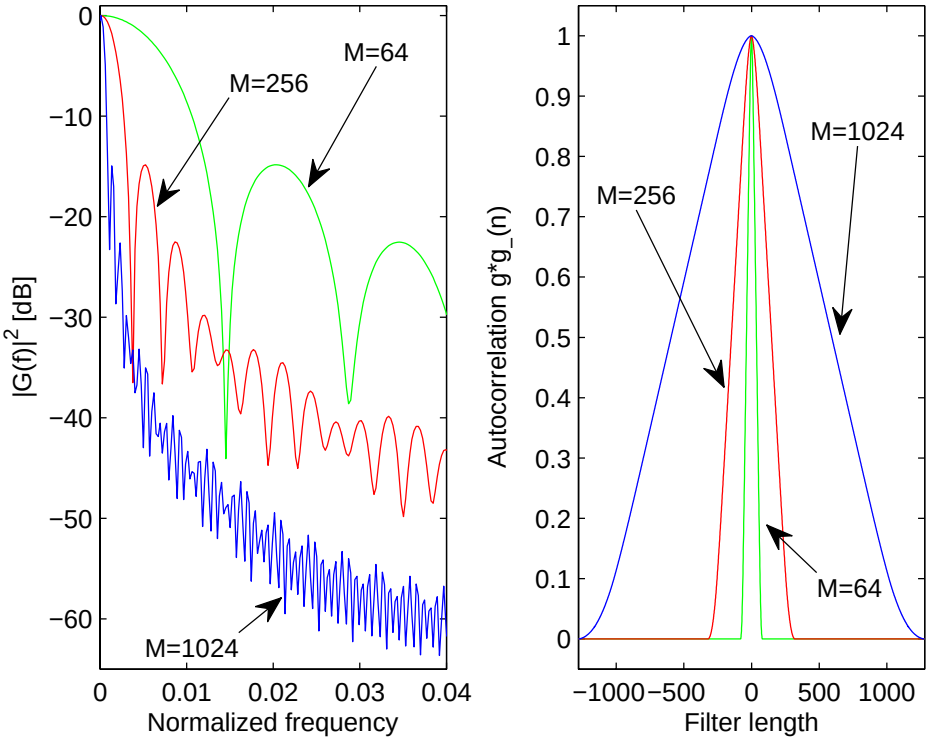

Figure 4.3: Frequency response and pulse autocorrelation for parameters $M_0 = 4$, $N_0 = 5$ and $L_f = N$.

The system can be parameterized with angles which yields

$$\begin{cases} p_a = cos(\theta_{a,1}) \\ p_{M+a} = sin(\theta_{a,1}) \\ p^2_{(k+1)M+a-kN} = 1 \qquad k \in \{1, \cdots, M_0 - 1\} \end{cases} . \tag{4.26}$$

As an example, in Fig. 4.5 we show the obtained pulses for $M = 64,\ 256,\ 1024$, $M_0 = 8$, $N_0 = 9$ and $L_f = N$.

4.4 Performance in wireless fading channels

In order to evaluate the robustness of the FMT scheme with the proposed pulses, we first consider transmission over a wireless dispersive fading channel having

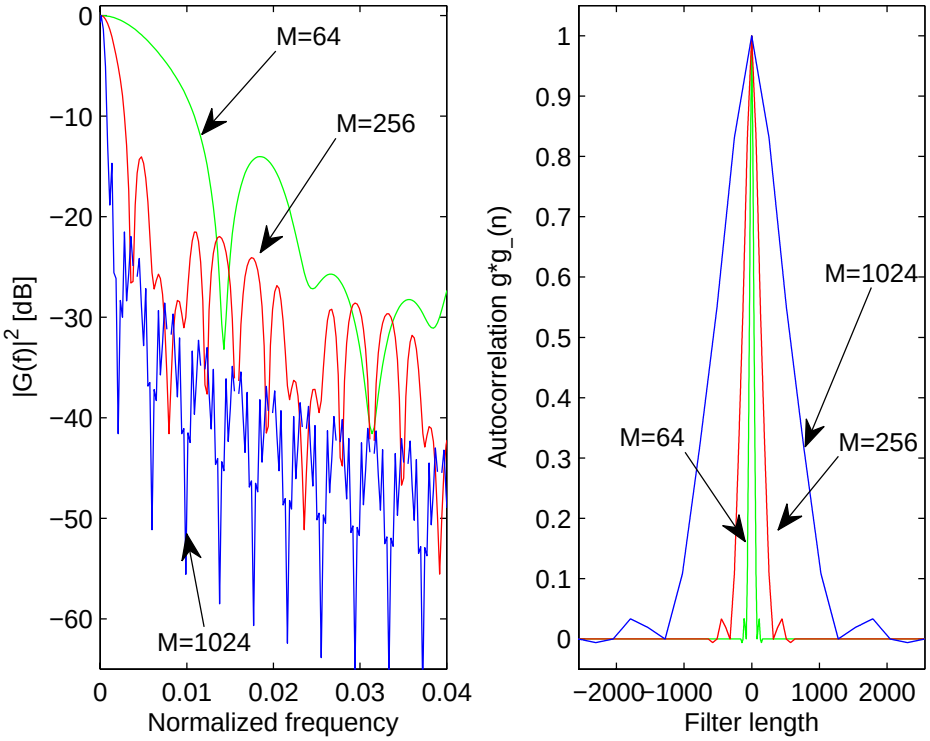

Figure 4.4: Frequency response and pulse autocorrelation for parameters $M_0 = 4$, $N_0 = 5$ and $L_f = 2N$.

impulse response $g_{ch}(n) = \sum_{p=0}^{N_p-1} \alpha_p \, \delta(n-p)$ where α_p are independent circular symmetric complex Gaussian variables with power $\Omega_p = \Omega_0 \, e^{-p/\gamma}$, and γ is the normalized delay spread. The channel is truncated at $-20dB$. This channel introduces a loss of system orthogonality that we evaluate in terms expected Signal-to-Interference Power Ratio SIR, versus delay spread γ. The SIR is evaluated as follows: first we compute the sub-channel signal-to-interference (ISI plus ICI) power ratio for a given channel realization. Then, we compute the average signal-to-interference ratio averaged over the sub-channels. Finally, we evaluate the expected (averaged over the channel realizations) signal-to-interference power ratio.

The simulation has been done for the case $M = 64, 256, 1024$, $L_f = N$, and $N = 3/2M$ in Fig. 4.6, $N = 5/4M$ in Fig. 4.7, $N = 9/8M$ in Fig.

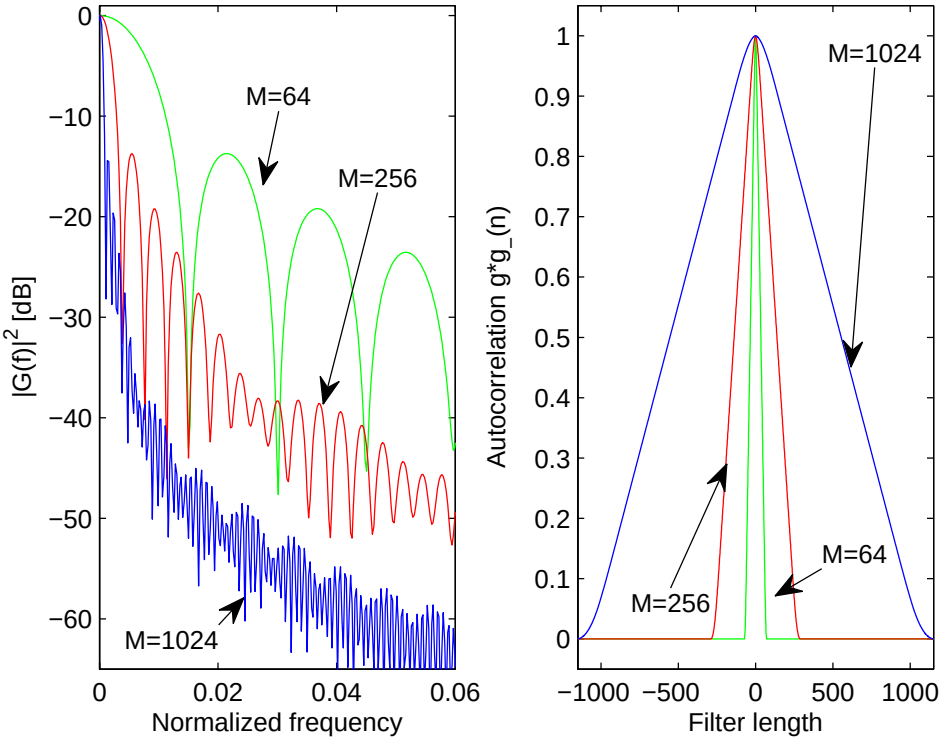

Figure 4.5: Frequency response and pulse autocorrelation for parameters $M_0 = 8$, $N_0 = 9$ and $L_f = N$.

4.8. To benchmark the performance of the proposed pulses, we consider the case $M = 64$ subcarriers with a conventional root-raised cosine (rrc) pulse with roll-of factor $R = 0.2$ and length $L_{RRC} = 2N, 6N, 20N$, and a IOTA pulse with length $L_{IOTA} = N$ which is a truncated version of the IOTA pulses family presented in [28].

Figs. 4.6-4.8 show that the FMT system, in the considered channel, has considerable better performance with the orthogonal pulses than with the rrc pulse of length $2N$, and the IOTA pulse of length N especially for low values of delay spread. For high delay spreads the IOTA pulse yields similar performance to the orthogonal pulse, and the rrc pulse has a better behavior only if it has large length ($6N$ and $20N$, in the figures) which however increases the complexity of the realization.

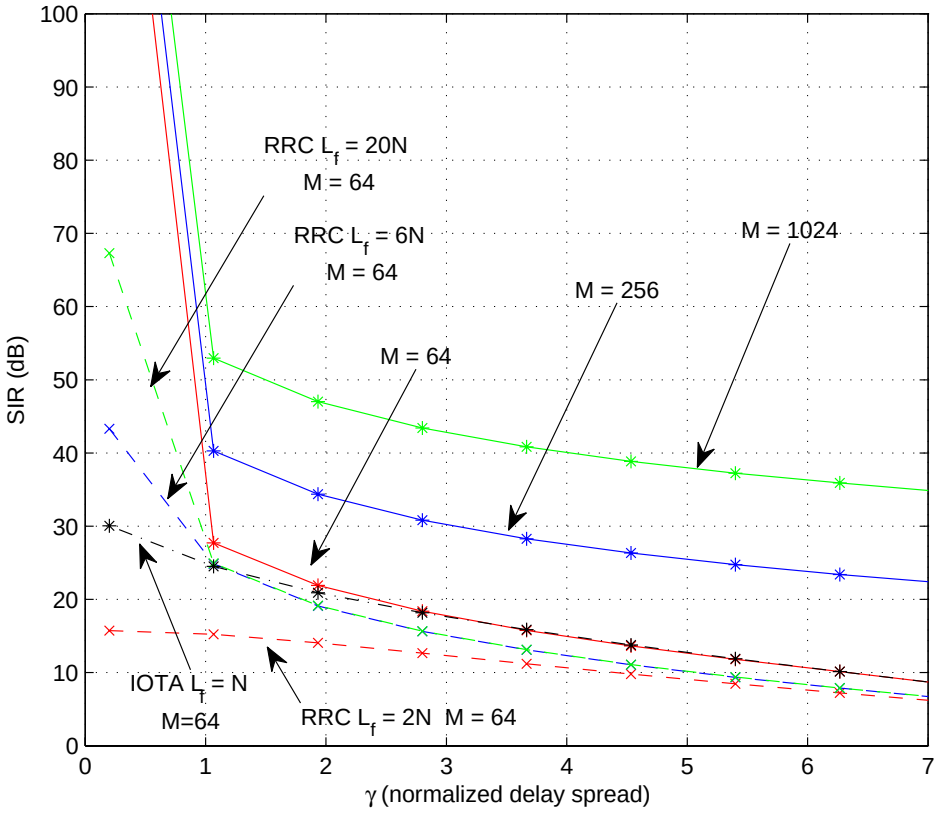

Figure 4.6: SIR vs. the normalized delay spread γ for orthogonal pulse with $M_0 = 2$, $N_0 = 3$ and $L_f = N$.

Furthermore, the figures show that better SIR is obtained by increasing the number of carriers since the sub-channels exhibit a flatter frequency response.

Now, we consider the application of FMT in indoor wireless LAN channels. We have used the IEEE 802.11 channel model presented in [18] and discussed in Section 2.4. Although the model allows us to consider MIMO channels, we restrict ourselves to the case of single-transmit/single-receive antenna. For a detailed description of the model, see [18] and references therein. The continuous time complex impulse response provided by such a model (with slow fading) can

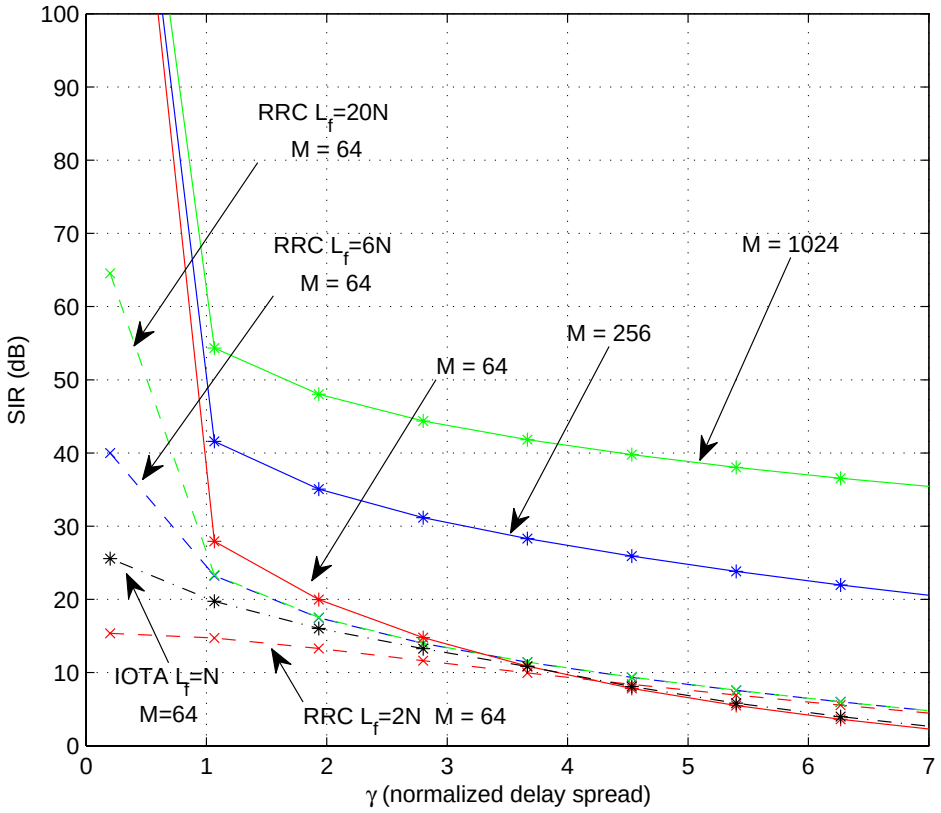

Figure 4.7: SIR vs. the normalized delay spread γ for orthogonal pulse with $M_0 = 4$, $N_0 = 5$ and $L_f = N$.

be written as

$$\hat{g}_{\text{ch}}(n, d) = A(d) \sum_{p=0}^{\nu-1} \beta(p)\, \delta(n - \tau_p)\,, \tag{4.27}$$

where $A(d)$ is the attenuation from path-loss when the transmitter and the receiver are at distance d, $\beta(p)$ is the tap amplitude and τ_p is the time delay. The number of multipath components is denoted with ν. We consider class B that assumes a LOS environment. The first tap has Rice amplitude, while the remaining $\nu - 1$ taps are Rayleigh distributed. To obtain the equivalent discrete time channel impulse response, we filter the channel response with a low pass

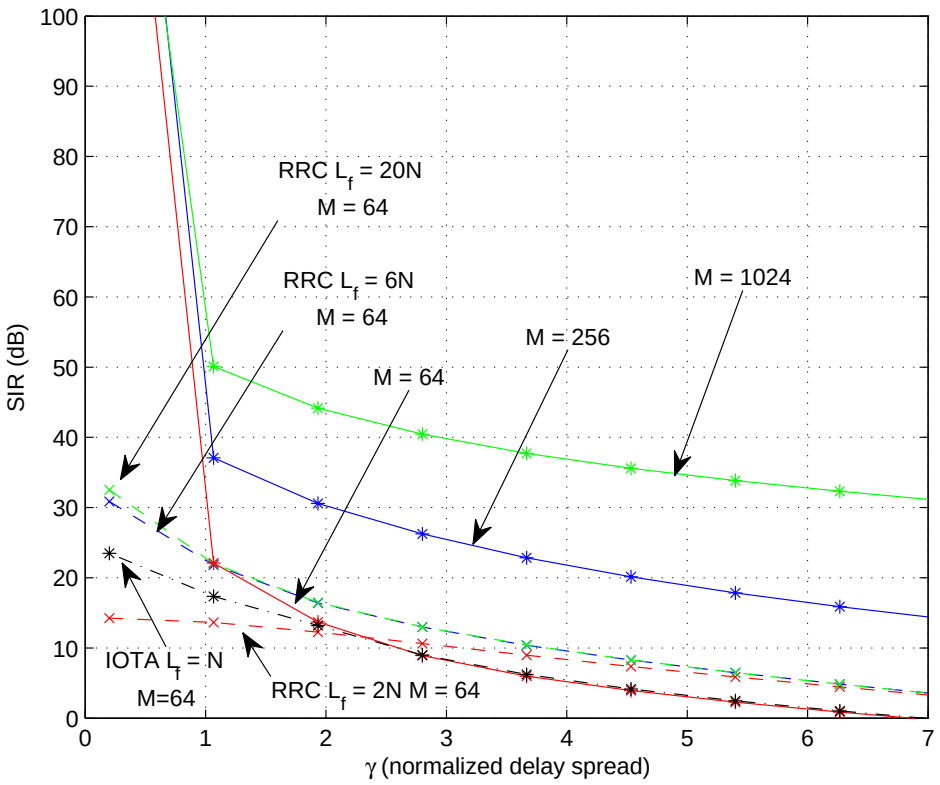

Figure 4.8: SIR vs. the normalized delay spread γ for orthogonal pulse with $M_0 = 8$, $N_0 = 9$ and $L_f = N$.

pulse, and we sample the outputs at rate $1/T$ that is equal to the transmission bandwidth of 20 MHz.

Now, we evaluate the system capacity with the above channel model assuming parallel Gaussian channels. That is, we assume additive white Gaussian noise, and independent and Gaussian distributed input signals, which renders ISI and ICI also Gaussian. Furthermore, we use of single tap sub-channel equalization, i.e., no attempt is made to suppress ISI and ICI. Then, the maximal data rate, for a given channel realization, is

$$C = \frac{1}{NT} \sum_{k=0}^{M-1} \log_2 \left(1 + SINR^{(k)}\right) \qquad [\text{bit/s}] \; . \tag{4.28}$$

In (4.28), $SINR^{(k)}$ denotes the signal over interference plus noise ratio experienced in sub-channel k for a given channel realization.

In Fig. 4.9 we show the complementary cumulative distribution function of the capacity (4.28). The results have been obtained assuming the class B channel with distances between transmitter and receiver equal to 20 m, 40 m, and 60 m. The FMT system uses the pulse in Fig. 4.3 with $M = 64$ sub-channels, and single tap equalization. As a comparison we also report the performance of OFDM with $M = 64$ sub-channels and a cyclic prefix of length 16 samples (0.8 μs) as defined in the IEEE 802.11 standard. The two systems have identical overhead. We assume a transmitted power spectra density (PSD) of -53 dBm/Hz and a noise PSD of -168 dBm/Hz.

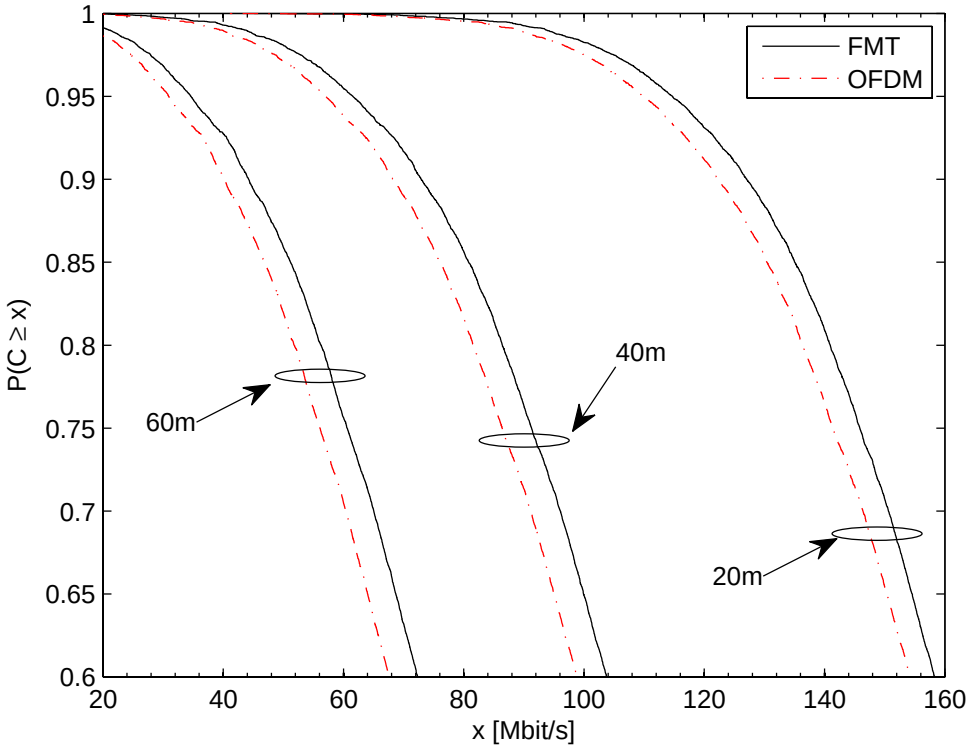

Figure 4.9: Capacity of the FMT with $M = 64$, $N = 80$ and $L_f = 80$ vs. OFDM with $M = 64$, $CP = 16$ samples.

The results show that in the considered scenario, FMT significantly outper-

forms OFDM yet having similar complexity since single tap equalization is used in both systems, and the pulse used in FMT has minimal length. For instance, for 80% of channel realizations, OFDM exceeds 81 Mbits/s at 40 m while FMT exceeds 86 Mbits/s. Performance improvements are expected if more powerful sub-channel equalization is deployed in FMT.

4.5 Conclusions

In this chapter we have considered the design of an orthogonal FMT system exploiting the matrix structure of the first efficient realization (the method in [13] described in Section 3.4), and we proposed a method that considerable simplifies the design of orthogonal FB for certain choices of the parameters and for arbitrarily large number of sub-channels.

Several examples of pulses with minimal length have been reported and the performance of the system in typical wireless multi-path fading channels has been shown. The comparison with a conventional truncated root-raised-cosine pulses and with IOTA pulses has shown that the proposed pulses yield significant improved robustness to multi-path fading. Furthermore, the comparison with cyclically prefixed OFDM using the IEEE 802.11 WLAN class B channel, has shown that FMT outperforms OFDM, yet having similar complexity.

Chapter 5

Co-channel Equalization

5.1 Introduction

As explained in Chapter 4, the deployment of long filters eliminates the ICI, but gives rise to non-negligible ISI, which severely limits the performance of the system. The use of sub-channel equalization copes with the ISI and can sensibly improve the performance not only by reducing ISI, but also by exploiting it gathering a diversity gain from the multipath channel.

Orthogonal FMT suffers from the presence of ICI which is not negligible at the receiver due to the short filters deployed that do not guarantee a perfect separation among the sub-channels when we signal over a time-dispersive channel. In this case we can adopt a linear equalizer applied across the sub-channels to cope with the interference. However, since the short filters do not have an high frequency confinement, some interference, mainly due to the signals belonging to adjacent sub-channels, affects the signal of interest, and thus a major part of ICI component arises.

In this chapter we present the design of a frequency domain equalizer that mitigates the unwanted ICI distortion effect. In conjunction with this linear equalization stage, we further propose to improve the performance by adopting a Decision Feedback Equalizer (DFE) to compensate the remaining inter-symbol interference effects. We present extensive numerical results considering the WLAN channel model [18], evaluating the performance in terms of capacity

of orthogonal FMT, and comparing the results with baseline OFDM used in the IEEE 802.11 protocol.

The chapter is organized as follows. In Section 5.2, we describe the general system model. In Section 5.3, we describe the frequency domain equalizer design. Then, in Section 5.4, we report numerical results showing the comparison in terms of capacity between orthogonal FMT and OFDM. Finally, in Section 5.5, the conclusions follow.

5.2 System model and capacity

5.2.1 System model

We consider a general FB system with a number of sub-channels equal to M, and interpolation-sampling factor equal to $N = M + \beta$, where we denoted as β the overhead (OH). The received signal at the kth sub-channel can be expressed as (see Section 2.1)

$$b^{(k)}(Nn) = \sum_{m\in\mathbb{Z}} y(m)h^{(k)}(Nn - m) \tag{5.1}$$

$$= U^{(k)}(Nn) + I^{(k)}(Nn) + \eta^{(k)}(Nn), \tag{5.2}$$

Equation (5.2) shows that the received signal at the k-th sub-channel can be decomposed into three components: the useful signal $U^{(k)}(Nn) = a^{(k)}(Nn)H^{(k)}$, the interference comprising ISI and ICI $I^{(k)}(Nn)$, and the noise component $\eta^{(k)}(Nn)$, where we defined the sub-channel gain as $H^{(k)} = g^{(k)} * h_{ch} * h^{(k)}(0)$. These components are in general all dependent on the OH factor $\beta = N - M$.

The channel is modeled as a linear time-invariant filter generated using the IEEE 802.11 TGn [18] model discussed in Section 2.4.

In order to obtain the equivalent discrete time channel impulse response, we use a low pass filter before sampling the signal with frequency $B = 1/T = 20MHz$, that is equal to the system transmission bandwidth considered in this chapter when showing numerical results.

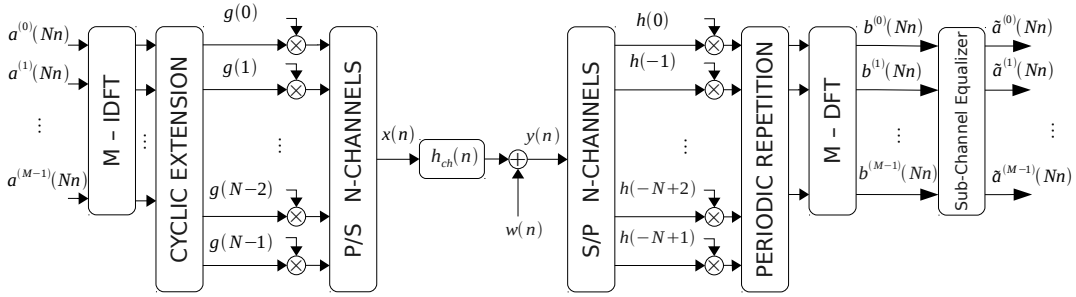

Figure 5.1: Efficient implementation of the orthogonal FMT scheme with M sub-channels, sampling interpolation factor equal to N, prototype pulse length $L_g = N$, and frequency domain equalizer.

5.2.2 SINR and Capacity

Having established the system signal model, we now define the signal to interference plus noise ratio (SINR), and the system requirements to estimate the information capacity, which allows us to evaluate the performance.

Since the system works in stationary conditions, the SINR experienced at the k-th sub-channel can be evaluated independently of any particular point in time, and thus it can be written as

$$SINR^{(k)}(h_{ch}) = \left(\frac{1}{SNR^{(k)}(h_{ch})} + \frac{1}{SIR^{(k)}(h_{ch})} \right)^{-1} \tag{5.3}$$

where in (7.18) we defined the signal to noise ratio (SNR) and the signal to interference ratio (SIR) given a channel realization $h_{ch}(n)$ at the k-th sub-channel respectively as

$$SNR^{(k)}(h_{ch}) = \frac{P_U^{(k)}(h_{ch})}{P_\eta^{(k)}(h_{ch})}$$
$$SIR^{(k)}(h_{ch}) = \frac{P_U^{(k)}(h_{ch})}{P_I^{(k)}}.$$

where we denoted the average powers of the useful signal, the interference, and

the noise as

$$P_U^{(k)}(h_{ch}) = E_a\{|U^{(k)}(0)|^2\} = |H^{(k)}|^2 P_a$$
$$P_I^{(k)}(h_{ch}) = E_a\{|I^{(k)}(0)|^2\}$$
$$P_\eta^{(k)} = E_a\{|\eta^{(k)}(0)|^2\}$$

and $E_a\{.\}$ is the expectation with respect to the transmitted data symbols $a^{(k)}(Nn)$ with statistical power P_a.

The system performance that we present in the following sections are based on the information capacity of the system. For this purpose, we assume parallel Gaussian channels and statistically independent Gaussian distributed input signals, which render ISI and ICI also Gaussian (cf. e.g. [35]).

$$C = \frac{1}{NT} \sum_{k=0}^{M-1} \log_2 \left(1 + SINR^{(k)}(h_{ch})\right). \tag{5.4}$$

5.3 Frequency domain equalizer

Despite designing the orthogonal FMT prototype pulse with maximum frequency confinement, in the presence of a non-ideal propagation media the system suffers from residual ICI. This is due to the fact that the pulses with minimal length have a frequency response not sufficiently confined to completely separate the sub-channels.

5.3.1 MMSE Frequency Domain Equalization

In this section we present the design of a frequency domain equalizer for orthogonal FMT to cope with the ICI. Our design can be adopted for a generic multi-carrier transceiver.

We begin by defining the output signals to the frequency domain equalizer

block depicted in Fig. 5.1, as

$$\begin{aligned}\hat{a}_m^i &= \hat{a}^{(i)}(Nm) = \\ &= \left(\mathbf{w}^i\right)^H \mathbf{b}_m^i \end{aligned} \tag{5.5}$$

In (5.5), we assumed that each sample output is a linear combination between the signals at a given time instant at the output of the DFT bock, and some appropriate weighing coefficients collected in the equalizer vector $\mathbf{w}^i = [w_0^i w_1^i \cdots w_{N_w}^i]^T$. The DFT output signal vector is denoted as $\mathbf{b}_m^i = [b_m^{i-(N_w-1)/2} \cdots b_m^i \cdots b_m^{i+(N_w-1)/2}]^T$ where we defined

$$b_m^i = b^{(i)}(Nm) = \tag{5.6}$$

$$= \sum_{k=0}^{M-1} \sum_{\ell \in \mathbb{Z}} g_{eq}^{(i,k)}(Nm - N\ell) a^{(k)}(N\ell) \tag{5.7}$$

In (5.7) we denoted the equivalent fitler responce between the transmitted signal $a^{(k)}(Nn)$ and the signal at input of the equalizer $b^{(i)}(Nn)$ as

$$\begin{aligned} &g_{eq}^{(i,k)}(Nm - N\ell) = \\ &= \sum_{n \in \mathbb{Z}} g^{(k)}(n - N\ell) \sum_{p \in \mathbb{Z}} h_{ch}(p-n) h^{(i)}(Nm - p) \end{aligned} \tag{5.8}$$

The equalizer vector associated to the i-*th* sub-channel has N_w taps, where N_w is considered to be an odd number. This means that the equalizer exploits $N_w - 1$ adjacent sub-channel signals (half on the right side and half on the left side), to compensate for the ICI distortion effect.

The equalizer we want to design belongs to the family of the Minimum Mean Squared Error (MMSE) equalizers. From the Wiener-Hopf filter theory, the coefficients that minimize the MSE can be obtained simply imposing the error orthogonal to the symbols at the output of the equalizer [36]

$$E[\hat{a}_m^i \, e^*(n)] = 0 \tag{5.9}$$

where we defined the error estimated at the receiver as the difference between

the original transmitted signal and the signal at the equalizer output

$$e^i(m) = a^i_m - \hat{a}^i_m \tag{5.10}$$

Relation (5.9) is referred to as the orthogonal condition property [36]. Substituting $e(n)$ and $\hat{a}^i_m$ in (5.9) we obtain

$$E[(\mathbf{w}^i)^H \mathbf{b}^i_m \; e^*(m)] = 0 \tag{5.11}$$

Defining $\mathbf{R}_b = E[\mathbf{b}^i_m (\mathbf{b}^i_m)^H]$ the correlation matrix of the vector $\mathbf{b}^i_m$, $\mathbf{r}_{b\,a} = E[\mathbf{b}^i_m \, (a^i_m)^*]$ the cross-correlation vector between the vector $\mathbf{b}^i_m$ and the desired symbol a^i_m, the expression in (5.11) can be rearranged as

$$\mathbf{R}_b \mathbf{w}^i = \mathbf{r}_{b\,a} \tag{5.12}$$

The relation (5.12) is the Wiener-Hopf equation from which we can derive the optimum equalizer coefficients that minimize the MSE as

$$\mathbf{w}^i_{opt} = \mathbf{R}_b^{-1} \, \mathbf{r}_{b\,a} \tag{5.13}$$

5.3.2 Decision Feedback Equalization

Linear equalizers are relatively simple, even though they often suffer of significant performance loss compared to optimal detector such as ML equalizer. This is due to the presence of remaining interference given by symbols transmitted in different instant of time w.r.t. the detected symbol. A trade-off can be achieved by joining the linear equalizer with a decision feedback equalizer (DFE) solution. The basic idea of the decision-feedback operation is to estimate and subtract the impact of those interfering symbols which have been detected earlier. Each symbol suffers from two different types of interferences: an ISI component given

by the term

$$ISI^{(i)} = \sum_{\substack{\ell \in \mathbb{Z} \\ \ell \neq 0}} g^{(i,i)}(Nm - N\ell)a^{(i)}(N\ell), \tag{5.14}$$

and an ICI contribution introduced by the previous transmitted symbols, herein denoted as Inter ICI (IICI), whose expression is

$$IICI^{(i)} = \sum_{\substack{k=0 \\ k \neq i}}^{M-1} \sum_{\substack{\ell \in \mathbb{Z} \\ \ell \neq 0}} g^{(i,k)}(Nm - N\ell)a^{(k)}(N\ell). \tag{5.15}$$

Linear equalization is applied to only compensate the impact of the ICI introduced by the undetected symbols itself. The DFE principle applies symbol-by-symbol detection with successive cancellation of the interference caused by the detected symbols. The remaining interference can be canceled by subtracting its impact.

More in detail, considering the received symbol $b^{(i)}(Nm)$, we apply a single tap DFE equalizer that compensates the ISI and IICI of the previous symbol only, i.e., $b^{(i)}(N(m-1))$.

In Fig. 5.2 the FMT scheme with linear and DFE equalization is depicted. As we can note the symbols $b^{(i)}(Nm)$ with $i \in \{0 \cdots M-1\}$, are fed back, and delayed by one sample time represented by Δ. Then, the DFE block evaluates the interference yielding at the output the signals

$$p^{(i)}(Nm) = \sum_{k=0}^{M-1} g^{(i,k)}(1)a^{(k)}(N(m-1)) \tag{5.16}$$

The signals $p^{(i)}(Nm)$ are finally subtracted to the detected signals $b^{(i)}(Nm)$.

5.4 Numerical results

In this section, we present the numerical results in terms of capacity, comparing orthogonal FMT and OFDM. The system parameters used are essentially those of the 802.11 protocol. The filter banks of the transmitter and the receiver

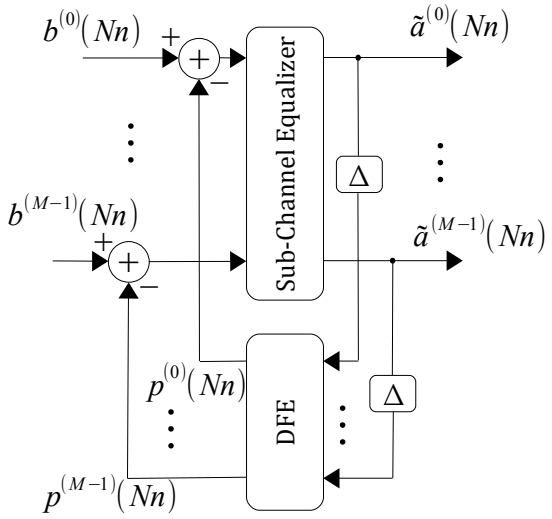

Figure 5.2: DFE equalization stage.

use a number of sub-channels equal to $M = 64$. The transmission bandwidth considered is equal to $B = 20MHz$. The transmitted power has a power spectral density (PSD) level equal to $-53dBm/Hz$. The noise at receiver is modeled as an Additive White Gaussian Noise (AWGN) process with the PSD level equal to $-168dBm/Hz$. Thus, with these set of parameters, the value of the Signal to Noise Ratio (SNR) experienced at the receiver with an ideal channel is equal to $115dB$. We use the Tgn channel model [18] considering the classes B,C, and D that have an RMS delay spread respectively of $\{15, 30, 50\}ns$.

We adopt an orthogonal FMT system presented in Chapter 4 with the prototype pulses having minimal length equal to $L_g = N$, and sampling/interpolation factor equal to $N = (9/8)M$. A single tap equalizer, and a MMMSE frequency domain equalizer with 11 taps and 41 taps are employed. Furthermore, we also consider a system deploying MMSE equalizer with 11 taps and 41 taps, combined with a single tap DFE equalizer.

We compare the performance with an OFDM system. In such a case the prototype filters has rectangular shape in the time domain, and the cyclic prefix used is equal to $\mu = 0.8\mu s$, or equivalently, over a bandwidth of $20MHz$, it has an over-head equal to $\beta = N - M = 16$ samples.

Fig. 5.3 and 5.4 report the curves representing the complementary cumula-

tive distribution function (CCDF) of the capacity for the classes B, C, and D considering several distances between the transmitter and receiver that are respectively {10, 30} mt using respectively 11 taps equalizer (Fig. 5.3) and 41 taps equalizer (Fig. 5.4). From Fig. 5.3 we can note that for a large distance, e.g., at 30 mt, orthogonal FMT can obtain higher values of capacity than OFDM. Furthermore, at the distance of 30 mt the frequency domain equalization has no significant effect on the performance of the orthogonal FMT, even using a large number of equalizer taps (Fig. 5.3). This can be explainable simply noting that for large distances the path loss is high, and then the power levels of the signal and the interferences are low. Thus, the factor that limits the performance in these conditions is the noise power level rather than the interference power level. As we can note in (7.18), if the power of the noise dominates the power of the interference, the SINR can be well approximated with the SNR itself. Since orthogonal FMT deploys match filtering, the SNR measured on the received data symbols is maximum [37]. On the contrary, OFDM does not deploy matched filtering due to the cyclic prefix, yielding a lower SNR. In other words, for large distances the use of the CP is useless since it removes power to the interference that is negligible compared to the power of the noise, resulting in a decrease of SINR and capacity (7.21). This behavior is also independent of the channel class considered, and thus independent of the delay spread. Fig. 5.3-5.4 show that at the distance of $30\,mt$ with probability equal to 0.9, independently of the number of equalizer taps deployed, orthogonal FMT outperforms OFDM by 18%, 19% and 15% for channel classes B, C and D respectively.

For shorter distances the path loss is lower so that the power level of the noise tends to be negligible compared to the power level of the interference, and in (7.18) we can approximate the SINR with the SIR. These considerations are confirmed by the simulations. As we can note from Fig. 5.3-5.4 at distance 10 mt, by removing part of interference on orthogonal FMT with the frequency domain equalizer, we can effectively improve the maximum achievable transmission rate. The performance shows that with probability equal to 0.9, orthogonal FMT with frequency domain equalizer outperforms FMT with single tap equalizer by $(1.8\%, 2\%)_{class\ B}$, $(4.3\%, 7.8\%)_{class\ C}$ and $(8\%, 12\%)_{class\ D}$ respectively using $(11, 41)$ taps. On the other side, with probability 0.9 orthogonal FMT with

frequency domain equalizer has a gain w.r.t. OFDM of $(11.3\%, 11.5\%)_{class\ B}$, $(6.1\%, 9.5\%)_{class\ C}$, and a loss of $(-11.5\%, -8\%)_{class\ D}$ respectively using $(11, 41)$ taps. The use of the DFE scheme further improve the performance, and it consistently outperforms OFDM even in those scenarios where the inter-symbol interference components are not negligible (i.e. Class D at 10 mt). It results that with probability 0.9 at 10 mt the gain of FMT with MMSE-DFE w.r.t. OFDM is equal to $(12\%, 20\%)_{class\ B}$ $(4\%, 10\%)_{class\ C}$ $(-8\%, 7\%)_{class\ D}$ respectively for 11 and 41 taps equalizer.

Clearly, the improvement given by the use of the frequency domain equalizer is paid in terms of computational complexity.

5.5 Conclusions

In this chapter, we have considered an FMT system deploying an orthogonal pulse with minimal length to reduce the ISI, in conjunction with an MMSE frequency domain equalizer to cope with the ICI, and a DFE sub-channel equalizer to cope with the residual inter symbol interference. Numerical results have shown that orthogonal FMT has the potentiality to improve the capacity in the WLAN scenario compared to OFDM. In particular when the distance between the transceivers is large, (i.e., with low SNR), single tap equalization performs well. For shorter distances, (i.e., with high SNR), FMT can further improve the performance with the use of frequency domain equalizer with and without DFE. However, this is paid in terms of computational complexity.

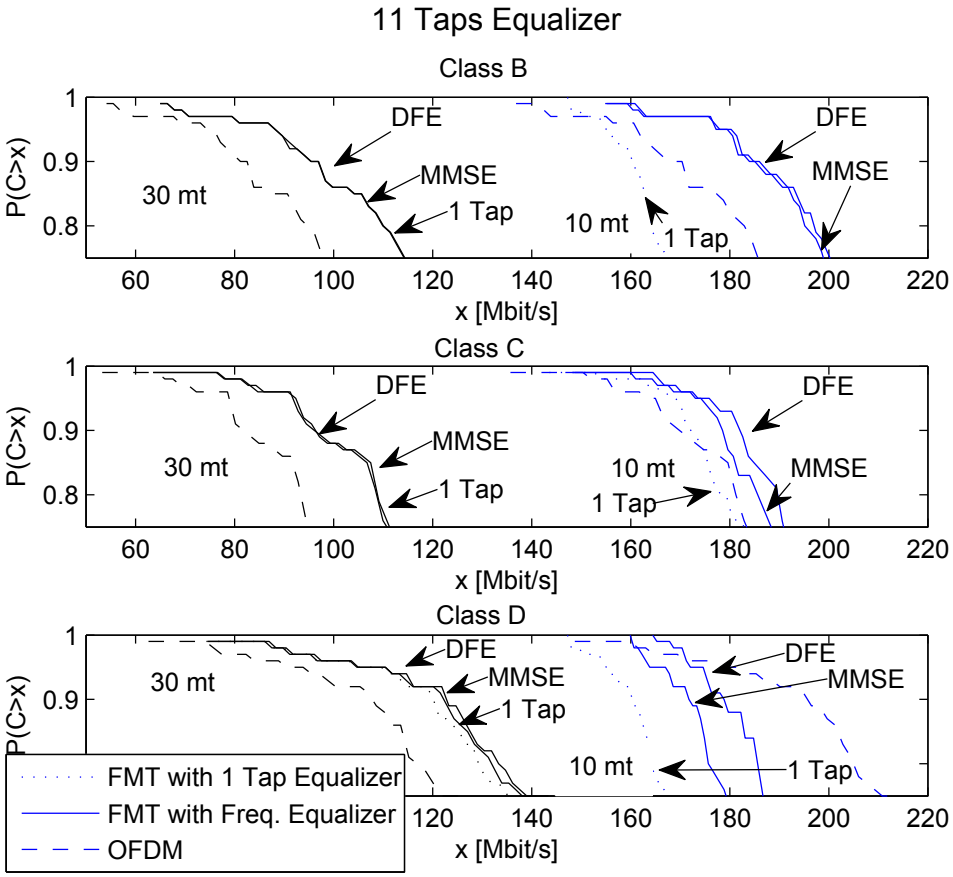

Figure 5.3: Complementary Cumulative Distribution Function (CCDF) of the capacity considering the orthogonal FMT with single tap equalizer (1 Tap-arrow in figure), with 11-taps MMSE frequency domain equalizer (MMSE-arrow in figure), with 11-taps MMSE combined with single-tap DFE equalizer (DFE-arrow in figure), and OFDM deployed in the IEEE 802.11 standard.

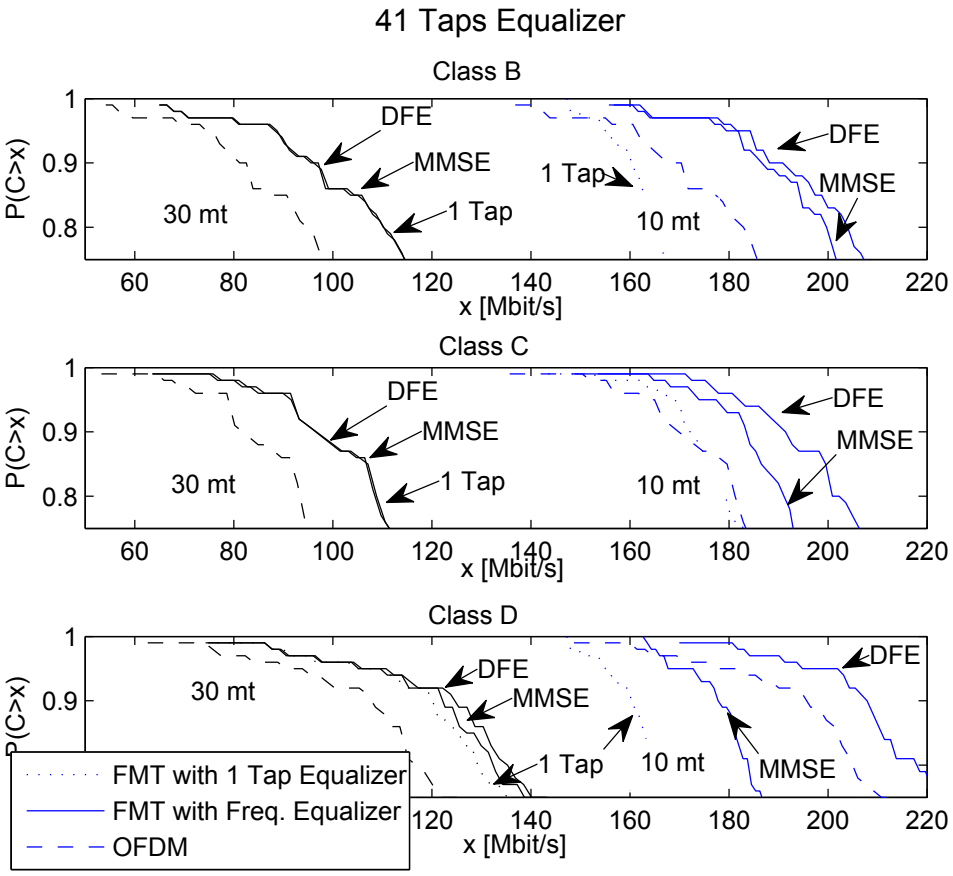

Figure 5.4: Complementary Cumulative Distribution Function (CCDF) of the capacity considering the orthogonal FMT with single tap equalizer (1 Tap-arrow in figure), with 41-taps MMSE frequency domain equalizer (MMSE-arrow in figure), with 41-taps MMSE combined with single-tap DFE equalizer (DFE-arrow in figure), and OFDM deployed in the IEEE 802.11 standard.

Chapter 6

Hybrid FMT for WLAN Applications

6.1 Introduction

In this chapter we present a hybrid transceiver scheme, that exploits the peculiarities of two different FB architectures, namely OFDM and FMT. We aim at setting up a system that can switch between the two architecture considered by choosing the one that grants the maximum information capacity as function of the channel state information.

As it was introduced in Chapter 2, the OFDM system uses prototype pulses with rectangular shape of impulse response. In the presence of a frequency selective channel, the cyclic prefix (CP) is needed to mitigate the interference components. If the CP is longer than the channel impulse response, the system maintains its perfect reconstruction properties, thus, the interference is perfectly coped at the decision stage. Nevertheless, this benefit is paid in term of a decrement of capacity that depends on the signal over noise ratio (SNR) level which is decreased by a factor of $M/(M+\beta)$, where we recall that β is the CP length in number of samples. Clearly, when the CP is shorter than the channel duration, ISI and ICI terms arise [35].

On the other side, we generally have that the FMT system has two main paradigms on which it can be designed. The first one uses a frequency confined prototype pulse to make the sub-channels quasi-orthogonal to each other. The second one adopts a minimal length orthogonal prototype pulse designed

following the procedure presented in Chapter 4, and this allows the system to counteract part of the ICI by maintaining low the computational complexity. In this chapter we will refer to this scheme as Short-Orthogonal-FMT (SO-FMT).

In [38], the authors found that by using OFDM over typical WLAN channels, the CP has not to be necessarily as long as the channel duration to maximize the achievable rate. Furthermore, for each channel class of the IEEE 802.11n WLAN channel model [18], it was found a nearly optimal value of CP designed according to the statistic of the capacity-optimal CP duration. It was shown that the capacity improvements for the WLAN standard are attainable by adapting the CP to the experienced channel class, and this is applicable for both the single and the multi user scenario. This scheme was referred to Adaptive-OFDM (A-ODFM).

Comparing the performance of SO-FMT and A-OFDM, we have found that depending on the channel condition it is convenient to use one scheme rather than the other. Therefore, we propose to exploit the similarities of both schemes by using a hybrid FMT architecture herein denoted as H-FMT. This new scheme can switch between SO-FMT and A-OFDM according to the experienced channelization. The central point that enables us to merge these two architectures together is the similar efficient implementation of both SO-FMT and A-OFDM. The efficient realization of H-FMT introduces a marginal increase of the computational complexity w.r.t. conventional OFDM. The performance improvements that are attainable with H-FMT are studied for the WLAN application scenario. It is worth noting that the use of hybrid schemes seems to be a new direction for next telecommunication systems. In fact, new home networking standards as IEEE P1901 and ITU G.hn [39] propose the use of different modulation techniques, e.g., IEEE P1901 allows transceivers to deploy both OFDM and wavelet OFDM. Furthermore, also the research interest for the hybrid architectures is increasing. As an example, in [40] a hybrid architecture based on hermitian symmetry - offset quadrature amplitude modulation (HS-OQAM) and discrete multitone (DMT) modulation is proposed for communication over power line channels.

This chapter is organized as follows. In Section 6.2 we present the general system model. In Section 6.3 we present the novel H-FMT architecture. In Sec-

tion 6.4 we report extensive numerical results showing that over typical WLAN channels [18] the use of H-FMT increases the system capacity and further renders the system more reliable than the conventional OFDM adopted in the WLAN standard [3]. Finally, in Section 6.5 the conclusions follow.

6.2 System Model

We consider a general FB scheme with M sub-channels, where $N = M + \beta$ is the sampling-interpolation factor, with β equal to the overhead (OH) duration in samples. We consider the WLAN scenario and we adopt the IEEE 802.11 TGn [18] channel model discussed in Section 2.4.

In order to evaluate the system performances, we assume parallel Gaussian channels and independent and Gaussian distributed input signals, which render ISI and ICI also Gaussian (cf. e.g. [35]). Therefore, the achievable rate in bit/s for a given channel realization, and supposing single tap zero forcing equalization, is given by

$$C(\beta) = \frac{1}{(M+\beta)T} \sum_{k=0}^{M-1} \log_2 \left(1 + SINR^{(k)}(h_{ch}, \beta)\right), \tag{6.1}$$

where $SINR^{(k)}(h_{ch}, \beta)$ denotes the signal over interference plus noise ratio experienced in sub-channel k when we transmit using an overhead of β samples (see Section 5.2.2). Here we recall that the SINR is related with the SNR and the SIR according to the following relation

$$SINR^{(k)}(\beta) = \left(\frac{1}{SNR^{(k)}(\beta)} + \frac{1}{SIR^{(k)}(\beta)}\right)^{-1}, \tag{6.2}$$

6.2.1 Adaptive OFDM (A-OFDM)

A-OFDM is an OFDM system which adapts the cyclic prefix duration to the channel condition an was presented in [38]. The cyclic prefix OFDM scheme can be obtained setting the coefficients $g(n) = 1/\sqrt{N} rect(nN)$ and $h(n) = 1/\sqrt{(M)} rect(n/M)$ (see Section 2.2). Note that $N = M + \beta$, and β is the

duration of the CP in samples.

Since the CP lasts more than the channel duration, the received signal is neither affected by ISI nor by ICI [35]. Nevertheless, in [38], the author showed that the CP has not to be necessarily as long as the channel duration to maximize the achievable rate. The rationale behind is that the level of interference can be raised in noise-limited systems without loosing in achievable rate (see (6.1)).

From the statistics of the optimal CP duration, in [38], it was found a limited set of CP values over which to adapt the OFDM system to the channel condition. We have denoted this set as $\mathbb{P}_{OFDM} = \left\{\beta_B^{(99\%)}, \beta_C^{(99\%)}, \beta_D^{(99\%)}, \beta_E^{(99\%)}, \beta_F^{(99\%)}\right\}$. That is, depending on the experienced channel class, the A-OFDM picks the corresponding CP value from the set $\mathbb{P}_{OFDM}$. For more details see [41].

6.3 Hybrid FMT (H-FMT)

In this section we describe a novel MC architecture able to exploit the strong points of both SO-FMT and A-OFDM.

To motivate the use of such scheme we make the following observations. We have numerically found that over typical WLAN channels, A-OFDM and SO-FMT respectively experience an interference level which is in average 80 dB and 40 dB under the level of the useful signal (see Section 6.4). Besides, we note that in A-OFDM the analysis and the synthesis pulses are not matched. This causes a loss in SNR of a factor $M/(M+\beta)$ w.r.t. SO-FMT. Having said that, we observe that when the channel attenuation is high, and both systems are noise limited, the SINR (6.2) can be approximated with the SNR. Consequently, in such a case (supposing the OH of FMT shorter or equal to the CP of OFDM) the use of FMT gives an higher value of achievable rate than the one obtained with A-OFDM (see (6.1)). In other words, when the SNR is low it is better to use FMT than OFDM. On the contrary, when the channel attenuation is low, namely when the SNR is high, and both systems are interference limited, the SINR (6.2) can be approximated with the SIR. In such a case, the interference experienced by SO-FMT is higher than the one of A-OFDM and thus the use of SO-FMT gives lower achievable rate than A-OFDM. It is therefore justified the use of a hybrid architecture able to dynamically switch, according to the

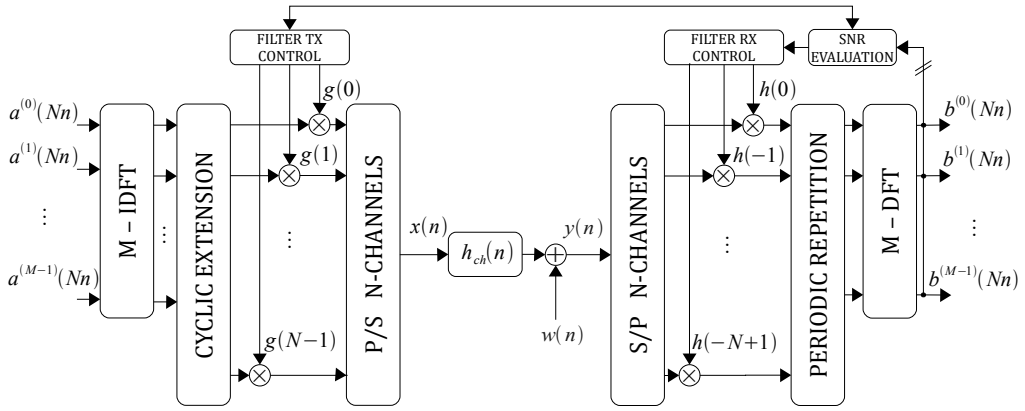

Figure 6.1: Hybrid FMT scheme.

channel condition, between SO-FMT and A-OFDM. We call such an architecture H-FMT.

We propose to implement the H-FMT using the efficient implementation of a modulated FB discussed in Chapter 3. Fig. 6.1 shows the H-FMT architecture. As we can see, at the transmitter the M data signals are processed by an M points IDFT. The N output samples from the cyclically extension, are multiplied by the coefficients $g(n)$, with $n = 0, \ldots, N-1$. $g(n)$ correspond to the prototype synthesis pulse coefficients of SO-FMT or A-OFDM. Finally, the outputs are parallel-to-serial converted. The receiver comprises the following operations. The signal is serial-to-parallel converted with a converter of size N. Depending on the modulation scheme used at the transmitter, namely SO-FMT or A-OFDM, the output signals are multiplied by the corresponding prototype analysis pulse coefficients $h(-n)$ with $n = 0, \ldots, N-1$. Then, the periodic repetition with period M of the block of coefficients of size N is applied. Finally, the M-point DFT is performed. Note that the A-OFDM analysis pulse has length M which is shorter than the pulse used for the synthesis stage with length N, but it can be considered with length N simply padding β zeros.

The choice about the usage of A-OFDM or SO-FMT (see Section 6.4) is made by the block SNR Evaluation. That is, depending on the experienced SNR, this block selects the appropriate modulation scheme and accordingly the TX and RX Controllers set the corresponding coefficients $g(n)$ and $h(n)$ at the

transmitter and at the receiver side. Note that the SNR evaluation can be done using OFDM with a CP longer than the channel duration. In this case the received signal results free of interference and the SINR (6.2) corresponds to the SNR. Furthermore, to adapt the system to the channel condition, the SNR evaluation is done periodically.

Taking into account that in SO-FMT only β coefficients of the prototype pulse differ from a constant, the complexity of this scheme is $(\alpha M \log M + \beta)/N$, and $(\alpha M \log M + 2\beta)/N$ operation per sample for the synthesis and the analysis stages respectively where the α factor takes into account the FFT implementation. Hence, the complexity of H-FMT is almost the same of the efficient implementation of OFDM which is $(\alpha M \log M)/N$ for both synthesis and analysis stages.

6.4 Numerical Results

To obtain numerical results, we have chosen the following system parameters that are essentially those of the IEEE 802.11 standard [3]. The MC system uses $M = 64$ sub-channels with a transmission bandwidth of 20 MHz. The signal is transmitted with a constant power spectral density (PSD) of -53 dBm/Hz. At the receiver side, we add white Gaussian noise with PSD equal to -168 dBm/Hz. Thus, the SNR, without path loss and fading, on each sub-channel is 115 dB. To show the performance of H-FMT, we use an OFDM baseline system which deploys a fixed CP of 0.8 μs ($\beta = 16$ samples), that is the value of CP employed in the IEEE 802.11 standard [3].

The H-FMT deploys SO-FMT with fixed OH of 0.4 μs ($\beta = 8$ samples, $N = 9/8M$), and A-OFDM with values of CP equal to $\mathbb{P}_{OFDM} = \{\beta_B^{(99\%)} = 0.4\mu s,\ \beta_C^{(99\%)} = 0.5\mu s,\ \beta_D^{(99\%)} = 0.6\mu s,\ \beta_E^{(99\%)} = 0.9\mu s,\ \beta_F^{(99\%)} = 1.1\mu s\}$ [38]. Both schemes use single tap zero forcing sub-channel equalization.

Fig. 6.2 shows the complementary cumulative distribution function (CCDF) of the achievable rate obtained using SO-FMT, A-OFDM, and the baseline system. For the sake of readability, we only show results for channel classes B, C, and D and for distances between transmitter and receiver equal to 10 m, 30 m, and 60 m. More results for the baseline OFDM and for A-OFDM can be found in

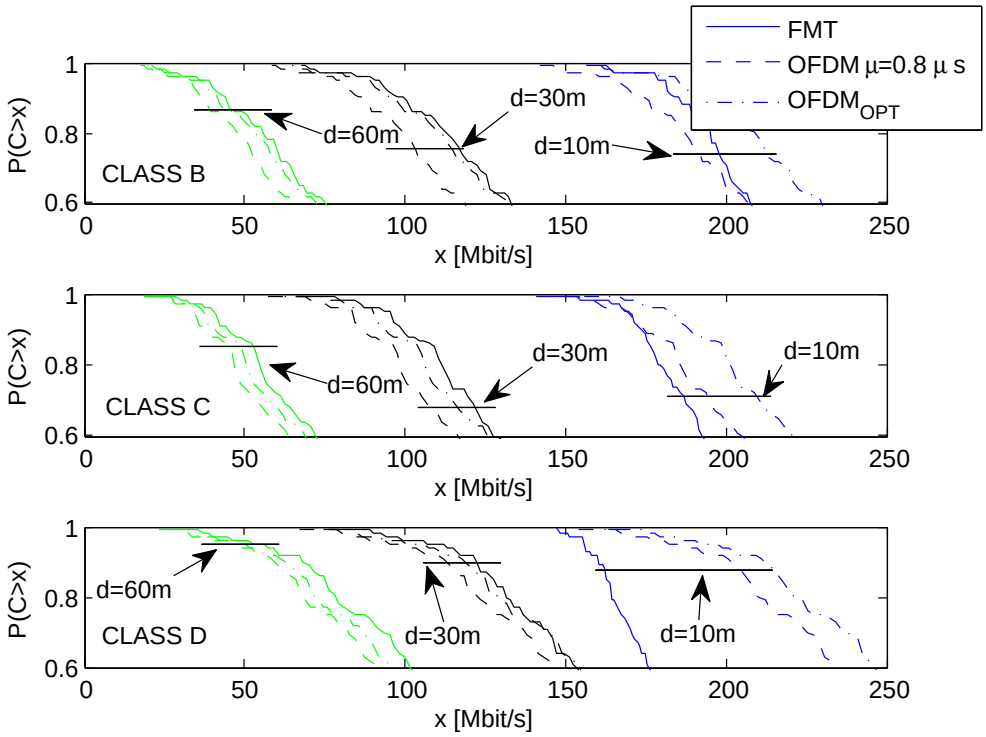

Figure 6.2: Achievable rate CCDF obtained using SO-FMT, A-OFDM, and OFDM with a fixed CP of 0.8 μs. The employed channel classes are the B,C, and D. The distance between transmitter and receiver is set to 10 m, 30 m, and 60 m.

[38]. From Fig. 6.2 we can observe how for high values of distance $d = \{30, 60\}m$, and thus in the low SNR region, the SO-FMT shows better performance than both A-OFDM and baseline OFDM. On the contrary, for a short distance of 10 m, A-OFDM is able to achieve higher rate than FMT. Although not shown, the results obtained with a distance of 3 m behave as the ones obtained with a distance of 10 m. From Fig. 6.2 we notice that with probability 0.9, the average gain obtained using SO-FMT and A-OFDM w.r.t. the baseline system is respectively of 17.3% and 8.3% at a distance of 60 m, of 13.4% and 8.7% at a distance of 30 m, and of -5% and 5% at a distance of 10 m.

In Fig. 6.3 we report the average SNR for each channel class and for distances between transmitter and receiver of 3 m, 10 m, 30 m, and 60 m. Each point

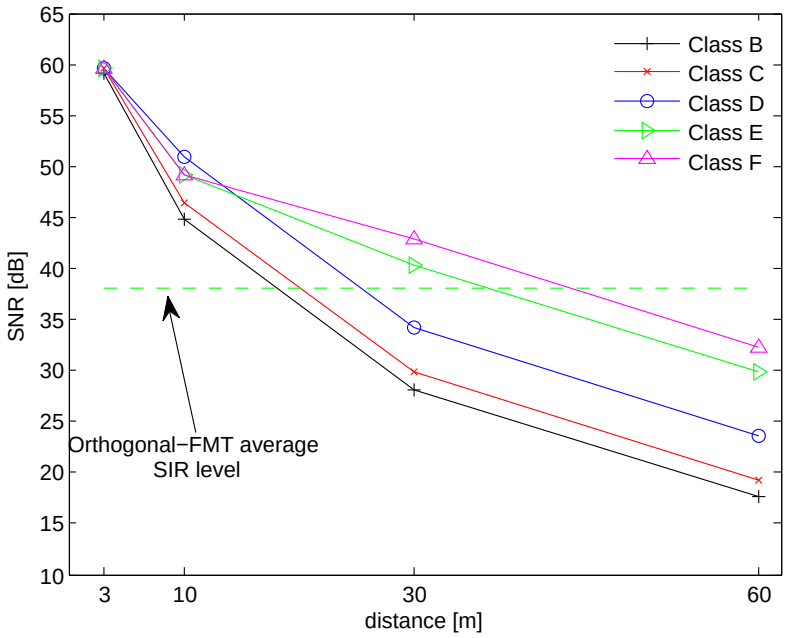

Figure 6.3: SNR and average SIR of SO-FMT as function of the distance.

has been computed as the ratio between the power of the transmitted signal attenuated by the average channel path loss, and the power of the noise. It is worth noting that the SNR experienced by SO-FMT corresponds to the showed one. Whereas, to obtain the SNR experienced by A-OFDM, we must lower the showed SNR of a factor $10log_{10}\left(M/(M+\beta)\right)$. For instance, for the highest used value of OH $\beta_F^{(99\%)} = 1.1\mu s$ (22 samples) we have to lower the SNR of Fig. 6.3 by 1.28 dB. Fig. 6.3 also shows the average SIR (averaged across all the channel classes and across all the distances) of the SO-FMT. Regarding A-OFDM, it always experiences a SIR that is several dBs higher than the one of SO-FMT.

Now the question is: *how does the system select the modulation to be used*? Looking at Fig. 6.3 and thus focusing of SO-FMT, we observe that when the SNR is higher than the SIR, the SINR (6.2) can be approximated by the SIR. Recalling that the SIR of A-OFDM is higher than that of SO-FMT, we deduce that is such a case is better to use A-OFDM than SO-FMT. Viceversa, when the SNR is lower than the SIR, the SINR (6.2) can be approximated by the SNR. Recalling that the SNR of A-OFDM is lower than that of SO-FMT, we deduce

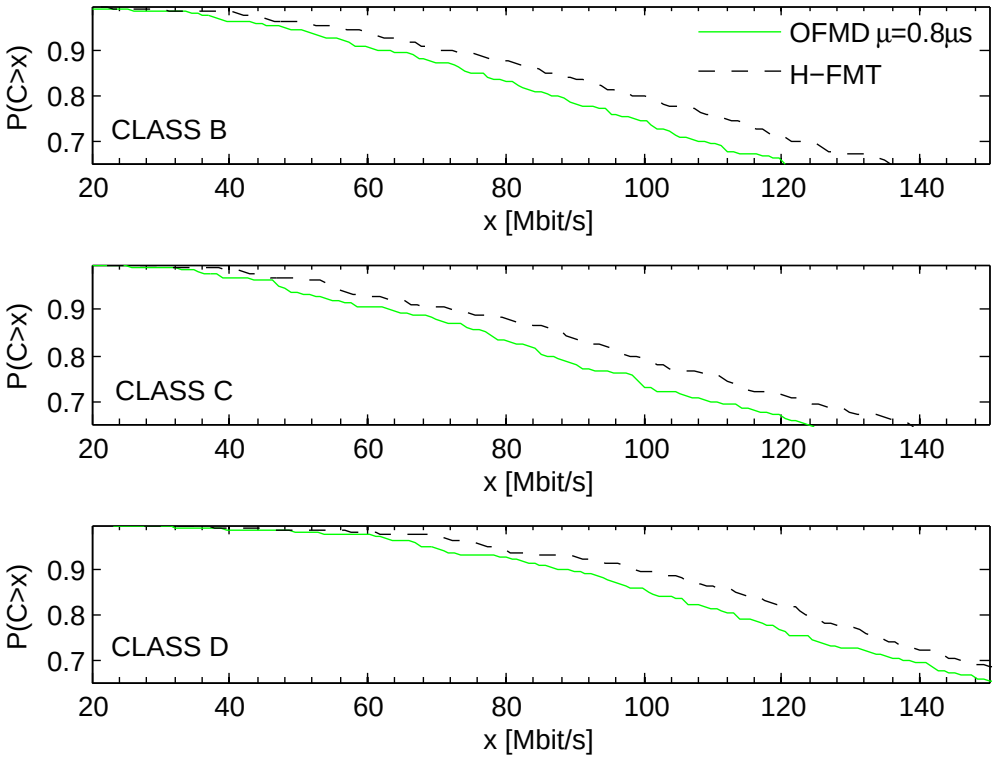

Figure 6.4: Achievable rate CCDF using H-FMT and OFDM with fixed CP equal to 0.8 μs for channel class B, C, and D.

that in such a case is better to use SO-FMT than A-OFDM.

Summarizing, when the SNR is below the SIR line of Fig. 6.3 it is convenient to use SO-FMT. Otherwise, we use A-OFDM.

Fig. 6.4 shows the achievable rate CCDF for the baseline system and for H-FMT. The simulated channel classes are the B, C, and D. For each class, the curves are computed considering random distances from the set $\{3, 10, 30, 60\}m$. We notice that with probability 0.9, H-FMT provides gains in achievable rate of $\{16\%, 15\%, 12\%\}$ w.r.t. OFDM for channel classes B, C, and D respectively. More precisely, with probability 0.9, for channel classes B, C, and D, OFDM exceeds $\{60, 64, 85\}Mbit/s$, while H-FMT exceeds $\{72, 74, 98\}Mbit/s$.

Finally, looking at Fig. 6.2, it should be noted that also if not explicitely highlighted before, the achievable rate CCDF of H-FMT for each distance and

for each class corresponds to the right most curve.

6.5 Conclusions

We have investigated the use of adaptive FB modulation over WLAN channels and proposed a hybrid architecture based on the use of adaptive OFDM and FMT with minimal length pulses. H-FMT provides significant achievable rate gains over OFDM with a static CP and it has marginal increased complexity.

Chapter 7

MIMO FMT with PSVD Precoding

7.1 Introduction

Multiple-input multiple-output (MIMO) channels arise in several scenarios in communications since they improve the capacity compared to a single-input single-output (SISO) channel. Many scenarios where the MIMO concept can be applied are present in several context such as in wireless application where multiple antenna transceivers are adopted, or in powerline systems when data are transmitted exploiting the phases of the electrical grid. Filter bank systems themselves can also be described as MIMO systems.

More specifically in this chapter we focus on the wireless scenario where MIMO transmission exploits multiple antennas. With this approach, wireless MIMO systems are able to exploit the spatial diversity of the channel to achieve throughput levels that are much higher than those achieved with single antenna realizations.

Under the availability of the full channel state information (FSI) at the transmitter and the receiver, several different precoding and equalization methods have been proposed in order to cope with the interference created by the MIMO spatial channel [42]. In this chapter we consider precoding for broadband channels that introduce inter-symbol (ISI). For this scenario, a precoding approach has been proposed in [43]. It is based on the singular value decomposition (SVD) of polynomial matrices (PSVD) which it is also referred to as broadband SVD

(BSVD). PSVD can be implemented with the algorithm proposed in [44].

To limit the residual interference introduced by the ISI channel, it was proposed in [45] to concatenate the PSVD decomposition stage with a further precoder and equalizer stage. This technique is characterized by high computational complexity that is $O(L^3)$ where L is the order of the channel, or equivalently the channel length in number of taps.

To address this limitation, in this chapter we analyze the possibility of combining the PSVD decomposition of the broadband MIMO channel with a filter bank (FB) modulation transmission system. As explained in Chapter 2, the FB modulator, divides the broadband channel in many narrow band sub-channels. This renders each sub-channel less frequency selective and therefore, less dispersive in time.

Thus, if each FB sub-channel is not affected by inter-channel interference, it will be possible to apply the PSVD on each sub-channel. This allows one to reduce the complexity of the PSVD algorithm since it operates at sub-channel level which has a length shorter than that of the broadband channel.

In this chapter, we consider both OFDM and FMT. Due to the cyclic prefix (CP), OFDM can cancel the interference, however, paying a price in terms of a decrement of signal-to-noise ratio at the receiver since the receiver FB is not matched to the transmitter one contrarily to FMT. However, while precoding in MIMO OFDM can be based on the SVD of the channel, precoding in MIMO FMT requires the PSVD of the channel since it exhibits some inter-symbol interference.

This chapter is organized as follows: in Section 7.2-7.3 we discuss the PSVD decomposition applied to a broadband channel. In Section 7.4, we describe the design of the MIMO FB with the PSVD. The evaluation of the capacity (under a uniform power distribution) is discussed in Section 7.5, while in Section 7.6 we report numerical results for typical WLAN channels, and finally, in Section 7.7 the conclusions are given.

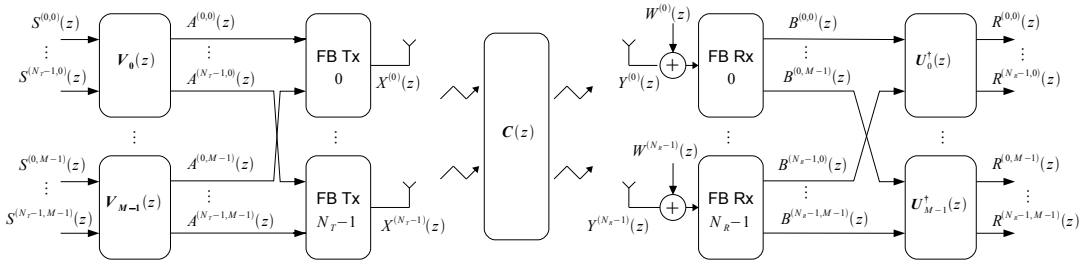

Figure 7.1: MIMO FB transceiver with sub-channel precoder and equaliser based on the a polynomial SVD of the channel matrix.

7.2 Polynomial SVD-Based Precoding and Equalisation

We consider a general linear time invariant (LTI) MIMO channel with N_T transmit and N_R receive antennas which is characterised by an $N_R \times N_T$ matrix of impulse response

$$\mathbf{c}(n) = \begin{bmatrix} c_{1,1}(n) & \cdots & c_{1,N_T}(n) \\ \vdots & \ddots & \vdots \\ c_{N_R,1}(n) & \cdots & c_{N_R,N_T}(n) \end{bmatrix}, \tag{7.1}$$

where $c_{i,k}(n)$ represents the finite channel impulse response between the kth transmit and the ith receive antennas. This channel matrix in (7.1) can also be written as

$$\mathbf{c}(n) = \sum_{\ell=0}^{L_c-1} \mathbf{c}_\ell \, \delta(n-\ell), \tag{7.2}$$

where $\delta(n)$ is the Kronecker function, L_c is the channel order, and the matrix $\mathbf{c}_\ell \in \mathbb{C}^{N_R \times N_T}$ contains the ℓth time slice of the FIR MIMO channel, i.e. $\mathbf{c}_\ell = \mathbf{c}[\ell]$. The z-transform of $\mathbf{c}(n)$, denoted by $\mathbf{C}(z) = Z\{\mathbf{c}(n)\} \in \mathbb{C}^{N_R \times N_T}(z)$, is a polynomial matrix of size $N_R \times N_T$ and order $L_c - 1$. Mathematically, $\mathbf{C}(z)$ can

be written as

$$\mathbf{C}(z) = \sum_{n=0}^{L_c-1} \mathbf{c}_n \; z^{-n} \quad . \tag{7.3}$$

In analogy to optimal processing of narrowband MIMO systems by means of an SVD [46], [43] and [45] a precoding and equalization design for a single carrier transceiver is proposed, which exploits the polynomial SVD (PSVD) in order to decouple a broadband MIMO system matrix into $\min\{N_T, N_R\}$ independent SISO subchannels. The PSVD of the polynomial channel matrix yields

$$\mathbf{C}(z) = \mathbf{U}(z)\mathbf{\Sigma}(z)\mathbf{V}^{\dagger}(z), \tag{7.4}$$

where $\mathbf{V}_i^{\dagger}(z) = \mathbf{V}_i^H(1/z^*)$ denotes the parahermitian operation, and $\mathbf{U}(z) \in \mathbb{C}^{N_R \times N_R}(z)$ and $\mathbf{V}(z) \in \mathbb{C}^{N_T \times N_T}(z)$ are paraunitary matrices. Paraunitary matrices fulfill $\mathbf{U}(z)\,\mathbf{U}^{\dagger}(z) = \mathbf{I}_{N_R}$, where $\mathbf{I}_{N_R}$ is the $N_R \times N_R$ identify matrix.

We assume that the MIMO system possesses a number of receive antennas greater or equal to the number of transmit antennas, $N_R \geq N_T$, and that the channel $\mathbf{C}(z)$ has no common zeros across all its transfer functions $Z\{c_{i,k}(n)\}$, $i = 0 \cdots (N_T - 1)$. In such a case, the polynomial matrix $\mathbf{\Sigma}(z) \in \mathbb{C}^{N_R \times N_T}(z)$ can be written as

$$\mathbf{\Sigma}(z) = \begin{bmatrix} \tilde{\mathbf{\Sigma}}(z) \\ \mathbf{0}_{(N_R - N_T) \times N_T} \end{bmatrix}, \tag{7.5}$$

where we define the diagonal matrix $\tilde{\mathbf{\Sigma}}(z) = \mathrm{diag}\{\Sigma_0(z), \cdots, \Sigma_{N_T-1}(z)\}$, and $\mathbf{0}_{A \times B} \in \mathbb{C}^{A \times B}$ as a matrix with zero entries.

Using the matrix $\mathbf{V}(z)$ as a filter bank precoder and $\mathbf{U}^{\dagger}(z)$ as an equalizer matrix, the equivalent overall MIMO channel is decoupled into N_R independent subchannels, canceling co-channel interference. It is worth noting that this type of precoding and equalization is not designed to remove ISI, and dispersive subchannels with transfer functions $\Sigma_i(z)$ remain [45]. As a drawback, the computational complexity of the PSVD approach is of order $O(L_C^3)$ and can be prohibitive.

The remaining ISI caused by the frequency selective channels $\Sigma_i(z)$, can be addressed employing a modulated FB system on each antenna. If the number of sub-channels, M, approaches infinity, the equivalent sub-channel MIMO impulse responses are no longer time dispersive. However, in feasible implementations M might not be large enough and the equivalent sub-channel response could be still time dispersive.

We propose an architecture based on the use of a PSVD decomposition on each FB sub-channel to address both the inter-antenna interference and the inter-symbol interference. This approach has a lower computational complexity w.r.t the single carrier case, since the equivalent MIMO sub-channel impulse response is much shorter than the broadband MIMO channel.

7.3 Sequential Best Rotation Algorithm

In [44] a generalization of the Eigenvalue Decomposition Algorithm (EVD) for polynomial matrices has been presented, and it has been referred to as Sequential Best Rotation Algorithm (SBR2). The input of the SBR2 algorithm is a para-Hermitian polynomial matrix $\mathbf{R}(z)$. Thus, the SBR2 algorithm compute a paraunitary matrix $\mathbf{H}(z)$ such that

$$\mathbf{H}(z)\mathbf{R}(z)\mathbf{H}^{\dagger}(z) \approx \mathbf{\Lambda}(z), \tag{7.6}$$

where $\mathbf{\Lambda}(z)$ is a diagonal polynomial matrix. In general a perfect diagonalization is not always achieved, since the paraunitary matrix $\mathbf{H}(z)$ contains a set of finite order polynomials. However, if the order of the polynomials is sufficiently large, the approximation is negligible.

The decomposition after L iterations is based on a paraunitary matrix $\mathbf{H}_L(z)$ defined as

$$\mathbf{H}_L(z) = \prod_{i=0}^{L-1} \mathbf{G}_i(z), \tag{7.7}$$

where we defined the ith elementary paraunitary matrix $\mathbf{G}_i(z)$ as

$$\mathbf{G}_i(z) = \mathbf{Q}_i^{(j,k)}(\theta, \phi)\mathbf{B}_i^{(k,t)}(z).$$

$\mathbf{Q}_i^{(j,k)}(\theta, \phi)$ is a Jacobi rotation matrix defined as

$$\mathbf{Q}_i^{(j,k)}(\theta,\phi) = \begin{bmatrix} 1 & 0 & & \overset{j-th}{\downarrow} & \cdots & \overset{k-th}{\downarrow} & & 0 \\ 0 & \ddots & & & & & & \\ & & cos(\theta) & \cdots & sin(\theta)e^{j\phi} & & & \leftarrow j-th \\ \vdots & & & \ddots & & & & \\ & & sin(\theta)e^{j\phi} & \cdots & cos(\theta) & & & \leftarrow k-th \\ & & & & & & \ddots & \\ 0 & & & \cdots & & & & 1 \end{bmatrix}$$

and $\mathbf{B}_i^{(k,t)}(z)$ is the delay matrix which is paraunitary of the form

$$\mathbf{B}_i^{(k,t)}(z) = \mathbf{I} - \mathbf{u}_i\mathbf{u}_i^H + z^{-t}\mathbf{u}_i\mathbf{u}_i^H$$

where $\mathbf{u}_i = [0 \cdots 0\ 1\ 0 \cdots 0]$ is a vector containing zeros except for a unit element at the kth position. It results that $\mathbf{B}_i^{(k,t)}(z)$ is an identity matrix with the i-th diagonal element replaced by a delay z^{-t}.

The SBR2 generates a paraunitary matrix according to (7.7) in L iterations. Each stage of the iterative process applies a single elementary paraunitary matrix with parameters θ, ϕ, t, $j$and k appropriately chosen to eliminate the dominant off-diagonal polynomial coefficient. This is analogous to a single step of the Jacobi algorithm deployed for Hermitian matrices.

After the final iteration the para-hermitian matrix $\mathbf{R}(z)$ can be written as

$$\mathbf{R}(z) = \mathbf{H}(z)(\mathbf{\Lambda}(z) + \mathbf{E}(z))\mathbf{H}^\dagger(z) \tag{7.8}$$

with $\mathbf{\Lambda}(z)$ diagonal. The $\mathbf{E}(z)$ matrix takes into account the error due to the finite iteration process. SBR2 allows for setting of an iteration stop criteria by

choosing a threshold coefficient. The iteration process continues until the magnitude of the dominant off-diagonal coefficient is under the selected threshold.

In general the MIMO broadband channel is represented by a rectangular matrix since the number of transmitting antennas differ from the number of receiving antennas. The SBR2 algorithm can be exploited to attain a SVD decomposition simply by noting that

$$\mathbf{A}(z) = \mathbf{C}(z)\mathbf{C}^{\dagger}(z) = \mathbf{U}(z)\mathbf{\Sigma}(z)\mathbf{\Sigma}^{\dagger}(z)\mathbf{U}^{\dagger}(z)$$
$$\mathbf{B}(z) = \mathbf{C}^{\dagger}(z)\mathbf{C}(z) = \mathbf{V}(z)\mathbf{\Sigma}(z)\mathbf{\Sigma}^{\dagger}(z)\mathbf{V}^{\dagger}(z)$$

Thus, the SBR2 algorithm can be applied twice on the squared matrices $\mathbf{A}(z)$ and $\mathbf{B}(z)$ from we can derive the matrices $\mathbf{U}(z)$ and $\mathbf{V}(z)$, since the matrix $\mathbf{\Sigma}(z)\mathbf{\Sigma}^{\dagger}(z)$ is diagonal .

7.4 Precoded MIMO FB Modulation System

In this section we describe the proposed MIMO system model considering N_T antennas at the transmitter and N_R antennas at the receiver. The general scheme is depicted in Fig. 7.1.

7.4.1 MIMO FB Modulation Transmitter

The signal transmitted on the αth antenna is here denoted as $x^{(\alpha)}(n)$, which is obtained by the transmission FB (FB Tx) depicted in Fig. 7.2 filtering M data streams with equal statistical power M_a at low symbol rate

$$x^{(\alpha)}(n) = \sum_{k=0}^{M-1} \sum_{\ell \in \mathbb{Z}} a^{(\alpha,k)}(\ell)\; g^{(k)}(n - N\ell) \quad . \tag{7.9}$$

Applying the z-transform to (7.9) we obtain

$$X^{(\alpha)}(z) = \sum_{k=0}^{M-1} A^{(\alpha,k)}(z^N)\; G^{(k)}(z), \quad , \tag{7.10}$$

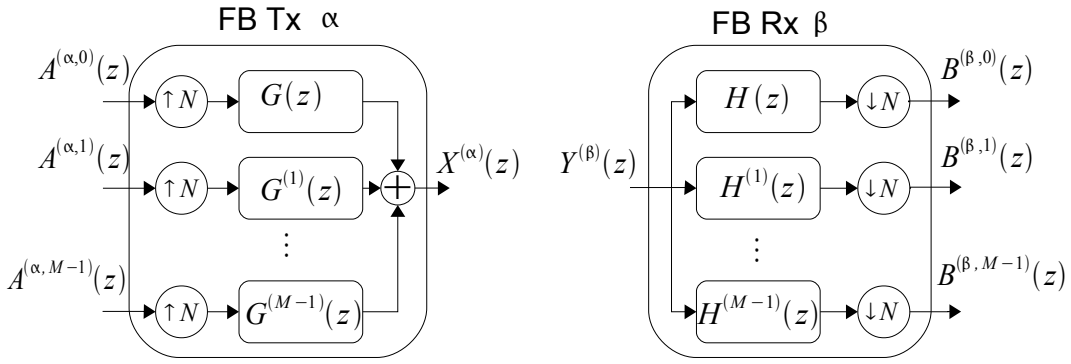

Figure 7.2: Synthesis FB providing the signal for the αth transmit antenna, and analysis FB operating on the βth receive antenna.

where M is the number of the transmitter sub-channels, and N is the interpolation factor to obtain transmit signals operated at N times the symbol rate. According to (7.10), the M symbol rate data streams $A^{(k)}(z)$ are upsampled by a factor N and then filtered by pulses $G^{(k)}(z) = G(z\, e^{-j\frac{2\pi}{M}k})$ which are modulated versions of a prototype pulse with transfer function $G(z)$. Thereafter, the sub-channel streams are summed and transmitted.

7.4.2 MIMO Precoding

The N_T streams at the kth input of each FMT system are obtained as

$$\mathbf{A}^{(k)}(z) = \mathbf{V}_k(z)\, \mathbf{S}^{(k)}(z), \tag{7.11}$$

where $\mathbf{A}^{(k)}(z) \in \mathbb{C}^{N_T \times 1}(z)$ denotes the N_T-element vector of transmit signals $A^{(\alpha,k)}(z)$ associated with the kth FMT sub-channel. The vector $\mathbf{S}^{(\alpha,k)}(z) \in \mathbb{C}^{N_T \times 1}(z)$ contains N_T signals $S^{(\alpha,k)}(z) = Z\{s^{(\alpha,k)}(n)\}$ where $s^{(\alpha,k)}(n)$ are spatially and temporally uncorrelated symbols belonging to a constellation set such as QAM with zero mean and variance σ_s^2. The polynomial precoder matrix $\mathbf{V}_k(z) \in \mathbb{C}^{N_T \times N_T}(z)$ defined in (7.4) as the polyphase synthesis matrix of a filter

bank of order L_v

$$\mathbf{V}_k(z) = \sum_{n=0}^{L_v-1} \mathbf{v}_{k,n}\, z^{-n} \quad , \tag{7.12}$$

which comprises of FIR filters whose nth time slide is given by $\mathbf{v}_{k,n} \in \mathbb{C}^{N_T \times N_T}$.

The N_T transmitted signals $X^{(\alpha)}(z)$ are sent over the MIMO channel $\mathbf{C}(z) \in \mathbb{C}^{N_R \times N_T}(z)$, whose transfer function is defined in (7.3).

7.4.3 MIMO FB Modulation Receiver

The received signal at the βth antenna denoted by $Y^{(\beta)}(n)$ is affected by additive white Gaussian noise $W^{(\beta)}(z)$, and processed by an analysis FB (FB Rx) whose outputs are

$$B^{(\beta,i)}(z) = \mathscr{C}_N \left[(Y^{(\beta)}(z) + W^{(\beta)}(z)) H^{(i)}(z) \right] \quad , \tag{7.13}$$

where we define the periodic repetition operation

$$\mathscr{C}_N[P(z)] = \frac{1}{N} \sum_{k=0}^{N-1} P(z^{1/N} e^{j\frac{2\pi}{N}k}) \quad . \tag{7.14}$$

According to (7.13), the signal $Y^{(\beta)}(z)$ is filtered by the modulated filters $H^{(i)}(z) = H(z\, e^{-j\frac{2\pi}{M}i})$, where $H(z)$ is the prototype pulse of the analysis bank.

7.4.4 MIMO Equalization

The ith outputs of the FMT receivers are processed by the equalization matrix $\mathbf{U}_i^{\dagger}(z) \in \mathbb{C}^{N_R \times N_R}(z)$ as

$$\mathbf{R}^{(i)}(z) = \mathbf{U}_i^{\dagger}(z)\, \mathbf{B}^{(i)}(z), \tag{7.15}$$

where $\mathbf{B}^{(i)}(z) \in \mathbb{C}^{N_R \times 1}(z)$ denotes a vector containing the N_R signals $B^{(\beta,i)}(z)$ associated with the ith FMT sub-channels and the βth receiver antenna. The vector $\mathbf{R}^{(\beta,k)}(z) \in \mathbb{C}^{N_R \times 1}(z)$ contains the N_R output signals $R^{(\beta,i)}(z)$. The equal-

izer matrix $\mathbf{U}_i(z) \in \mathbb{C}^{N_T \times N_T}$ is defined in (7.4) as a filter bank with polyphase analysis matrix of order L_u

$$\mathbf{U}_i(z) = \sum_{n=0}^{L_u-1} \mathbf{u}_{i,n}\, z^{-n}, \tag{7.16}$$

whose nth time slice is given by $\mathbf{u}_{k,n} \in \mathbb{C}^{N_T \times N_T}$.

7.5 Capacity

In this section we define the signal to interference plus noise ratio (SINR) and the capacity, that are used to evaluate the performance of the proposed system.

We consider the received signal at the βth antenna and the ith sub-channel $R^{(\beta,i)}(z)$ which can be written in the time domain as

$$r^{(\beta,i)}(n) = \underbrace{g_{\mathrm{EQ}}^{(\beta,i)}(0)\, s^{(\beta,i)}(n)}_{\mathrm{USE}^{(\beta,i)}(n)} + \underbrace{\sum_{\ell \neq n} g_{\mathrm{EQ}}^{(\beta,i)}(n-\ell)\, s^{(\beta,i)}(\ell)}_{\mathrm{ISI}^{(\beta,i)}(n)} + w^{(\beta,i)}(n) \quad , \tag{7.17}$$

where $g_{\mathrm{EQ}}^{(\beta,i)}(n)$ is the equivalent impulse response between the output $r^{(\beta,i)}(n)$ and the input $s^{(\alpha,k)}(n)$, $\mathrm{USE}^{(\beta,i)}(n)$ is the useful signal, $\mathrm{ISI}^{(\beta,i)}(n)$ the inter-symbol interference (ISI), and $w^{(\beta,i)}(n)$ the noise component. In (7.17), we assume that inter-carrier interference (ICI) is negligible, which is true for FMT in good approximation due to the very short spectral support of the pulses. For OFDM, it is assumed that the CP is sufficiently long to neglect ICI.

Assuming stationarity, the SINR experienced at the ith sub-channel and at the βth antenna can be written as

$$\mathrm{SINR}^{(\beta,i)} = \left(\frac{1}{\mathrm{SNR}^{(\beta,i)}} + \frac{1}{\mathrm{SIR}^{(\beta,i)}} \right)^{-1} \quad , \tag{7.18}$$

where in (7.18) we define the signal to noise ratio (SNR) and the signal to interference ratio (SIR) respectively as $\mathrm{SNR}^{(\beta,i)} = P_{\mathrm{USE}}^{(\beta,i)} / P_w^{(\beta,i)}$ and $\mathrm{SIR}^{(\beta,i)} =$

$P_{\mathrm{US}}^{(\beta,i)}/P_{\mathrm{ISI}}^{(\beta,i)}$, where we denote the average powers of the useful signal, the interference, and the noise respectively as $P_{\mathrm{USE}}^{(\beta,i)} = E\{|\mathrm{USE}^{(\beta,i)}[0]|^2\}$, $P_{\mathrm{ISI}}^{(\beta,i)} = E\{|\mathrm{ISI}^{(\beta,i)}[0]|^2\}$, and $P_N^{(\beta,i)} = E\{|w^{(\beta,i)}[0]|^2\}$, where $E\{\cdot\}$ is the expectation operator.

The average power of the useful signal and the ISI component can be expressed in the frequency domain as

$$P_{\mathrm{USE}}^{(\beta,i)} = P_s \left| \int_{-.5}^{.5} G_{\mathrm{EQ}}^{(\beta,i)}(e^{j2\pi f}) df \right|^2 \tag{7.19}$$

and

$$P_{\mathrm{ISI}}^{(\beta,i)} = P_s \left(\int_{-.5}^{.5} \left| G_{\mathrm{EQ}}^{(\beta,i)}(e^{j2\pi f}) \right|^2 df - \left| \int_{-.5}^{.5} G_{\mathrm{EQ}}^{(\beta,i)}(e^{j2\pi f})\, df \right|^2 \right), \tag{7.20}$$

where $G_{EQ}^{(\beta,i)}(z) = Z\{g_{EQ}^{(\beta,i)}(n)\}$, the power of the transmitted data symbols is denoted as P_s, and f represents normalized frequency relative to a sampling rate $f_{\mathrm{s}} = 1$.

The system performance that we present in the following sections is based on the information capacity of the system. For this purpose, we assume parallel Gaussian channels and statistically independent Gaussian distributed input signals, which render interferences also Gaussian (cf. e.g. [35]). Furthermore, by applying single tap zero forcing equalization, the capacity in [bit/s] for a given channel is

$$C(\beta) = \frac{B}{N} \sum_{\beta=0}^{N_R-1} \sum_{i=0}^{M-1} \log_2 \left(1 + \mathrm{SINR}^{(\beta,i)}(\beta) \right) \quad , \tag{7.21}$$

where B is the transmission bandwidth in Hz.

7.6 Numerical Results in WLAN Channel

In this section we present numerical results for the capacity of the proposed system when using either FMT or OFDM over typical WLAN channels.

7.6.1 Channel Model and Transmission Parameters

For our simulations, we adopt the IEEE 802.11 TGn channel model described in [18].

We assume the following system parameters. The transceiver has $N_T = 2$ transmitting and $N_R = 2$ receiving antennas. The transmit antennas are spaced by one wavelength of the highest frequency component, while the receive antennas are spaced at half that distance. [3]. The FB system uses $M = 64$ sub-channels with a transmission bandwidth of 20 MHz. In the following we set the level of the transmitted signal PSD mask to -53 dBm/Hz, which represents the total power transmitted by the N_T antennas. The receiver side experiences additive white Gaussian noise with a PSD equal to -168 dBm/Hz.

To show the performance of the proposed systems, we use an OFDM system which uses a fixed CP of 0.8 μs ($N = 80$, $\beta = N - M = 16$ samples), which is the CP value employed by the IEEE 802.11n standard [3]. The FMT system is derived from a root raised cosine (RRC) prototype pulse filter with length $L_g = 24N$, roll-off $\rho = 0.2$, and a sampling interpolation factor equal to $N = 80$. The analysis FMT pulses in the receiver are matched to the synthesis pulses used in the Rx FB. Both system use single-tap sub-channel equalization.

7.6.2 Simulation Results

For the class C and E models detailed in Sec. 7.6.1, large ensembles of random channel realizations for distances of 10m and 60m between Tx and Rx arrays have been simulated. For these ensembles, Fig. 7.3 and Fig. 7.4 show the complementary cumulative distribution functions (CCDF) for the system capacity. It is interesting to note that with probability 0.9, MIMO-FMT provides a capacity increase of 15% and 6% for class C over MIMO-OFDM for distances of 10m and 60m, respectively. While for class E, MIMO-FMT achieves a 7% ad-

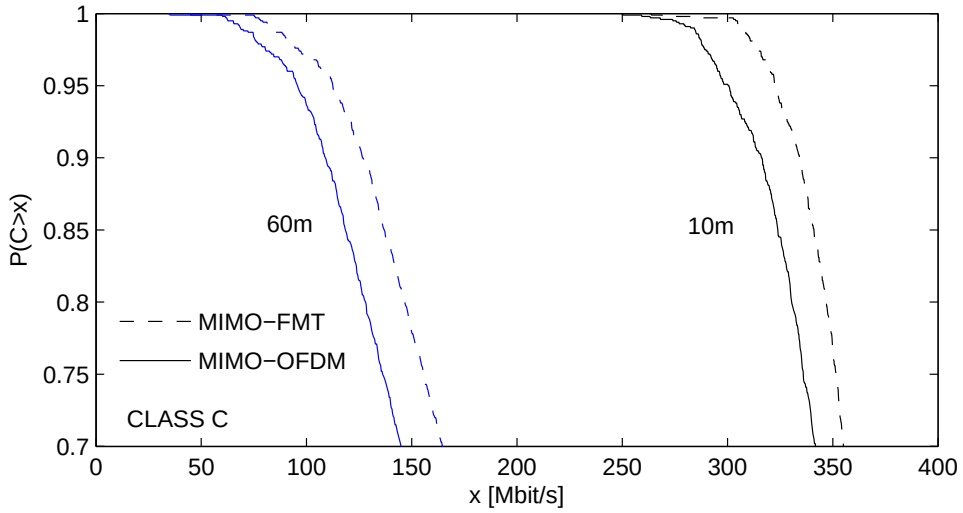

Figure 7.3: Complementary cumulative distribution function (CCDF) of the capacity considering a 2×2 antennas system using MIMO-FMT and MIMO-OFDM over an IEEE80.11TGn class C channel model.

vantage over MIMO-OFDM for the 60m distance. At the shorter distance of 10m, the advantage is reversed, and MIMO-OFDM achieves a 13% advantage over MIMO-FMT.

MIMO-OFDM provides an advantage in the case of channel class E for the shorter 10m distance, where the low path-loss provides relatively high SNR and the ISI dominates the performance of MIMO-FMT. While dispersive, the channel is however sufficiently short for OFDM to suppress all inter-block and inter-carrier interferences with its sufficiently long CP. In the cases where the SNR is not too high, MIMO-FMT gains from employing matched filtering for a superior performance in noise.

Although not reported, improved performance in FMT can be achieved with linear sub-channel equalization to better suppress the residual sub-channel ISI.

7.7 Conclusions

In this paper we have presented a MIMO transceiver based on FB modulation systems with PSVD precoding. In particular, we have considered two types of

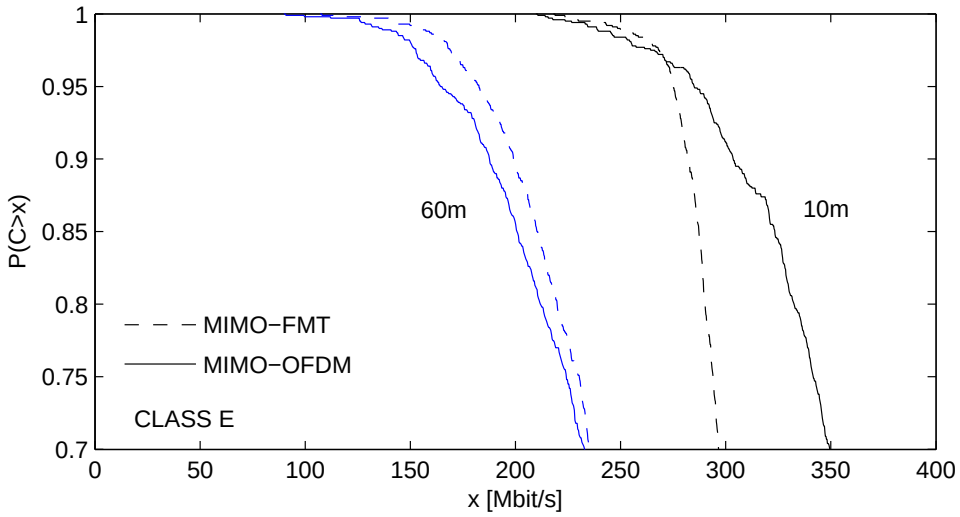

Figure 7.4: Complementary cumulative distribution function (CCDF) of the capacity considering a 2×2 antennas system using MIMO-FMT and MIMO-OFDM over an IEEE802.11TGn class E channel model.

FB which deploy either time confined prototype pulses (OFDM) or frequency confined prototype pulses (FMT). We have shown the performance in terms of capacity of the considered systems in typical WLAN channels. MIMO-FMT can afford higher capacity compared to MIMO-OFDM only in certain conditions, in particular when the power level of the noise at the receiver is higher than the power level of the interferences. At high SNRs, MIMO-OFDM is the best option because due to the CP it can cope with limit imposed by the interference.

Chapter 8

Analysis of Phase Noise in Modulated FB Systems

8.1 Introduction

Oscillators are one of the cores in a transceiver architecture since they are deployed in the RF for translating in frequency the signal of interest. Noise is a major concern in oscillators, because by introducing even a small noise into an oscillator leads to dramatic changes in frequency and timing properties. This phenomenon, peculiar to oscillators, is known as phase noise or time jitter. An ideal oscillator would have a localized tone at certain a frequency, but any corrupting noise spreads this perfect tone, resulting in high power level of neighboring frequency. This effect is the major contributor to undesired phenomena such as inter-channel interference leading to increased bit error rate (BER) in communications. Considerable effort was expended to understand phase noise and to develop a consistent analytical treatment and a coherent model suitable for the communication research.

Several authors studied phase noise in OFDM applications using different models. In [47] the critical effect of phase noise on OFDM was pointed out by using a model based on a non-stationary Wiener random process. On the other hand several authors modeled phase noise as a stationary, finite-power process [48], [49]. In addition, the assumption of low amplitude phase noise renders

simplified the analytical treatment.

In this chapter we study the effect of phase noise due to non ideal oscillators in filter bank (FB) modulation systems. In particular, we analyze the FMT (Filtered Multitone) system and the OFDM (Orthogonal Frequency Division Multiplexing) system that is also referred to as orthogonal frequency division multiplexing (OFDM).

Although FB modulation systems are robust to channel frequency selectivity, they are sensitive to fast channel time variations [20], as well as to carrier frequency offsets and phase noise (PN). An extensive literature exists on the performance analysis of multicarrier systems in the presence of phase noise, e.g., [48]-[52]. However, at the best of our knowledge, most of the work considers the OFDM scheme where the phase noise introduces a phase shift on the signal of interest often referred to as CPE, as well as inter-channel (ICI) interference due to the loss of sub-channel orthogonality. In [48]-[49] the authors focus on the CPE effects and analyze the performance considering a one-tap equalizer. In [50] the ICI component is also considered and an approach for its mitigation is proposed. Some early work on the capacity comparison between OFDM and FMT in the presence of PN was done in [51] although it was limited to simulation results. Preliminary error rate comparisons of OFDM and FMT with PN were reported in [52].

In this chapter, we provide a general framework to the analysis of the CPE and the interference components, i.e., the inter-symbol interference (ISI) and the ICI, in FB modulation. We focus the analysis on the FMT and OFDM systems. We propose approximated expressions of the symbol error rate for M-PSK and M-QAM constellations with both a non-coherent and a one-tap coherent receiver (equalizer), using a stationary model for the PN impairment process and under the Gaussian interference assumption. Several simulation results are reported to validate the theoretical results.

This chapter is organized as follows. In Section 8.2, we describe the system model. In Section 8.3, we study the CPE. In Section 8.4, we compute the power of the ISI plus ICI as a function of the system parameters. In Section 8.5, the symbol error rate is studied, while numerical results are reported in Section 8.6. Then, the conclusions follow.

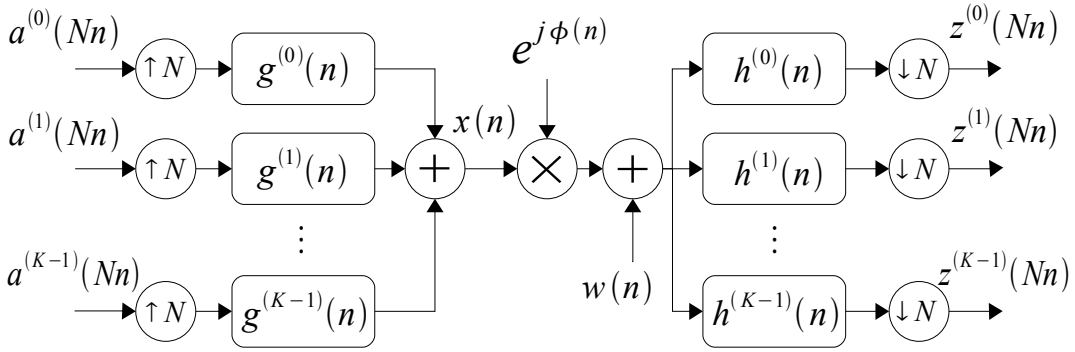

Figure 8.1: Filter bank modulation scheme including the phase noise

8.2 Filter Bank Modulation Scheme

We consider a FB scheme as depicted in Fig. 8.1 where the discrete-time transmitted signal at the output of the synthesis FB, $x(n)$, reads is obtained by the modulation of K data streams at low rate $a^{(k)}(Nn)$, with $k \in \{0, \cdots, K-1\}$, that belong to a constellation signal set, e.g., PSK or QAM. The transmitted signal can be written as

$$x(n) = \sum_{k=0}^{K-1} \sum_{\ell \in \mathbb{Z}} a^{(k)}(N\ell) g^{(k)}(n - N\ell), \tag{8.1}$$

The phase noise introduces a multiplicative distortion $\omega(n) = e^{j\phi(n)}$ to the transmitted signal $x(n)$, where the random process $\phi(n)$ is the phase noise whose statistical model is defined below. We furthermore consider an ideal propagation media to better understand the impact of the phase noise process on a FB system. The received signal is passed through an analysis FB with pulses $h^{(k)}(n)$. The sub-channel outputs of the FB are sampled by a factor N. If we define the equivalent (time variant) impulse response between the input sub-channel k and the output sub-channel i as $g_{eq}^{(i,k)}(Nm, N\ell) = \sum_n g^{(k)}(n - N\ell) h^{(\hat{k})}(Nm - n)\omega(n)$,

the analysis FB signal output, for sub-channel i, can be written as

$$\begin{aligned} z^{(i)}(Nm) &= g_{eq}^{(i,i)}(Nm, Nm)\, a^{(\hat{k})}(Nm) \\ &+ \sum_{\ell\in\mathbb{Z},\, \ell\neq m} a^{(i)}(N\ell) g_{eq}^{(i,i)}(Nm, N\ell) \\ &+ \sum_{k=0,\, k\neq i}^{K-1} \sum_{\ell\in\mathbb{Z}} a^{(k)}(N\ell) g_{eq}^{(i,k)}(Nm, N\ell) + w^{(i)}(Nm) \\ &= S^{(i)}(Nm) + I^{(i)}(Nm) + w^{(i)}(Nm), \end{aligned} \tag{8.2}$$

where the signal of interest is denoted with $S^{(i)}(Nm)$ (first term in (8.2)), while the inter-symbol plus inter-channel interference is denoted with $I^{(i)}(Nm)$ (second and third term in (8.2)). The interference is a function of both the prototype pulse and the phase-noise process. Furthermore, $w^{(i)}(Nm)$ is the additive Gaussian noise contribution.

The phase noise process $\phi(n)$ can be assumed to be a stationary Gaussian process with zero mean and periodic power spectral density (PSD)

$$R_\phi(f) = \sum_{n\in\mathbb{Z}} \hat{R}_\phi(f-n), \tag{8.3}$$

$$\hat{R}_\phi(f) = 10^{-c_\phi} + \begin{cases} 10^{-a_\phi} & |f| \leq f_{\phi_1} \\ 10^{-(|f|-f_{\phi_1})\frac{b_\phi}{f_{\phi_2}-f_{\phi_1}}-a_\phi} & |f| \geq f_{\phi_1}, \end{cases}$$

according to the model already used in [48], [52]. This PSD model allows us to describe a wide class of commercial oscillators. The coefficient c_ϕ determines the noise floor, while b_ϕ defines the slope, a_ϕ and f_{ϕ_1} establishes the white phase noise region, and finally f_{ϕ_2} is the frequency where the noise floor is dominant (Fig. 8.2a). If we assume the PN variance σ_ϕ^2 to be small, i.e., $\sigma_\phi^2 << 1$, the term $\omega(n)$ can be rewritten using Taylor series expansion as

$$\omega(n) = e^{j\phi(n)} \approx 1 + j\phi(n). \tag{8.4}$$

With this approximation that we use throughout this chapter, $\omega(n)$ can be

assumed to be stationary with PSD

$$R_\omega(f) = \sum_n \delta(f-n) + R_\phi(f)$$

and correlation

$$r_\omega(n_1 - n_2) = E[\omega(n_1)\omega^*(n_2)]$$

that is obtained via the inverse Fourier transform of the periodic PSD $R_\omega(f)$. Thus, there is a straightforward relation between the processes $\phi(n)$ and $\omega(n)$.

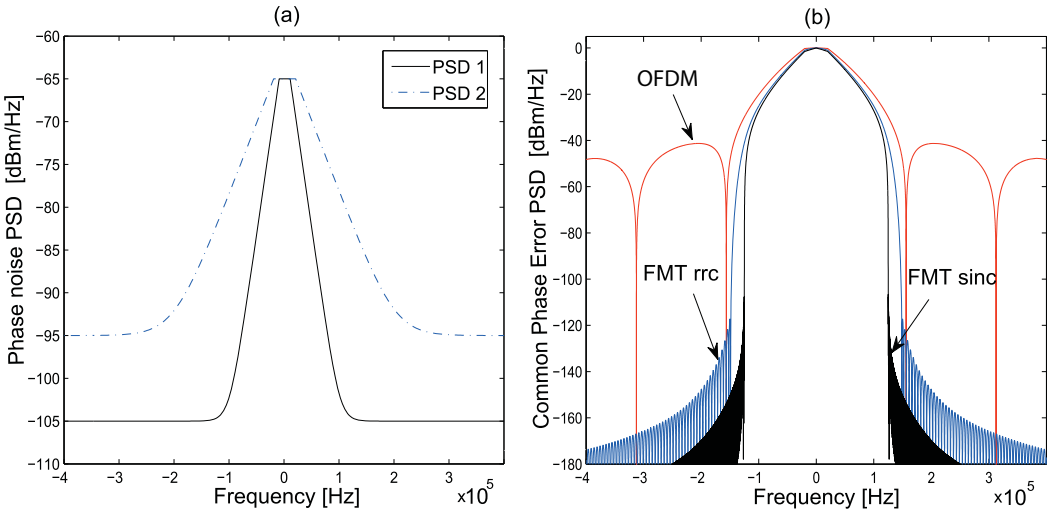

Figure 8.2: (a) - Phase noise PSD models with system transmission bandwidth $B = 10\,MHz$. PSD 1 has parameters $f_1 B = 10\ kHz$, $f_2 B = 100\,kHz$, $a = 6.5$, $b = 4$ and $c = 10.5$; PSD 2 has parameters $f_1 B = 20\ kHz$, $f_2 B = 200\ kHz$, $a = 6.5$, $b = 3$ and $c = 9.5$. (b) - PSD of the CPE considering OFDM and FMT, and the PSD 2 model. The parameters are $K = 64$, $N = 80$, and the rrc filter has a roll off factor 0.2 and length $L_g = 12N$.

8.3 Common Phase Error Analysis

In the signal of interest $S^{(i)}(Nm)$ in (8.2), the transmitted data symbol $a^{(i)}(Nm)$ is weighted by the factor

$$g_{eq}^{(i,i)}(Nm, Nm) = \sum_{n} g(n - Nm)\omega(n)h(Nm - n).$$

We denote the phase of this weighting factor with

$$\Theta(Nm) = \angle(g_{eq}^{(i,i)}(Nm, Nm)),$$

and we refer to it as *Common Phase Error* (CPE) [48] since it is identical for all the sub-channels. The CPE introduces a random phase rotation on the transmitted symbols. In this section, we analyze the CPE as a function of the prototype pulse deployed in the FB.

Assuming the model in (8.4) and with

$$\sum_{n} g(n)h(-n) = 1,$$

we can approximate the data symbol weighing factor as

$$g_{eq}^{(i,i)}(Nm, Nm) \approx 1 + j \sum_{n} g(n - Nm)h(Nm - n)\phi(n). \tag{8.5}$$

Furthermore, since (exploiting the Taylor series expansion of the $arctan(\cdot)$ function)

$$\Theta(Nm) \approx \Im[g_{eq}^{(i,i)}(Nm, Nm)],$$

we obtain

$$\Theta(Nm) \approx \sum_{n \in \mathbb{Z}} g(n - Nm)h(Nm - n)\phi(n). \tag{8.6}$$

Finally, the weighting factor can be approximated as

$$g_{eq}^{(i,i)}(Nm, Nm) \approx 1 + j\Theta(Nm) \approx e^{j\Theta(Nm)}$$

Now, if we define $g_-(n) = g(-n)$, the CPE is obtained by the convolution of the PN process with the pulse $g_-(n)\ h(n)$, i.e.,

$$\Theta(Nm) = \left[(g_-\ h)\ * \phi\right](Nm),$$

where $*$ denotes convolution. It follows that the PSD of the CPE can be written as

$$\begin{aligned} R_\Theta(f) &= \sum_{n=0}^{N-1} \hat{R}_\Theta(f - \frac{n}{N}), \\ \hat{R}_\Theta(f) &= |(G_- * H)(f)|^2\ R_\phi(f), \end{aligned} \tag{8.7}$$

where we denote with $G_-(f)$ and $H(f)$ the discrete time Fourier transform (DTFT) of the pulses $g_-(n)$ and $h(n)$, e.g.,

$$F[h(n)] = H(f) = \sum_n h(n) e^{-j2\pi f n}.$$

For certain choices of the prototype pulse, it is possible to derive (8.7) in closed form. For example, if we consider the OFDM system with K sub-channels and with cyclic prefix (CP) of length $N - K$ samples, the synthesis/analysis prototype pulses are

$$\begin{aligned} g(n) &= \frac{1}{\sqrt{K}} rect(n/N) \\ h(n) &= \frac{1}{\sqrt{K}} rect(-n/K), \end{aligned}$$

where we recall that we defined the rectangular function as $rect(n/K) = 1$ for $n \in \{0, \cdots, K-1\}$, and as 0 elsewhere. Since

$$g_-(n)h(n) = \frac{1}{K} rect(-n/K),$$

and considering that the DTFT of $rect(n/K)$ is equal to

$$F[rect(n/K)] = e^{-j\pi f(K-1)} \frac{sin(\pi f K)}{sin(\pi f)},$$

$\hat{R}_\Theta$ in (8.7) can be rewritten as

$$\hat{R}_\Theta^{OFDM}(f) = \left| \frac{1}{K} \frac{sin(\pi f K)}{sin(\pi f)} \right|^2 R_\phi(f). \tag{8.8}$$

Analogously, considering an FMT system deploying a root raised cosine (rrc) prototype pulse [37], with K sub-channels and oversampling factor N, we have that (8.7) can be written as

$$\hat{R}_\Theta^{FMT,rrc}(f) = \left| F[rrc^2\left(\frac{n}{N}\right)] \right| \tag{8.9}$$

The DTFT of the square of the rrc pulse in (8.9) cannot be expressed in a closed form except when the roll-off factor is set to 0, i.e., when the rrc pulse corresponds to the sinc pulse defined as

$$sinc(n) = \frac{sin(\pi n)}{\pi n}.$$

In such a case the prototype pulses are

$$g(n) = h(-n) = \frac{1}{\sqrt{N}} sinc(n/N).$$

Now, the DTFT of

$$g_-(n)h(n) = \frac{1}{N} sinc^2(n/N)$$

is equal to

$$F[\frac{1}{N} sinc^2(n/N)] = \sum_{k\in\mathbb{Z}} \Lambda(Nf - k)$$

where we have defined the triangle function as

$$\Lambda(f) = \begin{cases} 1 - |f| & \text{if} \quad |f| < 1, \\ 0 & \text{elsewhere} \end{cases}$$

Thus, for the FMT system deploying a sinc prototype pulse $\hat{R}_\Theta$ in (8.7) is equal to

$$\hat{R}_\Theta^{FMT,sinc}(f) = |\sum_{k\in\mathbb{Z}} \Lambda(Nf - k)|^2 \, R_\phi(f). \tag{8.10}$$

The analysis of (8.10) reveals that the PSD $\hat{R}_\Theta^{FMT,sinc}$ is perfectly set to zero outside the normalized band $2/N$, differently from $\hat{R}_\Theta^{OFDM}$ in (8.8) where the white component of the phase noise gives a contribution to the CPE power. In Fig. 8.2b, we report the PSD of the CPE for both OFDM and FMT, and we show that FMT has higher rejection to the CPE due to the sub-channel frequency confinement. As an example, we evaluate the CPE power derived from (8.7) with $K = \{64, 256, 1024\}$, $N = 5/4K$, and the PSD 2 model of Fig. 8.2a. The CPE power, in dB, is respectively equal to $\{-16.1, -19.5, -25.2\}$ for OFDM, $\{-17.0, -21.2, -27.3\}$ for FMT deploying a rrc pulse with roll-off factor 0.2 and filter length $L_g = 12N$, and $\{-17.4, -21.8, -27.8\}$ for FMT deploying a sinc pulse. The advantage of FMT w.r.t. OFDM in terms of coping with the CPE gets larger as the number of sub-channels increases.

8.4 Analytical Evaluation of the ISI and ICI Power

We now evaluate the power of the signal of interest and of the interference components defined in (8.2). We assume the data symbols to be i.i.d. with zero mean, with average power σ_a^2, and the model in (8.4) for $\omega(n)$ so that the received signal (8.2) is stationary. Thus, the total average power of the received

signal at time instant $Nm = 0$ for sub-channel of index i, reads

$$M_z^{(i)} = \sigma_a^2 \sum_{k=0}^{K-1} \sum_{\ell \in \mathbb{Z}} E[|g_{eq}^{(i,k)}(0, N\ell)|^2]. \tag{8.11}$$

Since it results that

$$g_{eq}^{(i,k)}(0, N\ell) = \sum_n g^{(k)}(n - N\ell) h^{(i)}(-n) \omega(n),$$

if we define the product filter response

$$gh^{(i,k)}(N\ell, n) = g^{(k)}(n - N\ell) h^{(i)}(-n),$$

we will obtain the following relation

$$\begin{aligned} E[|g_{eq}^{(i,k)}(0, N\ell)|^2] = & \sum_{n_1, n_2 \in \mathbb{Z}} gh^{(i,k)}(N\ell, n_1) r_\omega(n_1 - n_2) \\ & \times gh^{(i,k)^*}(N\ell, n_2). \end{aligned} \tag{8.12}$$

If we separate the power of the signal of interest from the power of the interference terms, we can write $M_z^{(i)} = M_S + M_I$ where

$$\begin{aligned} M_S &= E[|S^{(i)}(0)|^2] \\ &= \sigma_a^2 E[|g_{eq}^{(i,i)}(0,0)|^2] = \sigma_a^2 (1 + \sigma_\phi^2) \approx \sigma_a^2 \end{aligned} \tag{8.13}$$

$$\begin{aligned} M_I = E[|I^{(i)}(0)|^2] = & \sigma_a^2 \sum_{\ell \in \mathbb{Z},\, \ell \neq 0} E[|g_{eq}^{(i,i)}(0, N\ell)|^2] \\ & + \sigma_a^2 \sum_{k=0,\, k \neq i}^{K-1} \sum_{\ell \in \mathbb{Z}} E[|g_{eq}^{(i,k)}(0, N\ell)|^2]. \end{aligned} \tag{8.14}$$

It should be pointed out that in the presence of phase noise, the OFDM system suffers of only inter-channel interference (ICI), while the FMT system is predominantly affected by inter-symbol interference (ISI) due to its frequency confined pulses. Furthermore, given the symmetry of the prototype pulses and of

the phase noise PSD, the power of the signal of interest and of the interference is the same for all sub-channel indices. We can therefore define the average sub-channel signal-to-noise plus interference ratio as

$$SINR = \frac{M_S}{M_I + M_w},$$

where $M_w = \sigma_w^2$ is the power of the additive noise component in the sub-channel.

8.5 Error Rate Analysis in the Presence of Phase Noise

In this section we discuss the symbol error rate (SER) assuming two different types of receivers. Firstly, we consider a *non-coherent receiver* (NCR) that assumes no knowledge of the data symbol weighting factor, and uses the following decision metric for sub-channel i

$$\hat{a}^{(i)}(Nm) = \arg\min_{a \in A} ||z^{(i)}(Nm) - a||^2, \tag{8.15}$$

where the symbol alphabet is denoted with A.

Secondly, we consider a one-tap equalizer where, on the contrary, we take into account the perfect knowledge of the data symbol weighting factor using the decision metric

$$\hat{a}^{(i)}(Nm) = \arg\min_{a \in A} ||z^{(i)}(Nm) - g_{eq}^{(i,i)}(Nm, Nm)a||^2. \tag{8.16}$$

We refer to this receiver as the *one-tap coherent receiver* (CR). The weighting factor (related to the CPE) can be in practice estimated, for instance, with the method proposed in [48] for OFDM.

To proceed, the received signal can be approximated as

$$z^{(i)}(Nm) \approx a^{(i)}(Nm)e^{j\Theta(Nm)} + I^{(i)}(Nm) + w^{(i)}(Nm), \tag{8.17}$$

since $g_{eq}^{(i,i)}(Nm, Nm) \approx e^{j\Theta(Nm)}$ as discussed in Section 8.3. Furthermore, we

assume the interference to be Gaussian distributed, which holds true for a large number of interference components. These assumptions allow us to obtain quasi-closed form expressions for the SER of M-PSK and M-QAM that are in good agreement with simulation results.

8.5.1 Symbol Error Rate Analysis for the Non-Coherent Receiver (NCR)

1) SER conditioned by the CPE for M-PSK with the NCR
As it is proved in the Appendix C, for 4-PSK modulation the SER conditioned by Θ with the NCR, under the Gaussian approximation for the interference, is given by

$$P_e^{(4PSK)}(\Theta) = 1 - \left(1 - Q\left(\sqrt{SINR}\, sin(\frac{\pi}{4} + \Theta)\right) \times \left(1 - Q\left(\sqrt{SINR}\, cos(\frac{\pi}{4} + \Theta)\right)\right)\right), \tag{8.18}$$

where $Q(x) = 1 - \Phi(x)$ and $\Phi(x)$ is the the normalized Gaussian cumulative distribution function.

For M-PSK modulation, with $M > 4$, the conditional SER with the NCR can be approximated as (see the Appendix C).

$$P_e^{(MPSK)}(\Theta) \approx Q\left(\sqrt{SINR}\, sin(\frac{\pi}{M} - \Theta)\right) + Q\left(\sqrt{SINR}\, sin(\frac{\pi}{M} + \Theta)\right). \tag{8.19}$$

2) SER conditioned by the CPE for M-QAM with the NCR
Assuming M-QAM square constellations with data symbols

$$c_{i,k} = (2i - 1 - \sqrt{M}) + j(2k - 1 - \sqrt{M}) \quad \text{with} \quad (i,k) \in \{1, \cdots, \sqrt{M}\},$$

and the NCR, the probability to correctly receive a symbol, conditioned by the

CPE Θ, is (see the Appendix D)

$$\begin{aligned} P_c^{(QAM)}(\Theta) = & \sum_{i=2}^{S}\sum_{k=2}^{S}\frac{4}{M}\left[\Phi(\lambda\, R_{i,k}) - Q(\lambda\, L_{i,k})\right] \\ & \times \left[\Phi(\lambda\, U_{i,k}) - Q(\lambda\, D_{i,k})\right] \\ & + \sum_{i=2}^{S}\frac{4}{M}\Phi(\lambda\, U_{i,1})\left[\Phi(\lambda\, R_{i,1}) - Q(\lambda\, L_{i,1})\right] \\ & + \sum_{k=2}^{S}\frac{4}{M}\Phi(\lambda\, R_{1,k})\left[\Phi(\lambda\, U_{1,k}) - Q(\lambda\, D_{1,k})\right] \\ & + \frac{4}{M}\Phi(\lambda\, U_{1,1})\Phi(\lambda\, R_{1,1}), \end{aligned} \tag{8.20}$$

where

$$\begin{aligned} S &= \sqrt{M}/2 \\ \lambda &= \sqrt{\frac{3\,SINR}{2\,(M-1)}} \end{aligned}$$

and

$$\begin{aligned} R_{i,k} &= \left|\Re\left[c_{i,k}e^{j\Theta} - (c_{i,k}+1)\right]\right| \\ L_{i,k} &= \left|\Re\left[c_{i,k}e^{j\Theta} - (c_{i,k}-1)\right]\right| \\ U_{i,k} &= \left|\Im\left[c_{i,k}e^{j\Theta} - (c_{i,k}+j)\right]\right| \\ D_{i,k} &= \left|\Im\left[c_{i,k}e^{j\Theta} - (c_{i,k}-j)\right]\right|. \end{aligned}$$

The conditional SER for M-QAM is therefore

$$P_e^{(QAM)}(\Theta) = 1 - P_c^{(QAM)}(\Theta).$$

Average SER with the NCR

The average SER with the NCR is obtained from the conditional SER of M-PSK or M-QAM as follows

$$P_e = \int_{-\infty}^{+\infty} P_e(\theta) f_\Theta(\theta)\, d\theta, \tag{8.21}$$

where $f_\Theta(\theta)$ is the probability density function of Θ. Since Θ is a sum of several Gaussian components, as shown by (8.6), we assume it to be Gaussian distributed with zero mean and variance

$$\sigma_\Theta^2 = \int_{-1/2N}^{1/2N} R_\Theta(f) df,$$

where $1/N$ is the normalized sub-channel transmission band. The average SER in (8.21), then is obtained via numerical integration.

8.5.2 Symbol Error Rate Analysis for the One-Tap Coherent Receiver (CR)

We now consider the CR decision metric. Since in Section 8.3 we have shown that the signal weighting factor can be approximated as

$$g_{eq}^{(i,i)}(Nm, Nm) \approx e^{j\Theta(Nm)},$$

according to the model in (8.4), then its amplitude is constant, i.e.,

$$|g_{eq}^{(i,i)}(Nm, Nm)| \approx 1,$$

and the coherent receiver perfectly compensates the phase of the signal of interest. Therefore, the average SER can be simply computed using conventional formulas for the SER in AWGN [37] provided that we approximate the interference as a Gaussian process and we use the SINR defined in Section 8.4.

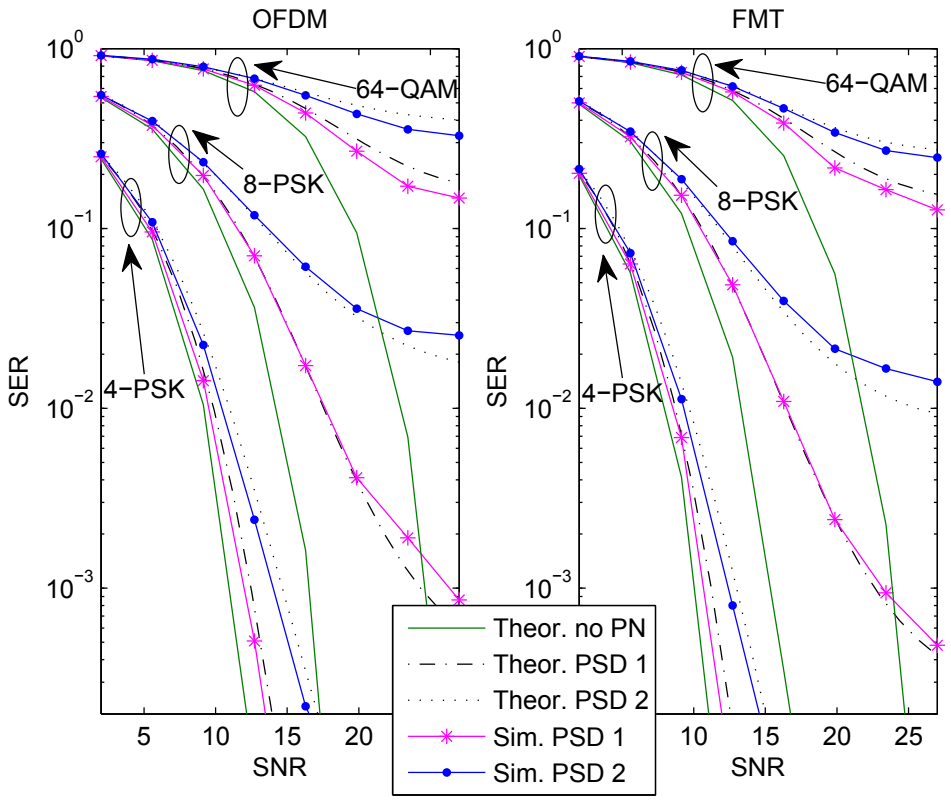

Figure 8.3: SER for OFDM and FMT with the non-coherent receiver, with $B = 10\ MHz$, $K = 64$ and $N = 80$ ($CP = 16$). Both simulation and theoretical results, from (8.19) and (8.20), are shown.

8.6 Numerical Results

We compare the OFDM and the FMT system in the presence of phase noise in terms of SER as a function of the $SNR = \sigma_a^2/\sigma_w^2$. We consider 4-PSK, 8-PSK, and 64-QAM constellations. We assume an overall transmission bandwidth equal to $B = 10\,MHz$, $K = 64$ sub-channels, and an interpolation/sampling factor $N = 80$. The pulses used in OFDM are $g(n) = \frac{1}{\sqrt{K}} rect(n/N)$ and $h(n) = \frac{1}{\sqrt{K}} rect(-n/K)$. The FMT system deploys a root-raised-cosine pulse ($g(n) = h(-n) = rrc(n/N)$) with roll-off factor 0.2 and number of coefficients $L_g = 12N$. The two systems have identical data rate.

Fig. 8.3 reports the Montecarlo simulation results and the theoretical SER curves using the NCR decision metric and with the phase noise PSD 1 or PSD

2 of Fig. 8.2a. In Fig. 8.4, we consider the CR with the same PN PSD models. The results show that the theoretical performance curves are close to those obtained via simulations, which proves that the proposed approximation for the received signal, including the Gaussian assumption for the ISI/ICI, allows us to predict the SER. Phase noise introduces a SER degradation which is more pronounced for high order constellations, and clearly, for the PSD 2 that is associated to heavier PN. Furthermore, the FMT system has better performance compared to the OFDM system, i.e., it has higher capability to cope with the PN, for all the PN PSD models considered, due to its higher sub-channel spectral containment. Furthermore, OFDM with cyclic prefix has a small SNR loss since the receiver FB is not matched to the transmitter FB. Fig. 8.4 shows that the CR can correct the distortion due to the CPE and therefore it yields better performance than the NCR which is close to the performance in the absence of PN. Although both systems suffer of the presence of interference components, in FMT the interference power is dominated by the ISI, while in OFDM by the ICI. Therefore, sub-channel equalization can in principle be useful to improve the SER performance in FMT .

8.7 Conclusion

We have analyzed the effect of phase noise on filter bank transmission systems. In particular, we have considered the OFDM and the FMT systems and reported a general analysis of the distortion due to the CPE and the interferences using a stationary model for the PN impairment process. We have considered a non-coherent and a one-tap coherent receiver where the first receiver assumes no knowledge of the CPE, while the second receiver assumes it perfectly known. The theoretical and simulation results are in good agreement and show that FMT, with a root-raised-cosine prototype pulse, has better performance than OFDM with both receivers. The compensation of the CPE yields significant improvements w.r.t. the non-coherent receiver.

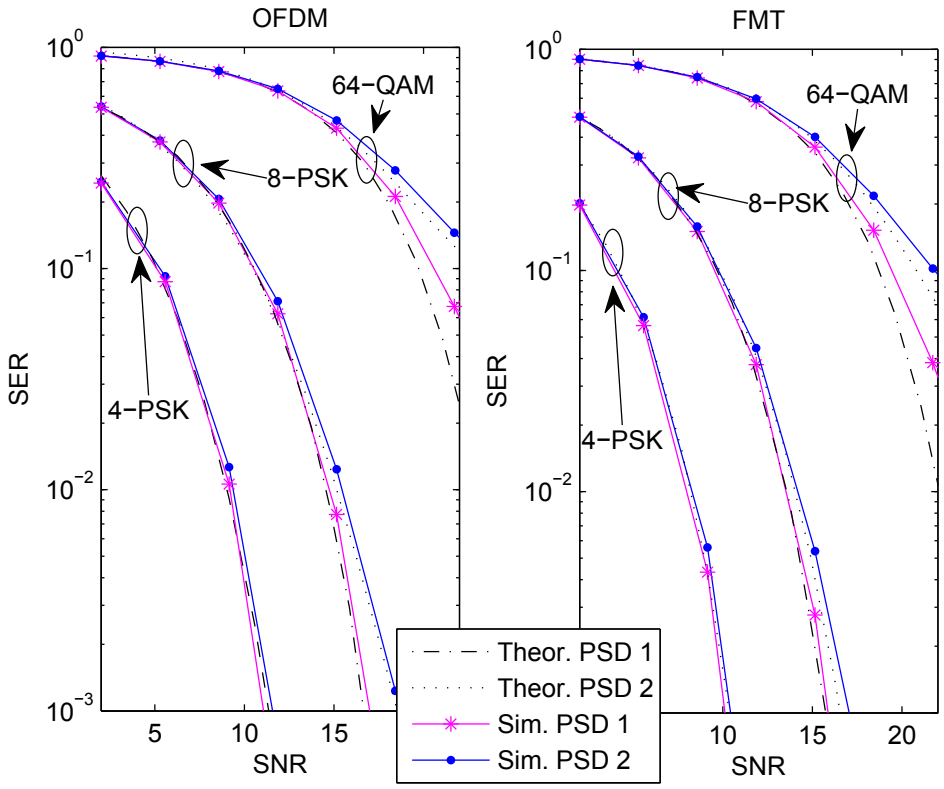

Figure 8.4: SER for OFDM and FMT with the single tap coherent receiver, with $B = 10\ MHz$, $K = 64$ and $N = 80$ ($CP = 16$). Both simulation and theoretical results are shown.

Chapter 9

Conclusions

In this thesis, modulated filter bank (FB) have been considered. We have introduced a notation based on operators that enables us to derive the efficient FB realizations exploiting a unique framework in the time domain. We compared three efficient realizations of the FB modulation system. We have shown that these implementations have the same complexity in terms of complex operations, and similar memory requirements, but they are different in terms of hardware implementation and matrix representation due to a different polyphase FB structure.

By starting from one of the efficient realization discussed in Chapter 3, we have considered the design of an orthogonal FMT system exploiting the matrix structure of this realization (the method in [13]). This allows us to derive a method that considerable simplifies the design of the orthogonal prototype pulse for certain choices of the parameters and for an arbitrarily large number of sub-channels. This scheme is referred to as orthogonal FMT or short-orthogonal FMT (SO) when minimal length pulses are used. Several examples of pulses with minimal length have been reported and the performance of the system in typical wireless multi-path fading channels has been shown. The comparison with a conventional truncated root-raised-cosine and with IOTA pulses has shown that the designed pulses yield significant improved robustness to multi-path fading. Furthermore, the comparison with cyclically prefixed OFDM using the IEEE 802.11 WLAN class B channel has shown that FMT outperforms OFDM, yet

having similar complexity.

We then have considered orthogonal FMT with minimal length pulses designed in Chapter 4, in conjunction with an MMSE frequency domain equalizer to cope with the ICI, and a DFE equalizer to cope with the residual inter symbol interference. Numerical results have shown that orthogonal FMT has the potentiality to improve the capacity in the WLAN scenario compared to OFDM, in particular when the distance between the transceivers is large, so that the SNR is low. For shorter distances, FMT can also attain high capacity due to the frequency domain equalizer, but this achievement is paid in terms of an increment of computational complexity.

We have then investigated the use of adaptive FB modulation over WLAN channels and proposed a hybrid architecture based on the use of adaptive OFDM (AOFDM) and SO-FMT, herein referred to as hybrid FMT (H-FMT). H-FMT provides significant achievable rate gains over OFDM with a static CP and it has marginal increased complexity.

We have also considered the multiple antenna communication scenario, and we have presented a multiple-input multiple-output (MIMO) transceiver based on FB modulation with precoding designed according to the polynomial singular value decomposition (PSVD). In particular, we have considered two types of FB transceiver, namely OFDM and FMT. We have shown their performance in terms of capacity in typical WLAN channels. MIMO-FMT can afford higher capacity compared to MIMO-OFDM only in certain conditions, in particular when the power level of the noise at the receiver is higher than the power level of the interferences. At high SNRs, MIMO-OFDM performs better because the CP lower the interference.

Finally, we have analyzed the effect of phase noise on FB transmission systems by considering ODFM and FMT. We here reported a general analysis of the distortion due to the CPE and the interferences using a stationary model for the PN impairment process. We have considered a non-coherent and a one-tap coherent receiver where the first receiver assumes no knowledge of the CPE, while the second receiver assumes it perfectly known. The theoretical and simulation results are in good agreement and show that FMT with a truncated root-raised-cosine prototype pulse, has better performance than OFDM with both receivers.

The compensation of the CPE yields significant improvements w.r.t. the non-coherent receiver.

Future activities related to the work presented in this thesis may include the development of further simplified algorithms for the design of orthogonal prototype pulse with arbitrary length in terms of number of samples. Moreover, the study of the hardware impairments on filter banks has been confined to only the phase noise effect. Nevertheless, it would be also worth considering other limitations such as the non-linearity distortion due to the amplifier adopted by transceivers in telecommunications.

Appendix A

Efficient Implementation Using Siclet et al. Method

In this appendix we derive the Method B proposed by Cvetković et al. in [14], and more recently by Siclet, Siohan, Pinchon in [15] and by McGee in [16].

A.1 Synthesis Bank (Method B)

The sub-channel pulse $g^{(k)}$ can be obtained from its A-type M_1 order polyphase decomposition as follows

$$g^{(k)}(n) = \sum_{i=0}^{M_1-1} \tau^{-i} \left[\mathcal{I}_{M_1}[\, g_i^{(k)}] \right] (n) \tag{A.1}$$

$$g_i^{(k)}(M_1 n) = g(M_1 n + i) W_M^{-k(M_1 n+i)} = g_i(M_1 n)\, W_M^{-ki} \ , \tag{A.2}$$

where g_i is the i-th polyphase decomposition of order M_1 of the synthesis prototype pulse.

Using this result the signal at the synthesis FB (8.1) can be written as

$$x = \sum_{k=0}^{M-1} \left[\mathcal{I}_N[a^{(k)}] \ * \ \sum_{i=0}^{M_1-1} \tau^{-i}[\mathcal{I}_{M_1}[g_i]] \ W_M^{-ki} \right] \tag{A.3}$$

$$= \sum_{i=0}^{M_1-1} \left[\mathcal{I}_N \left[\sum_{k=0}^{M-1} a^{(k)} \ W_M^{-ki} \right] \ * \ \tau^{-i}[\mathcal{I}_{M_1}[g_i]] \right] \ . \tag{A.4}$$

Let us define $A^{(i)}$ the M-point IDFT of the signal $a^{(k)}$. Then, since $M_1 = M_0 N$ we obtain

$$x = \sum_{i=0}^{M_1-1} \left[\mathcal{I}_N[A^{(i)}] \ * \ \tau^{-i}[\mathcal{I}_{M_0 N}[g_i]] \right] \tag{A.5}$$

$$= \sum_{i=0}^{M_1-1} \tau^{-i} \left[\mathcal{I}_N[A^{(i)}] \ * \ \mathcal{I}_{M_0 N}[g_i] \right] \qquad \text{(using (3.15))} \tag{A.6}$$

$$= \sum_{i=0}^{M_1-1} \tau^{-i} \left[\mathcal{I}_N \left[A^{(i)} \ * \ \mathcal{I}_{M_0}[g_i] \right] \right] \qquad \text{(using (3.13) and (3.16))}. \tag{A.7}$$

We now define the indices

$$\begin{aligned} i &= p + Mm \\ &= \alpha + Nb, \end{aligned}$$

with

$$\begin{cases} m \in \{0, 1, \ldots, N_0 - 1\} \\ p \in \{0, 1, \ldots, M - 1\} \\ \alpha \in \{0, 1, \ldots, N - 1\} \\ \beta \in \{0, 1, \ldots, M_0 - 1\}, \end{cases}$$

and

$$\begin{cases} p &= mod[a + N\beta, M] \\ m &= div[a + N\beta, M], \end{cases}$$

Finally, we can rearrange (A.7) as follows

$$x = \sum_{\alpha=0}^{N-1} \sum_{\beta=0}^{M_0-1} \tau^{-\alpha-N\beta} \left[\mathcal{I}_N \left[A^{(mod[\alpha+N\beta,M])} \ * \mathcal{I}_{M_0}[g_{(\alpha+N\beta)}]\right]\right] \tag{A.8}$$

$$= \sum_{\alpha=0}^{N-1} \sum_{\beta=0}^{M_0-1} \tau^{-\alpha} \left[\mathcal{I}_N \left[A^{(mod[\alpha+N\beta,M])} \right.\right.$$

$$\left.\left. * \ \tau^{-\beta}\mathcal{I}_{M_0}[g_{(\alpha+N\beta)}]\right]\right] \qquad \text{(using (3.6), (3.14) and (3.15))} \tag{A.9}$$

$$= \sum_{\alpha=0}^{N-1} \tau^{-\alpha} \ \mathcal{I}_N \left[\sum_{\beta=0}^{M_0-1} A^{(mod[\alpha+N\beta,M])} \ * \tau^{-\beta}\mathcal{I}_{M_0}[g_{(\alpha+N\beta)}]\right] \quad \text{(using (3.11)).} \tag{A.10}$$

According to (A.10), the transmitted signal is obtained by a S/P conversion of order N of the polyphase components (3.51).

A.2 Analysis Bank (Method B)

To start we can express the k-th sub-channel filter $h^{(k)}$ in the analysis FB (3.25) from its B-type M_1 order polyphase components $h_{-l}^{(k)} : \mathbb{Z}(M_1) :\to \mathbb{C}$ as follows

$$h^{(k)}(n) = \sum_{l=0}^{M_1-1} \tau^l \left[\ \mathcal{I}_{M_1} \left[\ h_{-l}^{(k)}\right]\right](n) \tag{A.11}$$

$$h_{-l}^{(k)} = h(M_1 n - l) W_M^{-k(M_1 n-l)} = h_{-l}(M_1 n)\ W_M^{kl}, \tag{A.12}$$

where h_{-l} is the l-th polyphase component of order M_1 of the analysis prototype pulse.

Then, the FB outputs (3.25) can be obtained as follows

$$b^{(k)} = \mathcal{C}_N \left[x \ * \ \sum_{l=0}^{M_1-1} \tau^l[\, \mathcal{I}_{M_1}[\, h_{-l}]]\, W_M^{kl} \right] \tag{A.13}$$

$$= \sum_{l=0}^{M_1-1} \mathcal{C}_N \left[\tau^l[x] \ * \ \mathcal{I}_{M_0 N}[\, h_{-l}] \right] \ W_M^{kl} \qquad \text{(using (3.7) and (3.15))} \tag{A.14}$$

$$= \sum_{l=0}^{M_1-1} \mathcal{C}_N \left[\tau^l[x] \right] \ * \ \mathcal{I}_{M_0}[\, h_{-l}]\, W_M^{kl} \qquad \text{(using (3.12) and (3.17))}. \tag{A.15}$$

Now, we redefine the indexes

$$\begin{aligned} l &= p + Mm \\ &= \alpha + N\beta, \end{aligned}$$

with

$$\begin{cases} m \in \{0, 1, \ldots, N_0 - 1\} \\ p \in \{0, 1, \ldots, M - 1\} \\ \alpha \in \{0, 1, \ldots, N - 1\} \\ \beta \in \{0, 1, \ldots, M_0 - 1\}, \end{cases}$$

and

$$\begin{cases} \alpha = mod[p + Mm, N] \\ \beta = div[p + Mm, N]. \end{cases}$$

Thus, we obtain

$$b^{(k)} = \sum_{p=0}^{M-1} \sum_{m=0}^{N_0-1} \left[\ \mathcal{C}_N \left[\tau^{\alpha+N\beta}[x] \right] * \mathcal{I}_{M_0}[\, h_{-p-Mm}] \ \right] \ W_M^{kp} \tag{A.16}$$

$$= \sum_{p=0}^{M-1} \sum_{m=0}^{N_0-1} \left[\ \tau^{\beta} \left[\mathcal{C}_N \left[\tau^{\alpha}[x] \right] \ * \ \mathcal{I}_{M_0}[\, h_{-p-Mm}] \right] \ \right] \ W_M^{kp} \quad \text{(using (3.10))}. \tag{A.17}$$

Since $\mathcal{C}_N\left[\tau^{\alpha}[x]\right]$ is the $\alpha - th$ polyphase component of x, we can define it as follows

$$x_{\alpha} = \mathcal{C}_N\left[\tau^{\alpha}[x]\right] \quad . \tag{A.18}$$

Substituting x_{α}, α and β, we obtain the realization of the analysis FB as in (3.54):

$$b^{(k)} = \sum_{p=0}^{M-1} \sum_{m=0}^{N_0-1} \left[\ \tau^{div[p+Mm,N]} \left[\ x_{mod[p+Mm,N]} \ * \ \mathcal{I}_{M_0}[\ h_{-p-Mm}]\right]\ \right] \ W_M^{kp}. \tag{A.19}$$

Appendix B

Efficient Implementation Using Weiss et al. Method

In this appendix we derive the Method C proposed by Weiss et al. in [17].

B.1 Synthesis Bank (Method C)

The transmitted signal x reads

$$x = \sum_{k=0}^{M-1} \left[\mathcal{I}_N[a^{(k)}] \ * \ \tilde{g}^{(k)} \right], \tag{B.1}$$

where the pulses have length equal to L_f samples. By performing an A-type polyphase decomposition of L_f-order on the filter $g^{(k)}$ we have

$$\begin{aligned} g_i^{(k)}(L_f n) &= g_i(L_f n + i) W_M^{-k(L_f n + i)} = g_i(L_f n)\, W_M^{-ki} \\ g^{(k)}(n) &= \sum_{i=0}^{M_1-1} \tau^{-i} \left[\mathcal{I}_{M_0 N}[\, g_i^{(k)}] \right](n)\, W_M^{-ki}, \end{aligned} \tag{B.2}$$

where $g_i^{(k)} : \mathbb{Z}(M_1) :\to \mathbb{C}$ is the $i-th$ polyphase component of $\tilde{g}^{(k)}$.
If we substitute (B.2) in (B.1) we obtain

$$x = \sum_{k=0}^{M-1} \left[\mathcal{I}_N[a^{(k)}] \ * \ \sum_{i=0}^{L_f-1} W_M^{-ki} \ \tau^{-i}[\mathcal{I}_{L_f}[g_i]] \right]. \tag{B.3}$$

If we define $A^{(i)}$ the M-point IDFT (Inverse Discrete Fourier Transform) of the signal $a^{(k)}$, i.e., $A^{(i)} = \sum_{k=0}^{M-1} a^{(k)} \ W_M^{-ki}$, we obtain

$$x = \sum_{i=0}^{L_f-1} \left[\mathcal{I}_N[A^{(i)}] \ * \ \tau^{-i}[\mathcal{I}_{L_f}[g_i]] \right] \tag{B.4}$$

$$= \sum_{i=0}^{L_f-1} \tau^{-i} \left[\mathcal{I}_N[A^{(i)}] \ * \ \mathcal{I}_{NL_M}[g_i] \right] \qquad \text{(using 3.15)} \tag{B.5}$$

$$= \sum_{i=0}^{L_f-1} \tau^{-i} \left[\mathcal{I}_N \left[A^{(i)} \ * \ \mathcal{I}_{L_M}[g_i] \right] \right] \qquad \text{(using 3.12 and 3.16).} \tag{B.6}$$

Since the polyphase decomposition on the filter g is of L_f-order, the polyphase component g_i has only one non-zero coefficient, that is equvalently to say that the ith polyphase filter is a dirac pulse

$$g_i(L_f n) = g(i) \ \delta(L_f n), \tag{B.7}$$

where $g(i)$ is the i-th coefficient of the filter g. Substituting we have:

$$x = \sum_{i=0}^{L_f-1} \tau^{-i} \left[\mathcal{I}_N \left[A^{(i)} \ \times \ g(i) \right] \right]. \tag{B.8}$$

We now decompose the indexes as

$$\begin{aligned} i &= \alpha + N\beta \\ &= p + Mm, \end{aligned}$$

with

$$\begin{cases} \alpha \in \{0, 1, \ldots, N-1\} \\ \beta \in \{0, 1, \ldots, M_0 - 1\} \\ m \in \{0, 1, \ldots, N_0 - 1\} \\ p \in \{0, 1, \ldots, M-1\}, \end{cases}$$

and

$$\begin{cases} p = mod[\alpha + N\beta, M] \\ m = div[\alpha + N\beta, M], \end{cases}$$

We then obtain the final expression

$$x = \sum_{\alpha=0}^{N-1} \sum_{\beta=0}^{L_M-1} \tau^{-\alpha-N\beta} \left[\mathcal{I}_N \left[A^{(p+Mm)} \times g(\alpha + N\beta)\right]\right] \tag{B.9}$$

$$= \sum_{\alpha=0}^{N-1} \tau^{-\alpha} \left[\mathcal{I}_N \left[\sum_{\beta=0}^{L_M-1} \tau^{-\beta} \left[A^{(mod[\alpha+N\beta,M])} \times g(\alpha + N\beta)\right]\right]\right]$$

(using 3.10 and 3.11). (B.10)

B.2 Analysis Bank (Method C)

The ith signal at the output of the analysis FB reads

$$b^{(i)} = \mathcal{C}_N[x * \tilde{h}^{(i)}] \qquad k \in \{0, 1, \cdots, M\}. \tag{B.11}$$

If we substitute the pulse $h(n)$ with its B-type L_f order polyphase decomposition

$$h_{-l}^{(i)}(n) = h_{-l}(L_f n - l) W_M^{-k(L_f n - l)} = h_{-l}\, W_M^{li} \tag{B.12}$$

$$h^{(i)}(n) = \sum_{l=0}^{L_f-1} \tau^l \left[\mathcal{I}_{L_f} \left[\, h_{-l}^{(i)}\right]\right](n)\, W_M^{li}, \tag{B.13}$$

where $h_l^{(i)} : \mathbb{Z}(M_1) \to \mathbb{C}$ is the $l-th$ polyphase component of $h^{(i)}$, we obtain

$$b^{(i)} = \mathcal{C}_N \left[x \ * \ \sum_{l=0}^{L_f-1} \tau^l [\, \mathcal{I}_{L_f} [\, h_{-l}]] \, W_M^{il} \right] \tag{B.14}$$

$$= \sum_{l=0}^{L_f-1} \left(\mathcal{C}_N \left[\tau^l [x] \ * \ \mathcal{I}_{NL_M} [\, h_{-l}] \right] \right) \, W_M^{il} \quad \text{(using 3.15 and 3.11)} \tag{B.15}$$

$$= \sum_{l=0}^{L_f-1} \left(\mathcal{C}_N \left[\tau^l [x] \right] \ * \ \mathcal{I}_{L_M} [\, h_{-l}] \right) \, W_M^{il} \quad \text{(using 3.17).} \tag{B.16}$$

We redefine the indexes

$$\begin{aligned} l &= p + Mm \\ &= \alpha + N\beta, \end{aligned}$$

where

$$\begin{cases} m \in \{0, 1, \ldots, L_N - 1\} \\ p \in \{0, 1, \ldots, M - 1\} \\ \alpha \in \{0, 1, \ldots, N - 1\} \\ \beta \in \{0, 1, \ldots, L_M - 1\}, \end{cases}$$

and the indexes are related with the following relation

$$\begin{cases} \alpha = mod[p + Mm, N] \\ \beta = div[p + Mm, N], \end{cases}$$

Thus, we obtain

$$b^{(i)} = \sum_{p=0}^{M-1} \sum_{m=0}^{L_N-1} \left[\, \mathcal{C}_N \left[\tau^{\alpha+N\beta} [x] \right] * \, \mathcal{I}_{L_M} [\, h_{-p-Mm}] \, \right] \, W_M^{ip} \tag{B.17}$$

$$= \sum_{p=0}^{M-1} \sum_{m=0}^{N_0-1} \left(\, \tau^\beta \left[\mathcal{C}_N \left[\tau^\alpha [x] \right] \ * \ \mathcal{I}_{L_M} [\, h_{-p-Mm}] \right] \right) \, W_M^{ip} \quad \text{(using 3.10).} \tag{B.18}$$

Considering that $\mathcal{C}_N\left[\tau^{\alpha}[x]\right]$ is the $\alpha - th$ polyphase component of x we write

$$x_{\alpha} = \mathcal{C}_N\left[\tau^{\alpha}[x]\right]. \tag{B.19}$$

If we substitute x_{α}, α and β in (B.18) we can write

$$b^{(i)} = \sum_{p=0}^{M-1} \left(\sum_{m=0}^{L_N-1} \tau^{div[p+Mm,N]} \left[x_{mod[p+Mm,N]} * \mathcal{I}_{L_M}[\, h_{-p-Mm}] \right] \right) W_M^{ip}. \tag{B.20}$$

Since $h(n)$ is assumed to be anticausal with length L_f that also corresponds to the order of the polyphase decomposition, the $-i$th polyphase pulse has only one non-zero component and can be written as

$$h_{-i}(L_f n) = h(-i)\ \delta(L_f n), \tag{B.21}$$

where $h(-i)$ is the i-th coefficient of the filter h, and we obtain the final expression

$$b^{(i)} = \sum_{p=0}^{M-1} \left(\sum_{m=0}^{L_N-1} \tau^{div[p+Mm,N]} \left[x_{mod[p+Mm,N]} \times h(-p-Mm) \right] \right) W_M^{ip}. \tag{B.22}$$

Appendix C

Probability of error for 4-PSK and M-PSK with the NCR

We consider 4-PSK modulation having symbols

$$c_k = e^{j(\pi/4+k\pi/2)} \quad \text{with} \quad k \in \{0,1,2,3\}.$$

The received signal (8.2) can be simply written as

$$z = ae^{j\Theta} + \eta,$$

since $g_{eq}^{(i,i)} \approx e^{j\Theta}$, where $a \in \{c_0, \cdots, c_3\}$, Θ is defined in (8.6), and η, that comprises ISI plus ICI and noise, is modeled as a stationary Gaussian process with variance σ_η^2. The SER is

$$P_e^{(4PSK)}(\Theta) = 1 - P_c^{(4PSK)}(\Theta),$$

where $P_c^{(4PSK)}(\Theta)$ is the correct decision probability with the NCR conditioned by the CPE. It is equal to

$$P_c^{(4PSK)}(\Theta) = 1/4 \sum_{k=0}^{3} P_c^{(4PSK)}(\Theta, c_k),$$

where $P_c^{(4PSK)}(\Theta, c_k)$ is the correct decision probability conditioned on the transmission of the symbol c_k.

We now consider the transmission of symbol $a = c_0 = e^{j\pi/4}$. It is correctly received if

$$\Re[\eta_k] > -d_{1,0}$$
$$\Im[\eta_k] > -d_{2,0}$$

where we defined

$$d_{1,0} = |\Re[c_0 e^{j\Theta}]| = cos(\pi/4 + \Theta)$$
$$d_{2,0} = |\Im[c_0 e^{j\Theta}]| = sin(\pi/4 + \Theta)$$

that are the minimum distances between $c_0 e^{j\Theta}$ and the boundaries of the decision region (axes). Thus, $P_c^{(4PSK)}(\Theta, c_0) = (1 - Q(d_{1,0}/\sigma_\eta)(1 - Q(d_{2,0}/\sigma_\eta))$. By symmetry, the same argument is valid if the other symbols $\{c_1, c_2, c_3\}$ are transmitted. Finally, we obtain that

$$P_c^{(4PSK)}(\Theta) = (1 - Q(d_{1,0}/\sigma_\eta)\,)(\,(1 - Q(d_{2,0}/\sigma_\eta)\,).$$

Considering M-PSK modulation, with $M > 4$ and symbols

$$c_k = e^{j(\pi/M + 2k\pi/M)} \quad \text{with} \quad k \in \{0, \cdots, M-1\},$$

we use the nearest neighbor symbol approximation. The minimum distances between the rotated symbol $ae^{j\Theta}$ and the adjacent boundaries of the decision region are

$$d_1 = sin(\pi/M - \Theta)$$
$$d_2 = sin(\pi/M + \Theta).$$

Thus, we can use the approximation

$$P_e^{(MPSK)}(\Theta) \approx Q(d_1/\sigma_\eta) + Q(d_2/\sigma_\eta),$$

which proves (8.19).

Appendix D

Probability of error for M-QAM with the NCR

In M-QAM modulation with square constellations, the symbols are defined as

$$c_{i,k} = (2i - 1 - \sqrt{M}) + j(2k - 1 - \sqrt{M}) \quad \text{with} \quad (i,k) \in \{1, \cdots, \sqrt{M}\}.$$

To obtain the SER with the NCR conditioned on the CPE, we start from the signal model

$$z = ae^{j\Theta} + \eta,$$

as in Appendix C. Furthermore, with the non-coherent metric in (8.16) we can identify three shapes of decision region depending on where the symbol is located: symbol in the constellation corner, symbol with three minimum distance neighbors, and symbol with four minimum distance neighbors. Furthermore, let us consider to transmit the symbol $a = c_{i,k}$, then we define

$$R_{i,k} = \left|\Re[c_{i,k}e^{j\Theta} - (c_{i,k} + 1)]\right|$$

as the minimum distance between the symbol affected by the CPE and the right boundary of the decision region associated to $c_{i,k}$. Analogously, we define

$$L_{i,k} = \left|\Re[c_{i,k}e^{j\Theta} - (c_{i,k} - 1)]\right|$$
$$U_{i,k} = \left|\Im[c_{i,k}e^{j\Theta} - (c_{i,k} + j)]\right|$$
$$D_{i,k} = \left|\Im[c_{i,k}e^{j\Theta} - (c_{i,k} - j)]\right|$$

as the minimum distances between the symbol affected by the CPE and, respectively, the left, the upper and the lower boundaries of the decision region.

Now, exploiting the symmetry of the problem, we need to compute the conditional probability of correct detection $P_c^{(QAM)}(\Theta, a = c_{i,k})$ only for the symbols $c_{i,k}$ with $i \in \{1, \cdots, \sqrt{M}/2\}$ and $k \in \{1, \cdots, \sqrt{M}/2\}$ (i.e. the symbols that are located on the lower-left quadrant of the Cartesian plane). Therefore, if the symbol belongs to the lower-left corner ($i = k = 1$) the probability of a correct decision is

$$P_c^{(QAM)}(\Theta, c_{1,1}) = \Phi(\frac{U_{1,1}}{\sigma_\eta})\Phi(\frac{R_{1,1}}{\sigma_\eta}).$$

For the symbols $c_{i,k}$ with $k = 1$, $i \in \{2, \cdots, \sqrt{M}/2\}$ we obtain

$$P_c^{(QAM)}(\Theta, c_{i,1}) = \Phi(\frac{U_{i,1}}{\sigma_\eta})\left(\Phi(\frac{R_{i,1}}{\sigma_\eta}) - Q(\frac{L_{i,1}}{\sigma_\eta})\right).$$

For the symbols $c_{i,k}$ with $i = 1$, $k \in \{2, \cdots, \sqrt{M}/2\}$) we obtain

$$P_c^{(QAM)}(\Theta, c_{1,k}) = \Phi(\frac{R_{1,k}}{\sigma_\eta})\left(\Phi(\frac{U_{1,k}}{\sigma_\eta}) - Q(\frac{D_{1,k}}{\sigma_\eta})\right).$$

Finally, for the symbols $c_{i,k}$ with $i \in \{2, \cdots, \sqrt{M}/2\}$, $k \in \{2, \cdots, \sqrt{M}/2\}$) we have that

$$P_c^{(QAM)}(\Theta, c_{i,k}) = \left(\Phi(\frac{R_{i,k}}{\sigma_\eta}) - Q(\frac{L_{i,k}}{\sigma_\eta})\right)\left(\Phi(\frac{U_{i,k}}{\sigma_\eta}) - Q(\frac{D_{i,k}}{\sigma_\eta})\right).$$

If we now define $S = \sqrt{M}/2$, we obtain

$$
\begin{aligned}
& P_c^{(QAM)}(\Theta) = \\
&= \sum_{i=2}^{S}\sum_{k=2}^{S} \frac{4}{M} P_c^{(QAM)}(\Theta, c_{i,k}) + \sum_{i=2}^{S} \frac{4}{M} P_c^{(QAM)}(\Theta, c_{i,1}) \\
&+ \sum_{k=2}^{S} \frac{4}{M} P_c^{(QAM)}(\Theta, c_{1,k}) + \frac{4}{M} P_c^{(QAM)}(\Theta, c_{1,1}).
\end{aligned} \tag{D.1}
$$

Since the average constellation energy is $\sigma_a^2 = 2(M-1)/3$, the signal to noise plus interference ratio can be written as $SINR = \sigma_a^2/\sigma_\eta^2$ with $\sigma_\eta^2 = E[|\eta|^2]$ (see the Appendix C). Thus, we obtain (8.20) from (D.1).

Bibliography

[1] M. Doelz, E. Heald, and D. Martin, "Binary data transmission techniques for linear systems," *Proceedings of the IRE*, pp. 656–661, 1957.

[2] J. Bingham, "Multicarrier Modulation for data Transmission, an Idea whose Time Has Come," *IEEE Commun. Mag.*, vol. 31, pp. 5 – 14, May 1990.

[3] IEEE, "802.11 Standard: Wireless LAN Medium Access Control and Physical Layer Specification," 2007.

[4] IEEE, "802.16 Standard: Air Interface for Broadband Wireless Access Systems," 2009.

[5] ETSI, "Radio Broadcasting Systems; Digital Audio Broadcasting (DAB) to mobile, portable and fixed receivers," 2006.

[6] ETSI, "Digital Video Broadcasting (DVB); A Guideline for the Use of DVB Specifications and Standards," 2008.

[7] Motorola, "Long Term Evolution (LTE): A Technical Overview," july 2010.

[8] S. Galli and O. Logvinov, "Recent Developments in the Standardization of Power Line Communications within the IEEE," *IEEE Communications Magazine*, vol. 46, july 2008.

[9] H. P. Alliance, "https://www.homeplug.org/home/,"

[10] F. Sjoberg, R. Nilsson, P. Odling, and P. Borjesson, "Asynchronous Zipper," *Proc. of IEEE International Conference in Communications(ICC)*, vol. 19, no. 5, pp. 231–235, 1999.

[11] G. Cherubini, E. Eleftheriou, and S. Olcer, "Filtered Multitone Modulation for Very High-Speed Digital Subscribe Lines," *IEEE J. Sel. Areas Commun.*, pp. 1016–1028, June 2002.

[12] P. Siohan, C. Siclet, and N. Lacaille, "Analysis and design of OFDM/OQAM systems based on filterbank theory," *IEEE Transactions on Signal Processing*, vol. 50, no. 5, p. 11701183, 2002.

[13] A. M. Tonello, "Time Domain and Frequency Domain Implementations of FMT Modulation Architectures," in *Proc. of IEEE Int. Conf. on Acoustic, Speech, and Signal Processing (ICASSP 2006)*, (Toulose, France), May 2006.

[14] Z. Cvetković and M. Vetterli, "Tight Weyl-Heisemberg Frames in $\ell^2(\mathbb{Z})$," *IEEE Trans. on Signal Processing*, vol. 46, May 1998.

[15] C. Siclet, P. Siohan, and D. Pinchon, "Perfect Reconstruction Conditions and Design of Oversampled DFT-Modulated Transmultiplexer," *EURASIP Journ. on Appl. Sign. Proc.*, vol. 2006, pp. 1–14.

[16] W. McGee, "Efficient Realization of Filtered Multitone Transmitters and Receivers and Oversampled Analysis/Synthesis Filterbank Pairs for Perfect and Non Perfect Reconstruction," *Personal correspondence*, August 2007.

[17] S. Weiss and R. Stewart, "Fast Implementation of Oversampled Modulated Filter Banks," *Electronic Letter*, vol. 36, August 2000.

[18] V. Ercegl, L. Shumacher, and et al, "IEEE P802.11 Wireless LANs, TGn Channel Models, doc.: IEEE 802.11-03/940r4," 2004.

[19] A. M. Tonello, "Performance Limits for Filtered Multitone Modulation in Fading Channels," *IEEE Trans. Wireless Commun.*, vol. 4, pp. 2121–2135, September 2005.

[20] A. Tonello and F. Pecile, "Analytical Results about the Robustness of FMT Modulation with Several Prototype Pulses in Time-Frequency Selective Fading Channels," *IEEE Trans. Wireless Commun.*, vol. 7, pp. 1634 – 1645, May 2008.

[21] A. Tonello and F. Pecile, "Efficient Architectures for Multiuser FMT Systems and Application to Power Line Communications," *IEEE Transaction on Communications*, pp. 1275–1279, May 2009.

[22] W. Kozek and A. Molisch, "Nonorthogonal Pulseshapes for Multicarrier Communications in Doubly Dispersive Channels," *IEEE J. Sel. Areas Commun.*, vol. 16, pp. 1579–1589, October 1998.

[23] M. Harteneck, S. Weiss, and W. Stewart, "Design of Near Perfect Reconstruction Oversampled Filter Banks for Subband Adaptive Filters," *IEEE Trans. Circuits Syst. II*, vol. 46, pp. 1081–1086, August 1999.

[24] A. Oppenheim and R. Schafer, "Digital Signal Processing," *Prentice Hall*, 1989.

[25] N. Mizutani, S. Muramatsu, and H. Kikuchi, "Memory Access Estimation of Filter Bank Implementation on Different DSP Architectures," *IEICE Trans. Fundam.*, vol. E84, pp. 1951–1959, August 2001.

[26] A. Tonello, "Asynchronous Multicarrier Multiple Access: Optimal and Suboptimal Detection and Decoding," *Bell Labs Technical Journal*, vol. 7 n. 3, pp. 191–217, 2003.

[27] T. Hunziker and D. Dahlhaus, "Transmission Employing Time-Frequency Concentrated Pulses," *IEEE Trans. on Comm.*, vol. 51, pp. 641–651, April 2003.

[28] B. L. Floch, M. Alard, and C. Berrou, "Coded Orthogonal Frequency Division Multiplex [TV Broadcasting]," *Proceedings of the IEEE*, vol. 83, pp. 982–996, June 1995.

[29] B. L. Floch, R. Halbert-Lassalle, and D. Castelain, "Digital Sound Broadcasting to Mobile Receivers," *IEEE Trans. Consum. Electron.*, vol. 35, pp. 493–503, August 1989.

[30] R. Haas and J.-C. Belfiore, "A Time-Frequency Well-Localized Pulse for Multiple Carrier Transmission," *Wireless Personal Communications*, vol. 5, pp. 1–18, July 1997.

[31] D. Schafhuber, G. Matz, and F. Hlawatsch, "Pulse-Shaping OFDM/BFDM Systems for Time-Varying Channels: ISI/ICI Analysis, Optimal Pulse Design, and Efficient Implementation," in *Proc. IEEE PIMRC 2002*, vol. 3, (Lisbon, Portugal), pp. 1012–1016, September 2002.

[32] T. Strohmer and S. Beaver, "Optimal OFDM Design for Time-Frequency Dispersive Channels," *EEE Trans. Commun.*, vol. 51, pp. 111–1122, July 2003.

[33] B. Borna and T. Davidson, "Efficient Design of FMT Systems," *IEEE Trans. Commun.*, vol. 54, pp. 794–797, May 2006.

[34] M. Vetterli and J. Kovacevic, "Wavelet and Subband Coding," *Prentice Hall PTR. Upper Saddle River*.

[35] J. Seoane, S. Wilson, and S. Gelfand, "Analysis of Intertone and Interblock Interference in OFDM when the Length of the Cyclic Prefix is Shorter than the Length of the Impulse Response of the Channel," in *Proc. of IEEE Global Telecommunications Conference (GLOBECOM)*, (Phoenix, AZ, USA), pp. 32–36, Nov. 1997.

[36] S. Hykin, *"Adaptive Filter Theory"*. Information and System Science Series, Practice Hall, 1996.

[37] J. Proakis, "Digital Communications, 4th Edition," *McGraw-Hill*, 1995.

[38] S. D'Alessandro, A. M. Tonello, and L. Lampe, "Improving WLAN Capacity via OFDMA and Cyclic Prefix Adaptation," in *Proc. of IEEE IFIP Wireless Days Conference (WD 2009)*, (Paris, France), Dec. 2009.

[39] V. Oksman and S. Galli, "G.hn: The new itu-t home networking standard," *IEEE Commun. Mag.*, vol. 47, no. 10, pp. 139–145, 2009.

[40] H. Lin and P. Siohan, "Modulation diversity in wideband in-home plc," *Proc. of Third Workshop on Powerline Commun. (WSPLC 2009)*, vol. 47, no. 10, pp. 86–88, 2009.

[41] S. D'Alessandro, "Adaptation and optimization in multi-carrier modulation schemes," *PhD Thesis, University of Udine*, 2011.

[42] D. P. Palomar, J. M. Cioffi, and M. A. Lagunas, "Joint Tx-Rx Beamforming Design for Multicarrier MIMO Channels: A Unified Framework for Convex Optimization.," *IEEE Trans SP*, vol. 51, no. 9, p. 23812401, 2003.

[43] S. Redif and T. Cooper, "Paraunitary Filter Bank Design via a Polynomial Singular Value Decomposition," *In Proc. IEEE ICASSP, Philadelphia, PA,*, vol. 4, p. 613616, 2005.

[44] J. G. McWhirter, P. D. Baxter, T. Cooper, S. Redif, and J. Foster, "An EVD Algorithm for Para-Hermitian Polynomial Matrices," vol. 55, pp. 2158–2169, May 2007.

[45] C. Ta and S. Weiss, "Design of precoding and equalisation for broadband MIMO transmission," *DSPenabledRadio, The 2nd IEE/EURASIP Conference*, 2005.

[46] M. Vu and A. Paulraj, "MIMO Wireless Linear Precoding," *IEEE Signal Processing Magazine*, vol. 24, pp. 86–105, Sept. 2007.

[47] T. Pollet, M. V. Bladen, and M. Moenclaey, "Ber sensitivity of ofdm systems to carrier frequency offset and wiener phase noise," *IEEE Trans. on Communications*, vol. 43, no. 2/3/4, pp. 86–88, 1995.

[48] P. Robertson and S. Kaiser, "Analysis of the effect of Phase-Noise in Orthogonal Frequency Division Multiplex (OFDM) System," *In Proc. IEEE ICC'95, Seattle*, pp. 1652–1657, June 1995.

[49] L. Piazzo and P. Mandarini, "Analysis of Phase Noise Effects in ODFM Modems," *IEEE Trans. on Communication*, vol. 50, pp. 1696–1705, October 2002.

[50] D. D. Lin, Y. Zhao, and T. J. Lim, "OFDM Phase Noise Cancellation via Approximate Probabilistic Inference," *Wireless Communications and Networking Conference, 2005 IEEE*, vol. 1, pp. 27–32, 2005.

[51] N. Benvenuto, G. Cherubini, and L. Tomba, "Achievable bit rates of DMT and FMT systems in the presence of phase noise and multipath," *Vehicular Technology Conference Proceedings, VTC 2000-Spring Tokyo*, May 2000.

[52] A. Assalini, S. Pupolin, and A. M. Tonello, "Analysis of the Effect of Phase Noise in Filtered Multitone (FMT) Modulated System," *Proc. of IEEE Globecom, Dallas*, pp. 3541–3545, November 2004.